National Library of Canada
Bibliothèque nationale du Canada

Canadian Theses Service
Service des thèses canadiennes

Ottawa, Canada
K1A 0N4

NOTICE

The quality of this microform is heavily dependent upon the quality of the original thesis submitted for microfilming. Every effort has been made to ensure the highest quality of reproduction possible.

If pages are missing, contact the university which granted the degree.

Some pages may have indistinct print especially if the original pages were typed with a poor typewriter ribbon or if the university sent us an inferior photocopy.

Previously copyrighted materials (journal articles, published tests, etc.) are not filmed.

Reproduction in full or in part of this microform is governed by the Canadian Copyright Act, R.S.C. 1970, c. C-30.

AVIS

La qualité de cette microforme dépend grandement de la qualité de la thèse soumise au microfilmage. Nous avons tout fait pour assurer une qualité supérieure de reproduction.

S'il manque des pages, veuillez communiquer avec l'université qui a conféré le grade.

La qualité d'impression de certaines pages peut laisser à désirer, surtout si les pages originales ont été dactylographiées à l'aide d'un ruban usé ou si l'université nous a fait parvenir une photocopie de qualité inférieure.

Les documents qui font déjà l'objet d'un droit d'auteur (articles de revue, tests publiés, etc.) ne sont pas microfilmés.

La reproduction, même partielle, de cette microforme est soumise à la Loi canadienne sur le droit d'auteur, SRC 1970, c. C-30.

Canada

SOME PROPERTIES OF THE SEMIMAGNETIC SEMICONDUCTOR ALLOY

$Cd_xZn_yMn_zSe$ $(x + y + z = 1)$

by

Sudershan Manhas

Thesis

Submitted to the University of Ottawa

in partial fulfillment of the

requirements for the degree of

Master in Physics.

Department of Physics

Ottawa, Ontario

K1N 6N5

1987

© Sudershan Manhas, Ottawa, Canada, 1987.

Permission has been granted to the National Library of Canada to microfilm this thesis and to lend or sell copies of the film.

The author (copyright owner) has reserved other publication rights, and neither the thesis nor extensive extracts from it may be printed or otherwise reproduced without his/her written permission.

L'autorisation a été accordée à la Bibliothèque nationale du Canada de microfilmer cette thèse et de prêter ou de vendre des exemplaires du film.

L'auteur (titulaire du droit d'auteur) se réserve les autres droits de publication; ni la thèse ni de longs extraits de celle-ci ne doivent être imprimés ou autrement reproduits sans son autorisation écrite.

ISBN 0-315-46811-4

UNIVERSITÉ D'OTTAWA
UNIVERSITY OF OTTAWA

ABSTRACT

This thesis investigates the crystallographic and magnetic properties of the pseudo-ternary alloy system, $Cd_x Zn_y Mn_z Se$, $(x + y + z = 1)$. These alloys also known as semi-magnetic semi-conductors or diluted magnetic semi-conductors is connected with their unique properties both from semi-conducting and magnetic point of view.

Samples with different composition were prepared and Debye-Scherrer x-ray powder photographs were used to investigate the equilibrium conditions and to determine the lattice parameters for each sample. These values were plotted as a function of composition z and f (where $f = y/x+y$) and thus the range of single phase solid solution was determined.

Measurements of low-field magnetic susceptibility were carried out using a SQUID magnetometer. From the susceptibility measurements, values were obtained for the spin-glass transition temperature T_g, the Curie-Weiss temperature θ, and the Curie constant C. The variation of these three parameters with composition was studied in some detail. A study of exchange interaction using the T_g values, suggested that the magnetic spins were indirectly coupled to each other by a mechanism which involved a virtual transition between the valence band and a Mn 3d level. Predictions of the exchange energy, based on these results, agreed with those of other researchers. As well, predictions of the Curie-Weiss temperature, also agreed with the measured values obtained in this work.

The ESR linewidth was studied as a function of composition and temperature. The linewidth was observed to increase with decreasing temperature. At lower temperature, the ESR line became asymmetrically broadened and then split into two parts well above any magnetic transition point. The dependence of the linewidth on temperature results were analyzed using a theory based on inhomogeneous broadening.

ACKNOWLEDGEMENTS

I would like to express my thanks to my supervisor Dr. J.C. Woolley for his assistance and invaluable suggestions during the course of this work.

Many thanks are also due to Dr. Gilles Lamarche for his help in the magnetic susceptibility measurements and for the useful discussions with him.

I would also like to thank Dr. Armen Manoogian for his help in ESR measurements and many useful discussions. Also thanks to B.W. Chan for handling the technical aspects of the ESR measurements.

I would also like to thank Mr. Tom Donofrio, for many useful discussions and for the help received on the use of the computing facilities.

My gratitude also goes to a very special person, my wife Anju, for her patience, understanding and love.

Finally, I wish to thank Mrs. Line Robitaille who did an excellent job in typing this thesis.

TABLE OF CONTENTS

LIST OF FIGURES

Chapter I

Introduction

Recent interest in semi-magnetic semi-conductors or diluted magnetic semi-conductors is connected with their unique properties both from semi-conducting and magnetic point of view. The name semi-magnetic semi-conductors (SMSC) was coined by R.R. Galazka [1] and name diluted-magnetic semi-conductor (DMSC) was suggested by Furdyna [2]. One example of semi-magnetic semi- conductors are the solid solutions of $A_{1-x}M_xB$ type which are formed by substitution of the 'A' component in an ordinary semi-conductor AB by the magnetic 3d or 4f 'M' component. If the MB compound is a magnetic semi-conductor, then $A_{1-x}M_xB$ solid solutions are continuously filling 'the gap' between normal non-magnetic and magnetic semi-conductors. In this case $A_{1-x}M_xB$ is the missing line between AB and MB and the terminology 'semi-magnetic semi-conductors' is used. Diluting magnetic compound MB with non-magnetic A ions we can refer to $A_{1-x}M_xB$ compound as diluted magnetic semi-conductors. In order to retain semi-conductor properties the M and A must have same number of valence electrons. Some of the typical examples of semi-magnetic semi-conductors are $Cd_{1-z}Mn_zSe$, $Zn_{1-z}Mn_zSe$, $Cd_{1-z}Mn_zTe$, $Zn_{1-z}Mn_zTe$, $Hg_{1-z}Mn_zTe$ etc.

Due to the presence of paramagnetic ions (Mn^{2+}) in these materials the interactions between the localized magnetic moments and mobile electrons play an important role.

Therefore in an external magnetic field a behaviour of the spin-split-energy levels is observed strongly different from that of

usual semi-conductors. On the other hand in the absence of a magnetic field the band structure in these materials exhibit a form similar to that of a typical semi-conductors, except at low temperature as shown by Tom Donofrio in his work [3] on $Cd_xZn_yMn_zTe$ alloys.

A large number of papers present physical properties of pseudo-binary alloys obtained by mixing $A^{II}B^{VI}$ semi-conductors with corresponding Mn compounds. There have been recent studies of the magnetic properties of the $Cd_{1-z}Mn_zTe$, $Hg_{1-z}Mn_zTe$ [4-7] $Zn_{1-z}Mn_zTe$ [8] $Cd_{1-z}Mn_zSe$ [9,10] alloys as well as studies of electron paramagnetic resonance (EPR) properties of the pseudo-ternary alloy system $Cd_xZn_yMn_zTe$ which links two pseudo-binary system [3]. In all these alloys, one main important effect stems from the disordered distribution of magnetic Mn ions on the cation sublattice which allows them to exhibit spin glass properties.

Brief history of spin glass physics

During the last twenty years, the physics of disordered systems has come to the forefront of theoretical physics.

The original material, on which were first observed the characteristic properties of spin glasses, were dilute alloys of transition impurities in noble matrices e.g. metal impurities (Fe,Mn) in noble metals (Au,Cu). In 1932 Louis Neel [11] in his experiments was hoping to get a better understanding of the magnetic properties of pure transition metals. It was only in 1956 that at lower temperatures the flattening of the magnetic susceptibility was first observed by J. Owen [12]. At that time this could only be interpreted as an

antiferromagnetic transition. However, in some respects (remanent magnetization hysteresis) the materials behaved like ferromagnets and besides it was hard to imagine a long range antiferromagnetic ordering in these alloys. The specific heat experiments at the end of the 50's, showing a contribution linear in T at low temperatures and a very round maximum, led to a different type of interpretation, which essentially negated the existence of a transition. This interpretation came to dominate in the 60's and found its expressions in the term "spin glass" coined by B.R. Coles at the end of the decade.

The name "spin glass" was introduced by Coles to denote the "entire class of (random) magnetic alloys of moderate dilution in which the magnetic structure no longer resembles that of a pure metal but is sufficiently similar that the exchange interaction dominates other energy contributions such as those from the Kondo effect and other free electrons interactions". Such an alloy after cooling to a very low temperature in zero field has the solute moments 'frozen' in local molecular fields. These fields having a distribution of magnitudes and directions such that the net magnetization of any region containing a few tens of solute atom is zero. So far as the nature of the exchange interaction is concerned the physical model has come to be accepted for these metallic materials so that the exchange interactions follow the RKKY theory.

During the last decade many other spin-glass system have been discovered where the physical origin of randomness of the spin orientation and the nature of the exchange interaction are different from the one considered above. Therefore Binder [13] defined spin-glass as "magnetic systems where the interactions between the spins are

in conflict" with each other due to some quenched (i.e. frozen in) disordered in the system.

Therefore for the metallic materials the essential ingredients of spin glass are the randomness and the mixed interactions but for semi-conductors materials this is not the case.

In order to produce a random magnetic system, we have to simply substitute a magnetic element for a non-magnetic one in a multi-component system as discussed earlier in the chapter. The method which we used to produce the random magnetic system was melt and anneal technique, in which we weighed the different elements according to their appropriate ratio and melt them together. The other method and more recent technique is by sputtering. But this is done mostly for metallic compounds.

In this present work we will be discussing semi-magnetic semi-conductor systems. Semi-conducting mixed crystals containing a magnetic component e.g. $Cd_{1-z}Mn_zSe$, $Hg_{1-z}Mn_zTe$, $Cd_{1-z}Mn_zTe$ and $Zn_{1-z}Mn_zSe$ have received considerable attention [4-10]. The presence of the paramagnetic Mn ion in these materials modifies the semi-conductor properties, particularly at low temperatures, and produces some interesting magnetic effects, one being the formation of a spin-glass phase.

In this present work an investigation of certain properties of the system $Cd_xZn_yMn_zSe$ and $Cd_xHg_yMn_zTe$ where $x + y + z = 1$ will be presented. The composition of these semi-magnetic semi-conductors may be represented by a composition triangle (Fig. I-A and I-B) in triangular co-ordinates.

Each point in the triangle represent a particular value of x,

y and z, and hence a particular composition. Each corner of the triangle represent a pure compound, CdSe, ZnSe, MnSe, CdTe, HgTe and MnTe, and each side of the triangle represent a pseudo-binary system e.g. $Cd_{1-z}Mn_zSe$, shown in Fig. I-A on the left side of the triangle, and similarly with the other sides.

Now the samples in this report with particular composition will be referred to by a label of the form (x,y,z) where x,y,z are percentage composition of Cd, Zn, Mn in Fig. I-A and Cd, Hg, Mn in (Fig. I-B).

Many measurements have been performed on the pseudo-binary systems $Cd_{1-z}Mn_zTe$, $Hg_{1-z}Mn_zTe$, $Cd_{1-z}Mn_zSe$ and $Zn_{1-z}Mn_zTe$ [4-10].

In this work the measurements will be extended to the pseudo-ternary systems $Cd_xZn_yMn_zSe$ and $Cd_xHg_yMn_zTe$. There are some advantages in performing these measurements on a pseudo-ternary rather than just on pseudo-binary alloys. For one, we have wide range of samples available over complete composition of the triangle (see Fig. I-A) to investigate and also a wide solid solution range. This can then provide much more data for analysis of those properties and may reveal previously undetected results.

The measurements which were carried out were as follows. First the variation of the lattice parameter with composition were measured for equilibrium samples. In doing so the limits of solid solution were also determined. Next the magnetic properties of the system were investigated. These measurements were made only on the system $Cd_xZn_yMn_zSe$, for the system $Cd_xHg_yMn_zTe$ only lattice parameter measurements were made, other measurements carried out by another student (D. Beckett). Because of the semi-magnetic nature of the

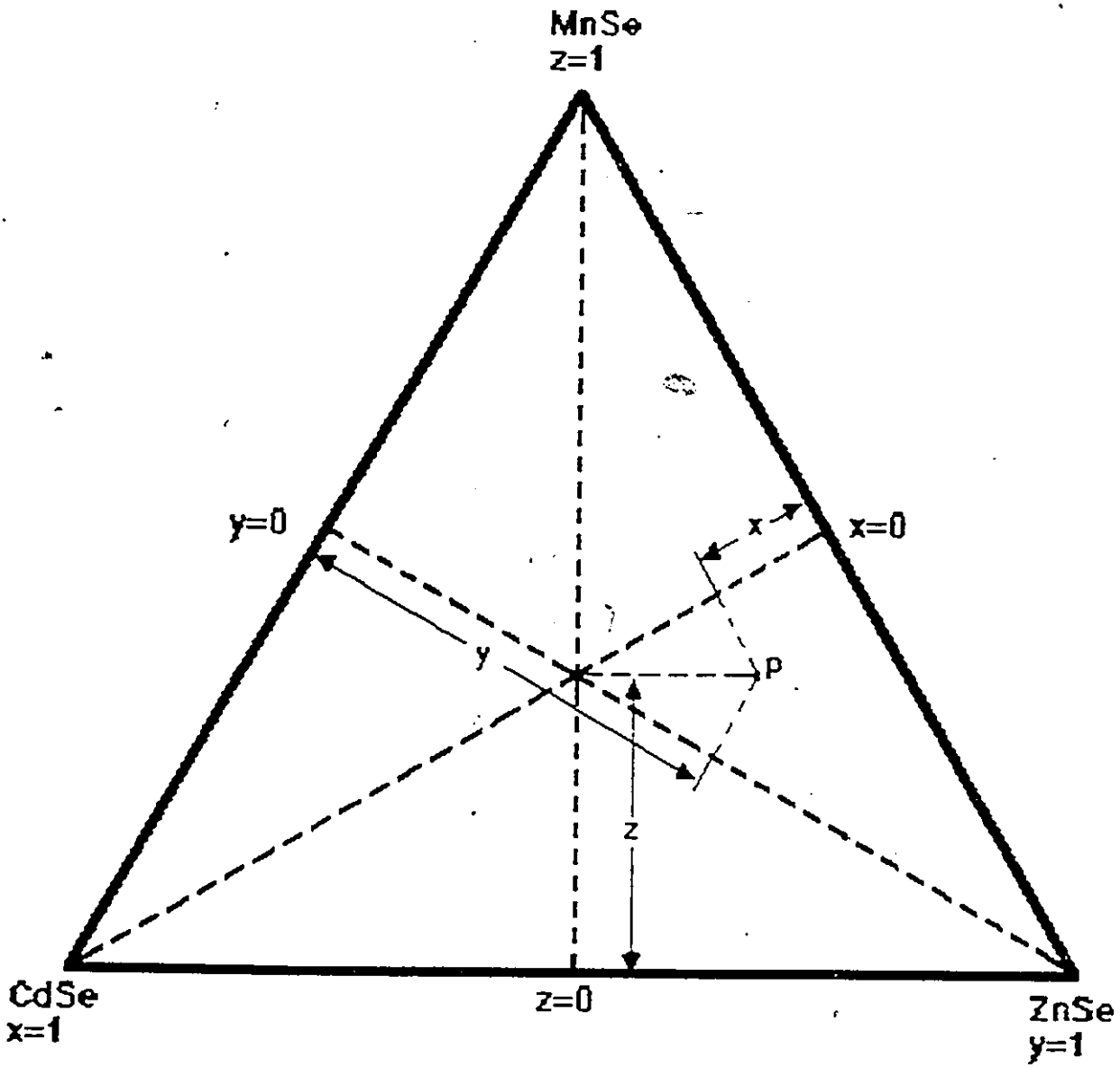

FIGURE 1-A *Triangular Coordinate System.*
Any point "P" in the diagram represents a sample of composition (x, y, z).

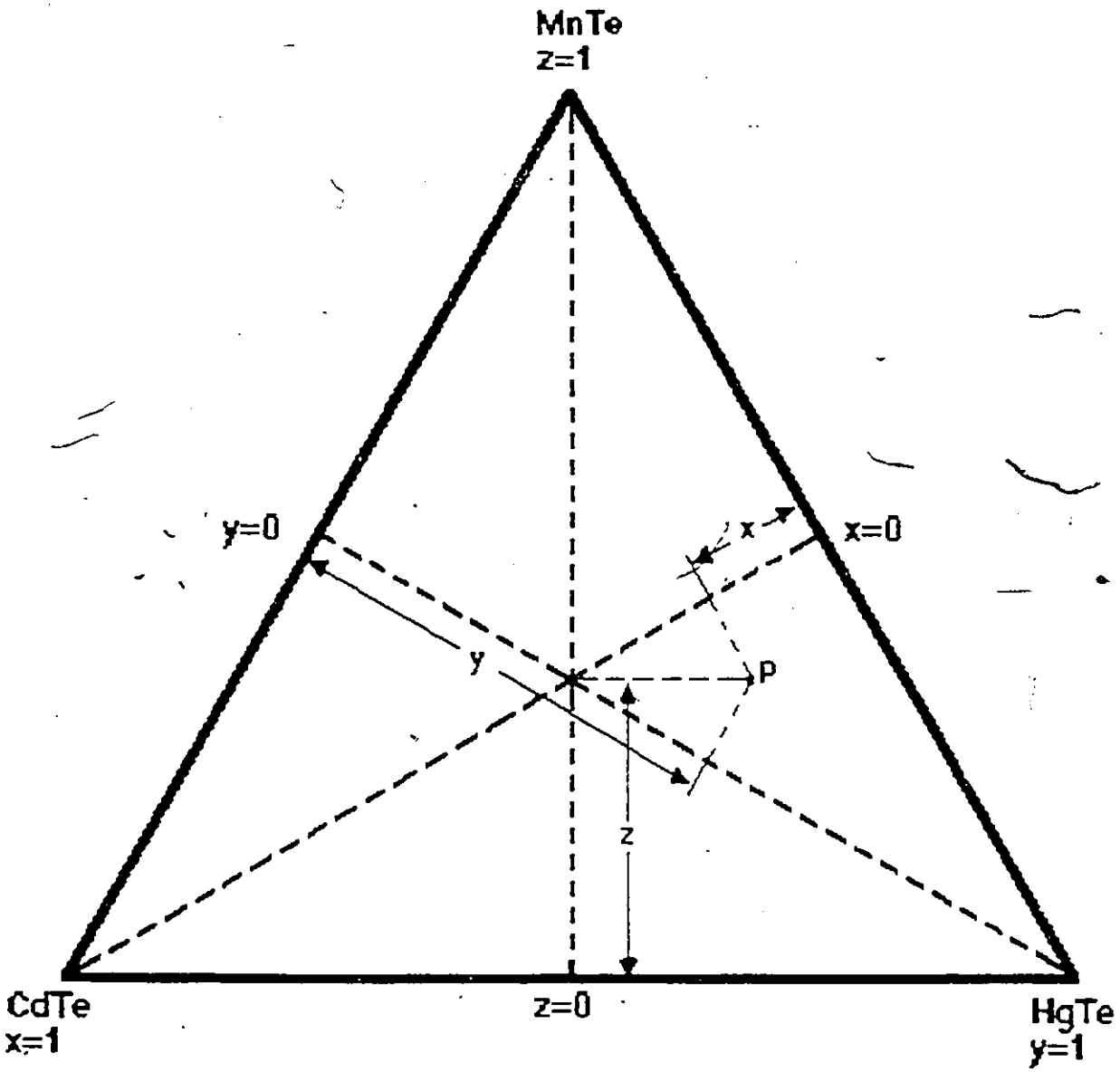

FIGURE 1-B Triangular Coordinate System.
Any point 'P' in the diagram represents a sample of composition ($x_c y, z$).

material, a magnetic state known as spin glass (as discussed earlier) can occur below a certain critical temperature. Measurements of susceptibility and of electron spin resonance were carried out to study this.

Polycrystalline samples were produced rather than single crystal, because a large numbers of samples with different compositions were required. The choice of polycrystalline samples allowed of the order ten or twenty times the number of composition to be investigated as compared with the case of single crystals were used. In all of the measurements made, the use of polycrystalline samples was no disadvantage.

REFERENCES

1. J.A. Gaj, Proc. 15th Int. Conf. Physics of semi-conductors Kyoto, (1980).

2. J.K. Furdyna, J. Appl. Phys. 53, 7637 (1982.

3. Tom Donofrio, Some properties of the semimagnetic semi-conductor alloy (thesis) University of Ottawa.

4. J.A. Gaj, R.R. Galazka, M. Nawrocki, Solid State Commun. 25, 193 (1978).

5. R.R. Galazka, S. Nagata, P.H. Keesom, Phys. Rev. B 22, 3344 (1980).

6. S. Nagata, R.R. Galazka, D.P. Mullin, H. Akbarzakeh, G.D. Khattak, J.K. Furdyna, P.H. Keesom, Phys. Rev. B 22, 3331 (1980).

7. G. Bastard, C. Rigaux, Y. Galdner, J. Mycielski, A. Mycielski, Journal de Phys. 39, 87 (1978).

8. T. Donofrio, G. Lamarche and J.C. Woolley, J. Appl. Phys. 57, 1937 (1985).

9. S. Oseroff, Phys. Rev. 25B, 6484 (1982).

10. H. Wiedemier and A.B. Sigai, J. Electrochem. Soc. 117, 551 (1970).

11. L. Neel, Ann. Phys. 17, 5 (1932).

12. J. Oæn, K.D. Bowers, Prepts. Prog. Phys. 18, 304 (1955).

13. K. Binder, in Fundamental Problems in Statistical Mechanics V, Ed. E.G.D. Cohen (North-Holland, Amsterdam) p.21.

Chapter II

CRYSTALLOGRAPHY AND X-RAY MEASUREMENTS

2.1 Preparation of samples

Polycrystalline samples of the alloy systems $Cd_xZn_yMn_zSe$ and $Cd_xHg_yMn_zTe$ were prepared from the elements by the standard melt and anneal technique. The components of one gram samples were sealed in small lengths of quartz tubing under vacuum. During all preparations, careful procedures were followed to ensure that the final alloy composition was in accordance with the initially measured quantity of elements.

It was found that if untreated quartz tubing were used, during the melting process, the material would react with quartz to such an extent that the tube would break upon cooling and all the sample would be lost. It was believed that this was due to the presence of manganese in the sample. In order to avoid this reaction the insides of quartz tubes were covered with a layer of carbon. This was done by inserting a piece of absorbent paper into the open end of tube, and then placing the absorbent paper in a beaker full of acetone for few minutes so that it soaked up some acetone. The other end of the quartz tube, which was sealed, was then heated in a flame. After this was done two or three times a layer of hot carbon began to collect at the hot end, and the process was continued until a good layer of carbon was deposited on the inner surface of the quartz tube. Carbonising the tube does not always prevent the sample reacting, as some times during melting layer of carbon will flake off. However the method was successful in the large majority of cases.

The samples were placed in a melting furnace at room temperature and heated to about 1200°C. This temperature was maintained for half an hour, during which time the tubes were shaken periodically in order to obtain a through mixing of the elements. Cooling to room temperature was carried out in approximately three to four hours, this rate of cooling being sufficiently slow to avoid breakage of the quartz tube upon solidification of the alloys. The samples were then placed in a furnace to anneal at a temperature of 800°C for two weeks.

After two weeks in the annealing furnace, the sample was taken out and in order to check whether equilibrium had been reached a Debye-Scherrer powder x-ray photograph was taken. Most of samples were found to be in good equilibrium condition except some with a higher concentration of manganese. These samples were resealed under vacuum and placed back in the annealing furnace for another two weeks.

2.2 X-ray Powder Diffraction Technique

Many materials particularly metals and alloys can be obtained only as a mass of randomly-oriented crystallites and consequently only the powder method can be applied to them. The interpretation of a powder pattern can be a simple or a difficult operation, depending upon the number and structural complexity of the phases composing the specimen. With the relatively simple structures involved in the present work, the unit cell dimension and lattice type of the cubic substance can be arrived at in a straight-forward manner from the diffraction pattern, and similar information can usually be deduced for tetragonal and hexagonal substances.

2.3 Method Used for X-ray Analysis

Debye-Scherrer x-ray powder photographs were obtained for each of the samples using Philips Debye-Scherrer 114.6 mm powder cameras and CuKα radiation.

Each specimen was ground into a smooth, fine powder and mounted in the camera by means of a spindle and thin glass fibre arrangement (shown in figure ?.1). The fibre was coated with powder using, as an adhesive, a grease known to give little absorption, care being taken to keep the fibre and powder in cylindrical form in order to minimize unsystematic absorption corrections. Kodak no-screen medical x-ray 35 mm film was used. The variation of exposure time depends upon the material and composition of the sample. In this case the exposure time required was from two to three hours. After the exposure, the film was developed for 5 minutes, fixed for 10 minutes and then washed for 30 minutes.

2.4 Measurements of X-ray Films

The position of the diffraction lines were measured using a travelling microscope and, after allowing for absorption effects, the Bragg angle of each line was calculated. The absorption effects mentioned above result from the specimen having finite width and high absorption so that diffraction is obtained from a limited region of sample. As seen from fig. (2.2), the effect of absorption will be greater in the center of the specimen compared to the edges, since the incident rays have travelled a greater distance within the sample. The resulting intensity distribution across the powder line is shown in fig. (2.2). For low Bragg angles this has the effect of doubling the

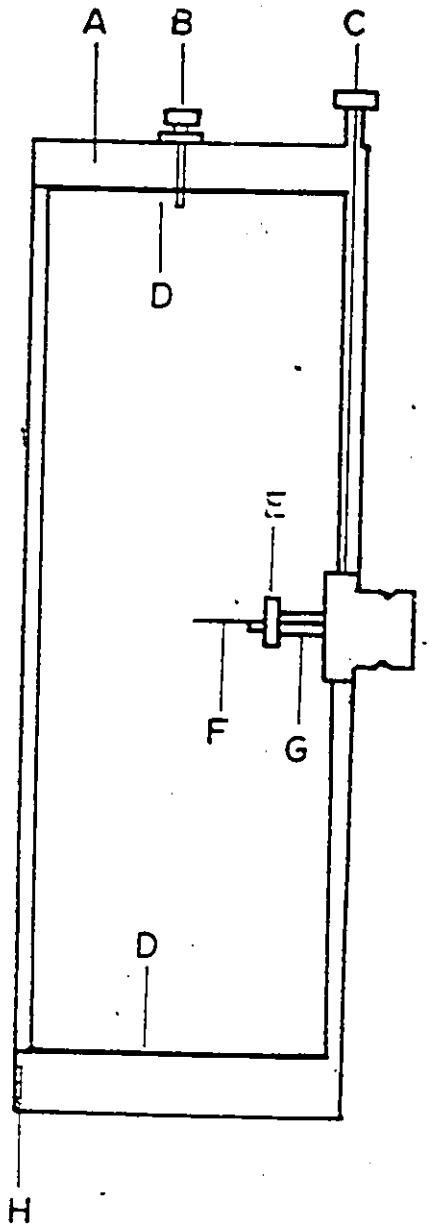

Figure 2.1 The powder camera and spindle-fibre arrangement used to take Debye-Scherrer x-ray photographs. The camera is shown in actual size with a radius of 114.6 mm. The part labelled A is the cylindrical camera body, B, are movable pins with a locking screw to hold the film in position, C, is a plugger to centre the specimen holder, E, in the x-ray beam. F is the fibre onto which the specimen is adhered, G, a drive spindle from a detachable motor, H a detachable lid, and D the film.

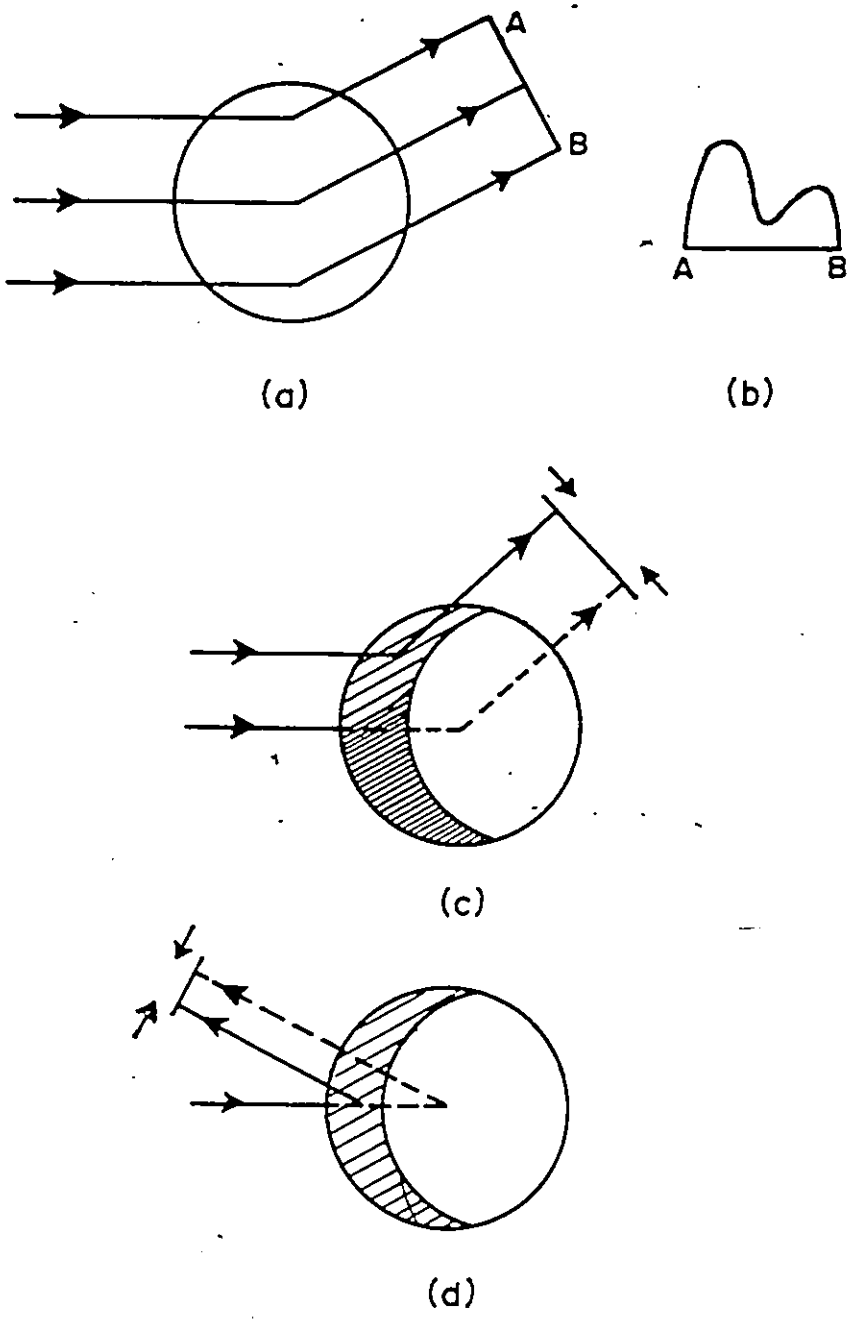

Figure 2.2 The effect of absorption in an x-ray specimen. An x-ray beam is diffracted as it passes through the specimen (a). The resulting intensity distribution is shown in (b). The diffraction line appears to be doubled. If absorption is high only part of the sample is irradiated. This region is shown by the shaded areas in (c) and (d). X-rays in the darkly shaded areas are absorbed within the sample after being diffracted. The effect of high absorption is to shift the diffraction line to a higher angle. The shift is greater for lower Bragg angles (c) and decreases as θ approaches 90° (d).

diffraction lines. In some cases, when absorption is high, only part of the specimen is irradiated as is shown in figure (2.2) where x-rays have penetrated throughout the shaded region only.

Two methods are used to correct the absorption effects, these being Nelson-Riley extrapolation [1] and the internal calibration technique. The Nelson-Riley technique is a method of linear extrapolation and was used mostly in the case of cubic structure to predict what value "a" (lattice parameter) would have at $\theta = 90^{o}$. Values of "a" were plotted against a function $f(\theta)$

$$f(\theta) = \frac{1}{2}\left\{\frac{\cos^2\theta}{\sin\theta} + \frac{\cos^2\theta}{\theta}\right\}$$

and the straight line intercept on the "a" axis, where $\theta = 90^{o}$, gives the value of the lattice parameter. A least squares fit is used to draw the best straight line through the experimental points which minimizes the effect of random errors.

The internal calibration [2] involves intimately mixing an internal standard of accurately known lattice parameter such as silicon with the sample being x-rayed and this was used, for samples with hexagonal structure. The powder of the specimen whose parameter is to be determined, is mixed with a small amount of silicon powder, and a pattern is obtained for the composite powder. The true angle θ for any diffraction line from the silicon can be calculated and then the difference between the observed and calculated values of $\sin^2\theta$ for silicon is calculated and plotted as a function of the observed values of $\sin^2\theta$. Thus a correction curve may be plotted showing the change in the Bragg angle θ, due to absorption, as a function of θ or more conveniently changes $\Delta\sin^2\theta$ in $\sin^2\theta$ as a function of $\sin^2\theta$. A typical correction curve is shown in figure (2.3). This is then used to

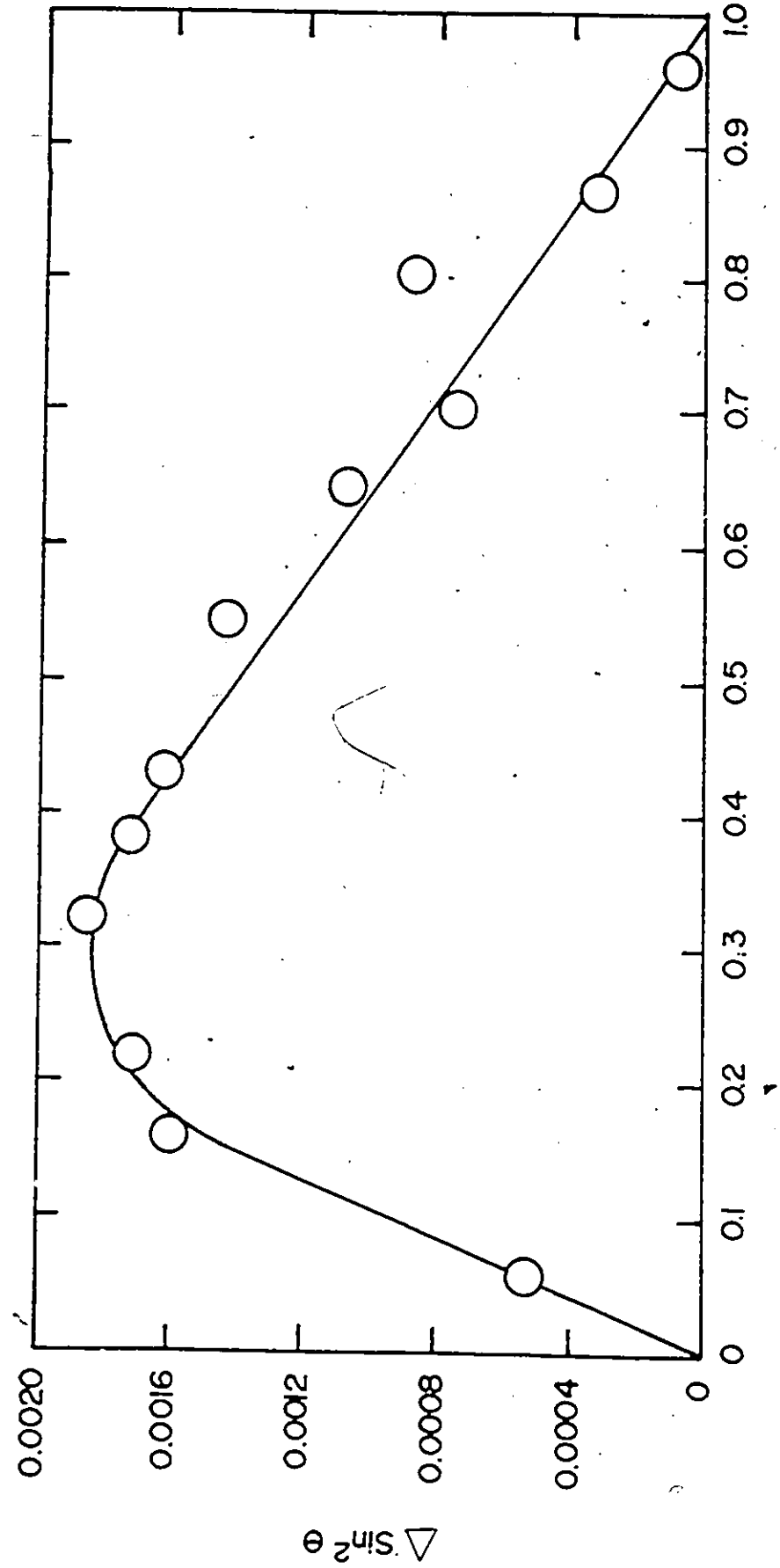

Figure 2.3 A typical silicon correction curve showing the change in $\sin^2\theta$, where θ is the Bragg angle, as a function of $\sin\theta$. The change in $\sin^2\theta$, ($\Delta\sin^2\theta$), results from absorption of x-rays in the specimen.

correct all lines for unknown sample. Knowing the true values of $\sin^2\theta$, one can apply the least squares method to the equation

$$Q = \frac{\sin^2\theta}{\lambda^2/4} = 4/3\ \frac{h^2 + hk + k^2}{a^2} + \frac{\ell^2}{c^2}$$

and values of a and c can be obtained.

2.5 Result and Analysis

In figure (2.4) the range of sample composition which was studied is shown. The compositions were chosen so that the variation of properties along lines of constant z and along lines of constant x:y ratio could be studied. Two single phase regions representing different solid state structures were observed in the ternary phase diagram. The dotted line in fig. (2.5) represents the boundary between the two regions. Samples whose compositions lie in the upper region of the triangle, i.e. the P region, consist of two phases, wurtzite and the sodium chloride structure of MnSe. Region Q has wurtzite single phase structure, and in the region R single phase of zinc blende structure was observed.

The x-ray pictures of some of the two phase samples were analyzed, but only to determine the limits of the single phase fields.

The variation in lattice parameter with composition for various fields is shown in Figs. 2.6 - 2.9. Fig. 2.6 shows the variation in the hexagonal phase of a (lattice parameter) versus z at constant f, where f (= y/(x+y)), is the zinc fraction of non-magnetic cations, while figure 2.7 show the variation of a (lattice parameter) versus f at constant z. Similarly in fig. 2.8 and 2.9 the variation of c (lattice parameter) versus z at constant f and variation of c versus f at constant z are shown.

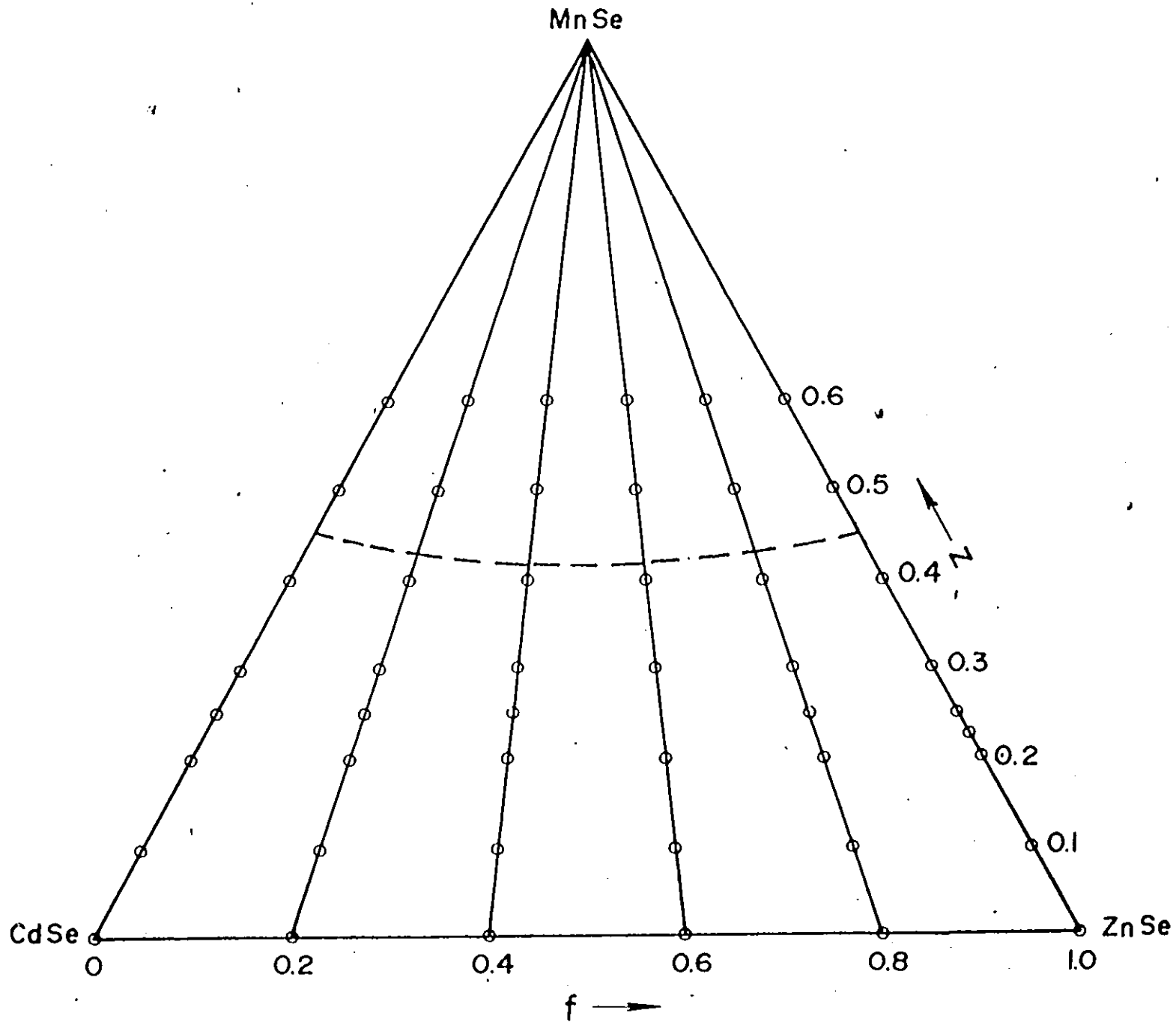

Figure 2.4 Samples studied by powder x-ray photographs. The curved line at the top of the diagram represents the limits of solid solution.

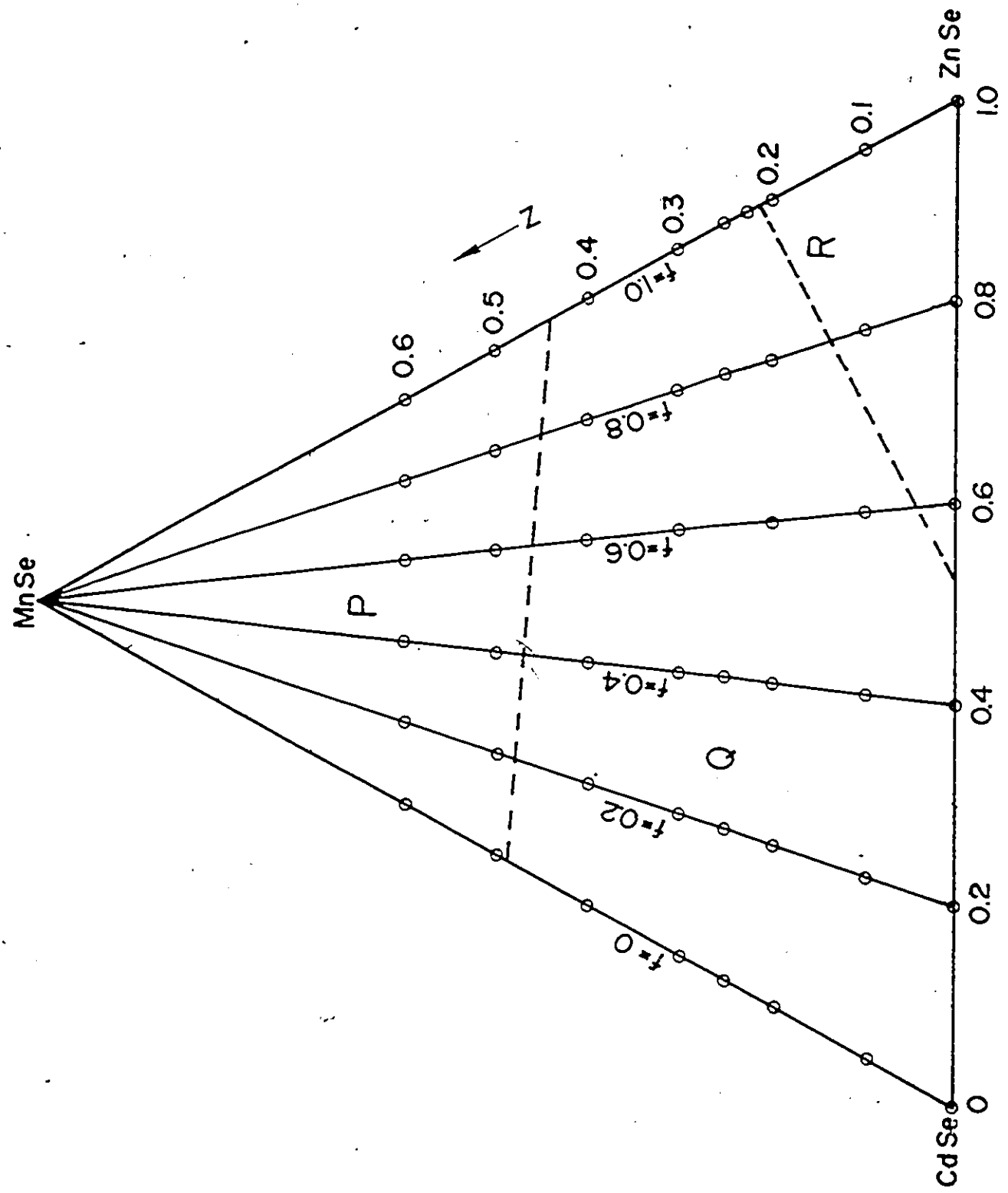

Figure 2.5 Diagram showing the limits of single phase regions in the $Cd_xZn_yMn_zSe$ alloys system.

These result can be used to determine the different phase boundaries since for any single-phase field, the lattice parameter always varies in smooth and continuous way with composition. In a two-phase region "tie lines" exist, along which the relative amounts of the two phases change but their compositions and hence lattice parameter remain constant. However, the compositions of the two phases and consequently their lattice parameters will vary along any line which is not a "tie line".

As a result of these rules in most cases, a break in curve of a (lattice value) against the relevant composition parameter gives a good indication of a field boundary. The lattice parameter usually changes at a different rate in the two-phase region than in the single phase region, which causes a break in the parameter-composition curve. Each break in each lattice parameter curve would then allow us to determine one point on the corresponding phase boundary on the isothermal section. Let us consider fig. 2.6. In this figure, the lattice parameter a shows a linear variation with f in the single-phase region as shown by the solid lines. The irregular behaviour of lattice parameters a starts at about z = 0.48 on f = 0 line at this point. The lattice parameter value a instead of following the dashed line shown in figure (2.6) deviates thus indicating the presence of a two phase region beyond z = 0.48. Similar results are observed for other lines in figure 2.6. Also as seen in figure 2.7, in which the variation of lattice parameter a versus f at constant z is shown, all the lines vary smoothly except at low value of z. In this latter case we have a zinc blende structure at higher value of y being compared with the hexagonal structure at low y values. However if we plot cation-cation spacing,

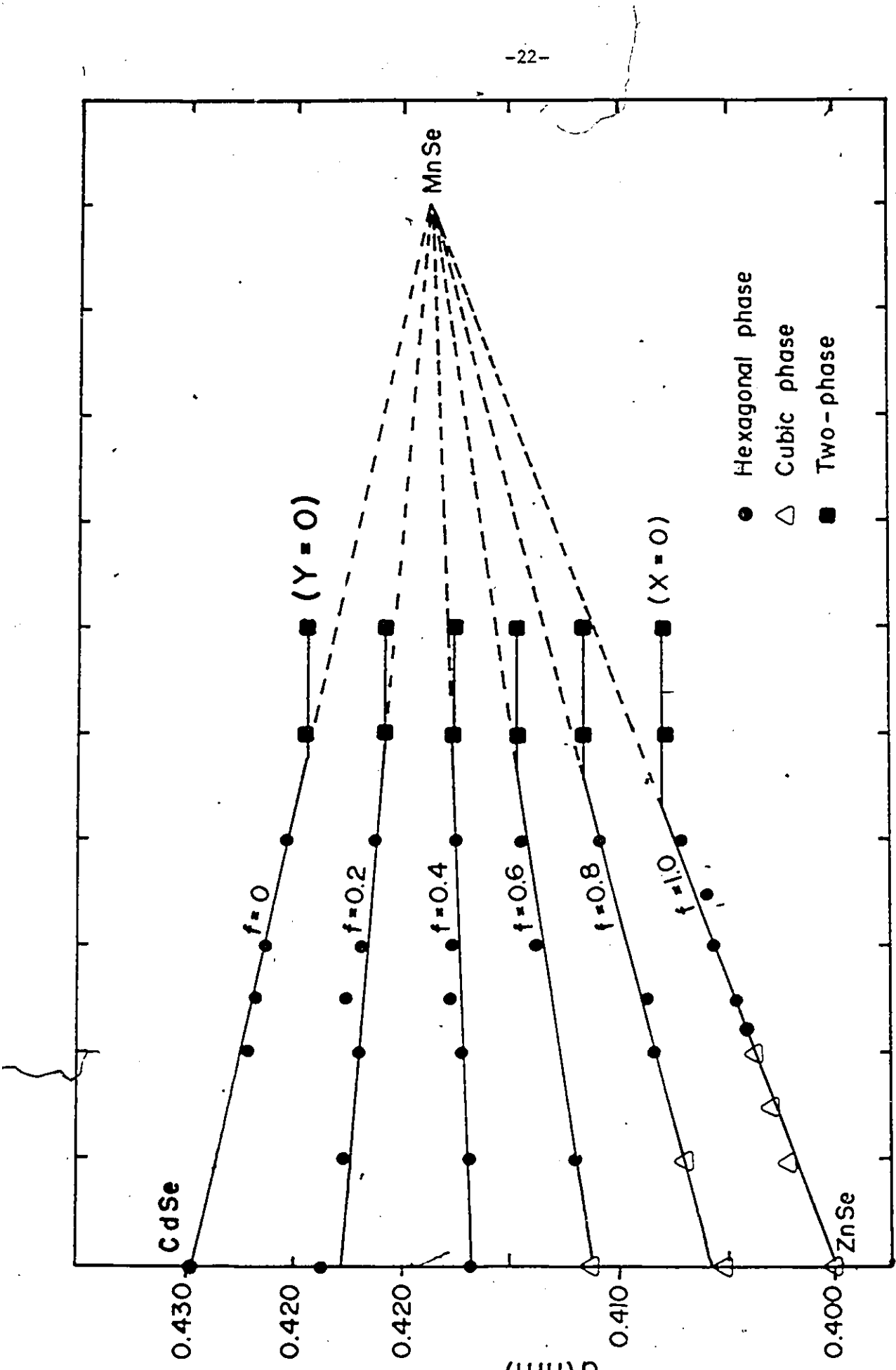

Figure 2.6 Variation of the lattice parameter a with Mn concentration z for lines of constant f(where f = y/x+y)
Hexagonal Phase Δ Cubic Phase Two-Phase

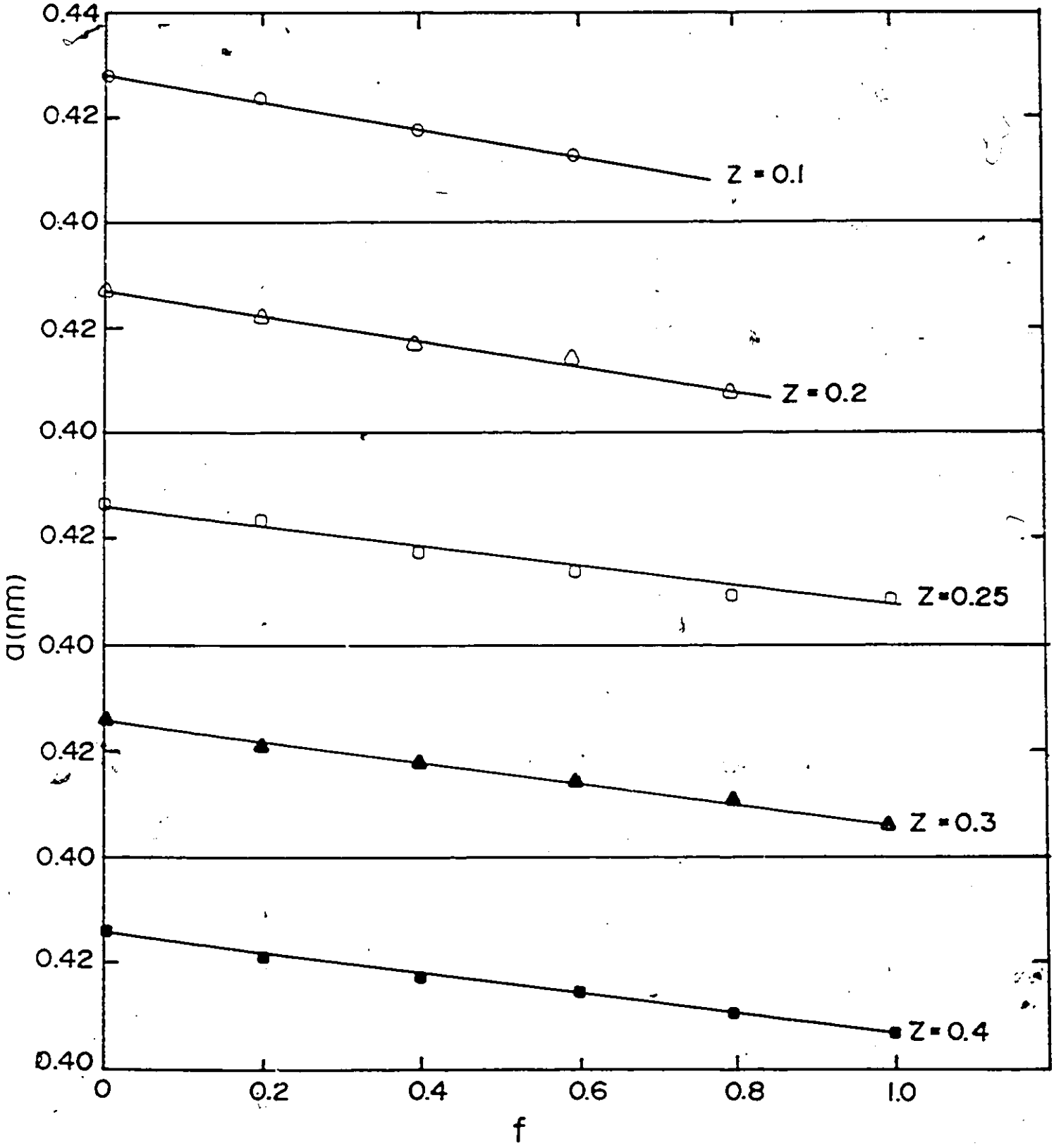

FIGURE 2.7 Variation of the lattice parameter a versus f at constant z. (where f = y/x+y).

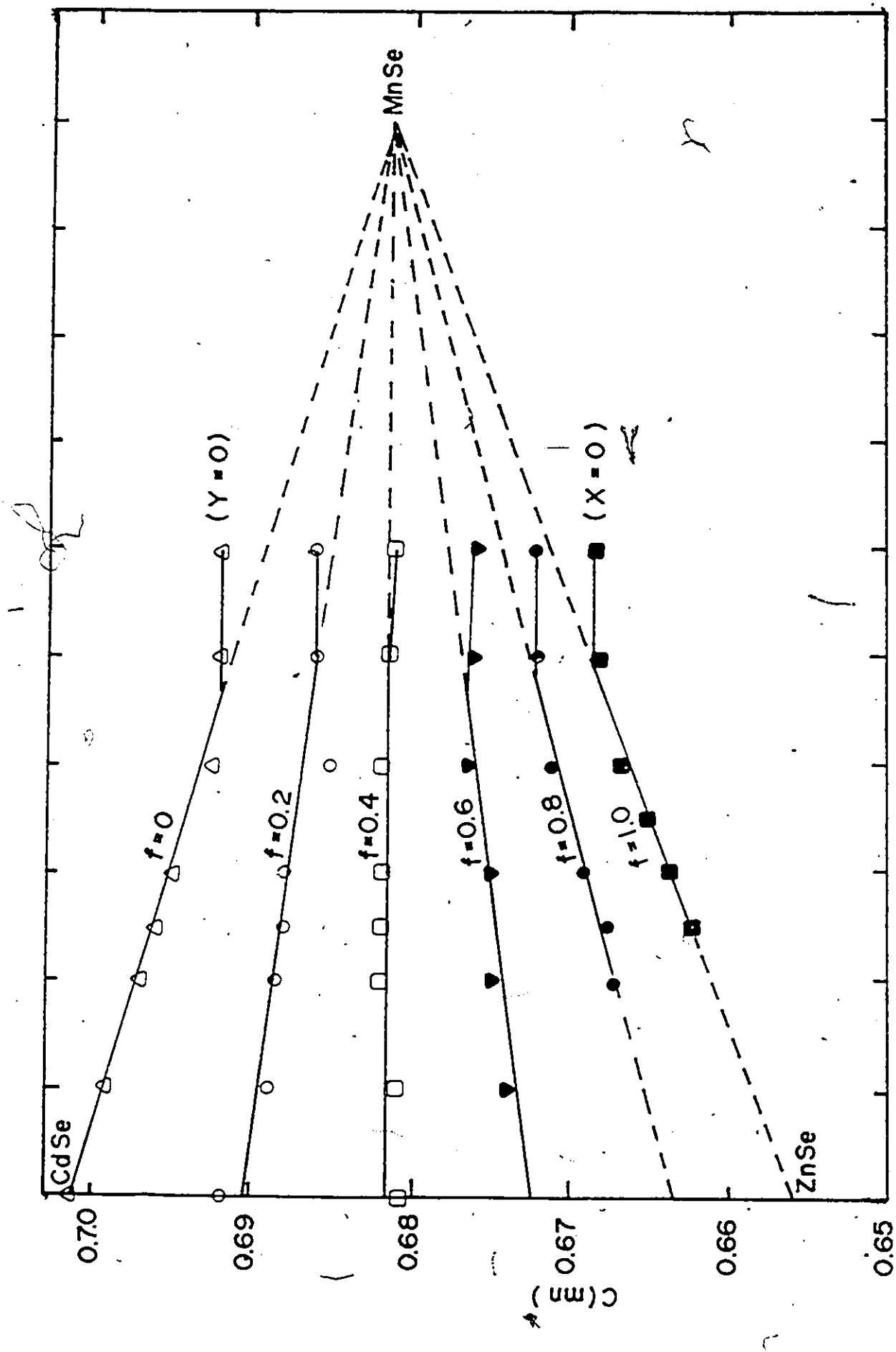

Figure 2.8 Variation of the lattice parameter c with Mn concentration z for lines of constant f(where f = y/x+y)

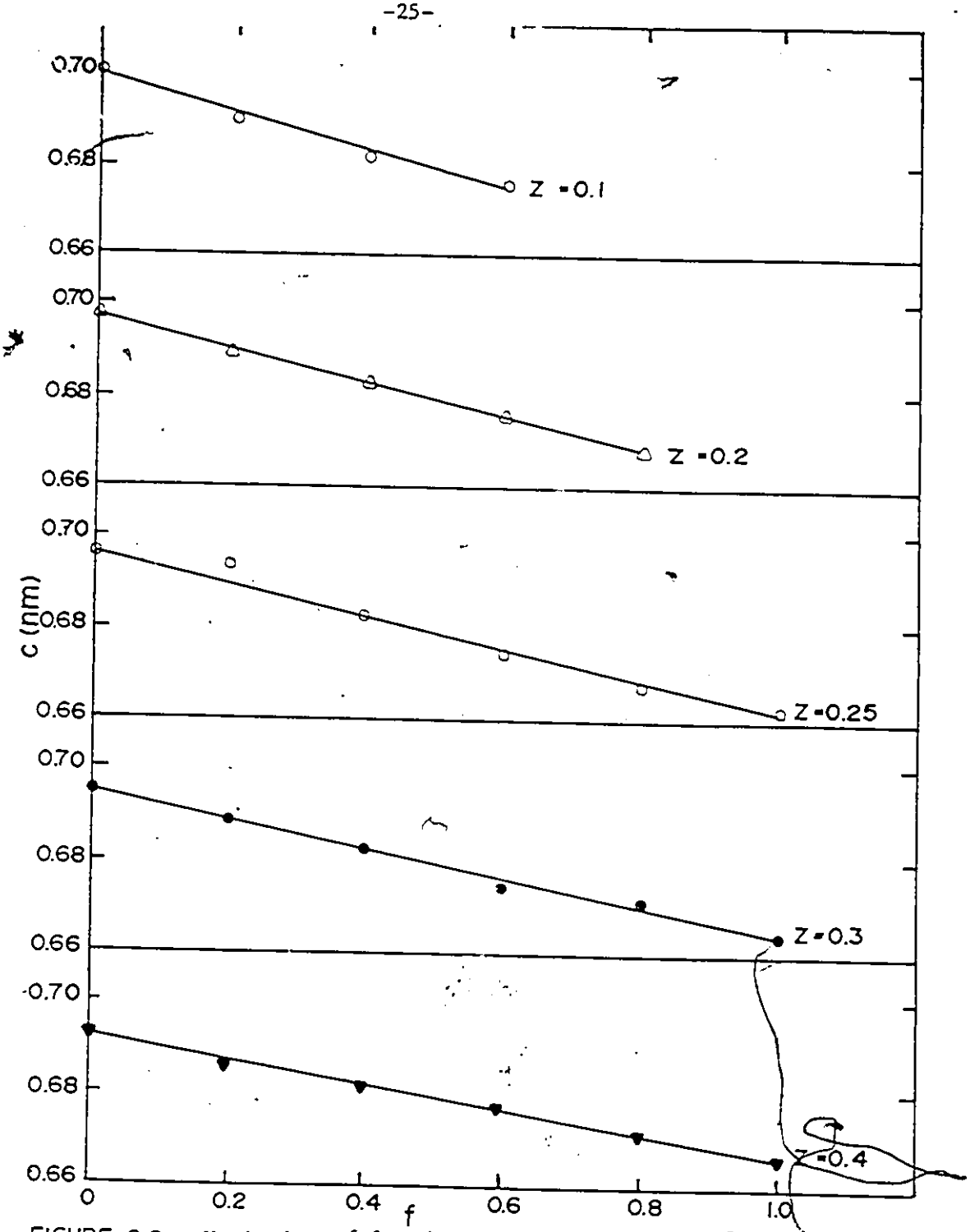

FIGURE 2.9 Variation of lattice parameter c versus f at constant z. (where f = y/x+y).

which in case of wurtzite structure is a (lattice parameter) and for cubic structure is $a/\sqrt{2}$, against f, a smooth variation is obtained.

Turning to the values of lattice parameter, it is usual in cases of this type to look for a convenient mathematical expression to represent the parameter as a function of composition variables. This is convenient for purposes of interpolation etc. It was found that for each single-phase field the dependence of the lattice parameter on f and z could be expressed by a simple mathematical equation of the form $a = mz + k$ where m and k are slope and intercept respectively, which were f-dependent in the case of constant f. The values of m and k obtained for all the lines of constant f were then plotted as a function of f, these plots showed a linear dependence of m and k on f. Similar kinds of results were obtained when the analysis was applied to other cases such as a plot of lattice parameter a against z. Thus the required mathematical equation would have the form,

$$a = A + Bz + Cf + Dfz$$

where A, B, C and D are constants. These constants were obtained from a least square fit calculation which was carried out using an Apple II Computer Programme (see Ref. 2). In the zinc blende region we have

$$a(nm) = 0.6483 - 0.0145z - 0.0437f + 0.0141zf$$

with a standard deviation σ of 0.0003(nm). In the wurtzite region we have

$$a(nm) = 0.4595 - 0.0294z - 0.0297f + 0.0177zf$$

$$c(nm) = 0.7615 - 0.0867z - 0.0601f + 0.0639zf$$

with a standard deviation σ for a 0.0002(nm) and for c of 0.0003 nm.

Discussion and conclusion: An isothermal section of the phase diagram of the semi-magnetic semi-conductor alloy system $Cd_x Zn_y Mn_z Se$ was obtained. In the alloy system under investigation one and two phase behaviour was observed. However, in the investigation of the properties of semi-magnetic semi-conductor only the single phase fields are of interest, and the wider the range of single solution the better it is for the comparison of magnetic and other properties.

REFERENCES

1. J.B. Nelson and D.P. Riley, Proc. Phys. Soc. 57, 160 (1945).

2. Science and Engineering Programm Apple II, edited by John Heiborn, Published by Osborne/McGraw-Hill.

3. B.D. Cullity, Elements of X-ray Diffraction, Addison Wesley Publishing Company (1956) Chap. 11, 12.

Chapter III

MAGNETIC SUSCEPTIBILITY MEASUREMENTS

3.1 Introduction

The magnetic moment of a free atom has three principal sources: (1) The spin with which electrons are endowed (2) their orbital angular momentum about the nucleus and (3) the change in the orbital moment induced by an applied magnetic field. The first two effect give paramagnetic contributions to the magnetization, and the third gives diamagnetic contribution. Atoms with filled electron shells have zero spin and zero orbital moment; these moments are associated with unfilled shells [1].

The magnetization M is defined as the magnetic moment per unit volume. The magnetic susceptibility per unit volume is defined as [2]

$$\chi = \frac{M}{B} \text{ (C.G.S)} \qquad 3.0\ a$$

$$\chi = \frac{\mu_o M}{B} \text{ (SI)} \qquad 3.0\ b$$

where B is the macroscopic magnetic field intensity, χ is dimensionless in both systems. Substance with a negative magnetic susceptibility are called diamagnetic. Substance with a positive susceptibility are called paramagnetic.

The magnetic moment of an atom in free space is given by

$$\mu_J = \gamma\hbar J = -g\mu_B J \qquad 3.1$$

the constant γ is the ratio of the magnetic moment to the angular momentum; γ is called gyromagnetic ratio or magnetic ratio. For electronic systems a quantity g, called the g factor or the spectroscopic splitting factors, is defined by

$$g\mu_B = -\gamma\hbar \qquad 3.2$$

For an electron spin g = 2.0023, usually taken as 2.00. For a free atom the g factor is given by the Landé equation

$$g = 1 + \frac{J(J+1) + S(S+1) - L(L+1)}{2J(J+1)} \qquad 3.4$$

The vector addition of the quantum numbers results in only partially filled electronic level possessing a non-zero resultant momentum. Therefore only atoms such as Mn can have a net magnetic moment. The five unpaired 3d electrons of Mn result in a value of spin momentum S equal to 5/2, as given by ground state configuration of Mn^{2+} which is $3d^5$ by applying Hund's rules.

M_S / M_L	1/2	-1/2
2	↑	
1	↑	
0	↑	
-1	↑	
-2	↑	

$M_S = 1/2 + 1/2 + 1/2 + 1/2 + 1/2 = 5/2$

$\therefore S = 5/2$

$M_L = 2 + 1 + 0 - 1 - 2 = 0$

$J = L + S = 5/2$

In a solid the angular momentum L may be quenched by the crystal field [2,3]. Therefore it may not contribute to the total magnetic moment. Now in the case of Mn by substituting S = 5/2, L = 0 and J = 5/2 in equation 3.4 we get the value of g = 2 for Mn.

Materials may be classified according to their magnetic properties into three general categories; diamagnetic, paramagnetic and exchange coupled magnetic systems. In an applied magnetic field the three general categories distinguish themselves especially as a function of temperature. For diamagnetic materials, the magnetic

susceptibility, which is defined as $\chi = M/H$, turns out to be negative and independent of temperature. Paramagnetic systems have a positive susceptibility and at high temperature follows the Curie Law given by

$$\chi = \frac{NJ(J+1)g^2\mu_B^2}{3k_BT} = \frac{Np^2\mu_B^2}{3k_BT} = \frac{C}{T} \qquad 3.5$$

Here p is the effective number of Bohr magnetons, defined as

$$p \equiv g[J(J+1)]^{\frac{1}{2}}$$

the constant C is known as Curie constant, N is the number of magnetic atoms, k_B is the Boltzman constant and T is temperature in Kelvin, g the spectroscopic splitting factor is given by equation (3.4).

Substances that obey Curie's Law at least up to a first approximation are called normal paramagnetic materials, the interaction between the magnetic dipoles is negligible and consequently is always overcome by the disordering effect of the temperature which tends to randomnize the magnetic dipoles orientations, so that the net magnetization vanishes as soon as the applied magnetic field is switched off. However in other paramagnetic materials, the magnetic dipole-dipole interaction is not small and as a result these materials obey the Curie-Weiss law

$$\chi = \frac{C}{T-\theta} \qquad 3.6$$

where θ is a constant which takes into account the effect of the inter-dipole interaction. If this is positive the internal interaction tends to line up the spins parallel to each other, resulting in ferro-magnetic behaviour.

An antiferromagnet interaction, on the other hand, aligns neighbouring spins in antiparallel orientation and θ is negative in this case. When the temperature is decreased in an antiferromagnet substance, the magnetic susceptibility increases and shows a

singularity in its curve at a critical temperature T_N, known as the Neel temperature below which the spin system is an ordered state of antiparallel alignment. Above the Neel temperature the alignment is lost and the material assumes a paramagnetic-like state.

Zero value of θ means the material is paramagnetic and the equation 3.6 reduces to equation 3.5.

In the class of magnetic material known as spin glass, the magnetic spins interact with each other in such a way that at low temperature spins end up being frozen in random directions [4-7]. This is due to "frustration" of the spin system, a term introduced by Toulouse [8,9] to indicate that not all the interactions can be satisfied simultaneously. Frustration occurs when there is a competition in the interactions between the spins. The frustration can occur in one of two ways. Firstly if both positive and negative exchanges are present in the lattice then any given ion can experience both positive and negative interactions from different neighbours and so frustration will occur. This is illustrated by the normal behaviour in metallic spin glasses. For metallic spin-glass systems such as CuMn, AgMn etc. the exchange interaction is an indirect one through the conduction electrons. The process is known as RKKY (Ruderman-Kettel-Kasuya- Yosida) [4] interaction. The exchange integral J_e oscillates between positive and negative values as it decays with distance (Fig. 3.1) [4]. This interaction results in a competition between ferromagnetic and antiferromagnetic interactions, between the randomly distributed spins, which becomes "frustrated" and freeze in a disordered fashion.

The RKKY interaction is important with the large charge carrier concentration [2,10] in metals semi-conductors with large

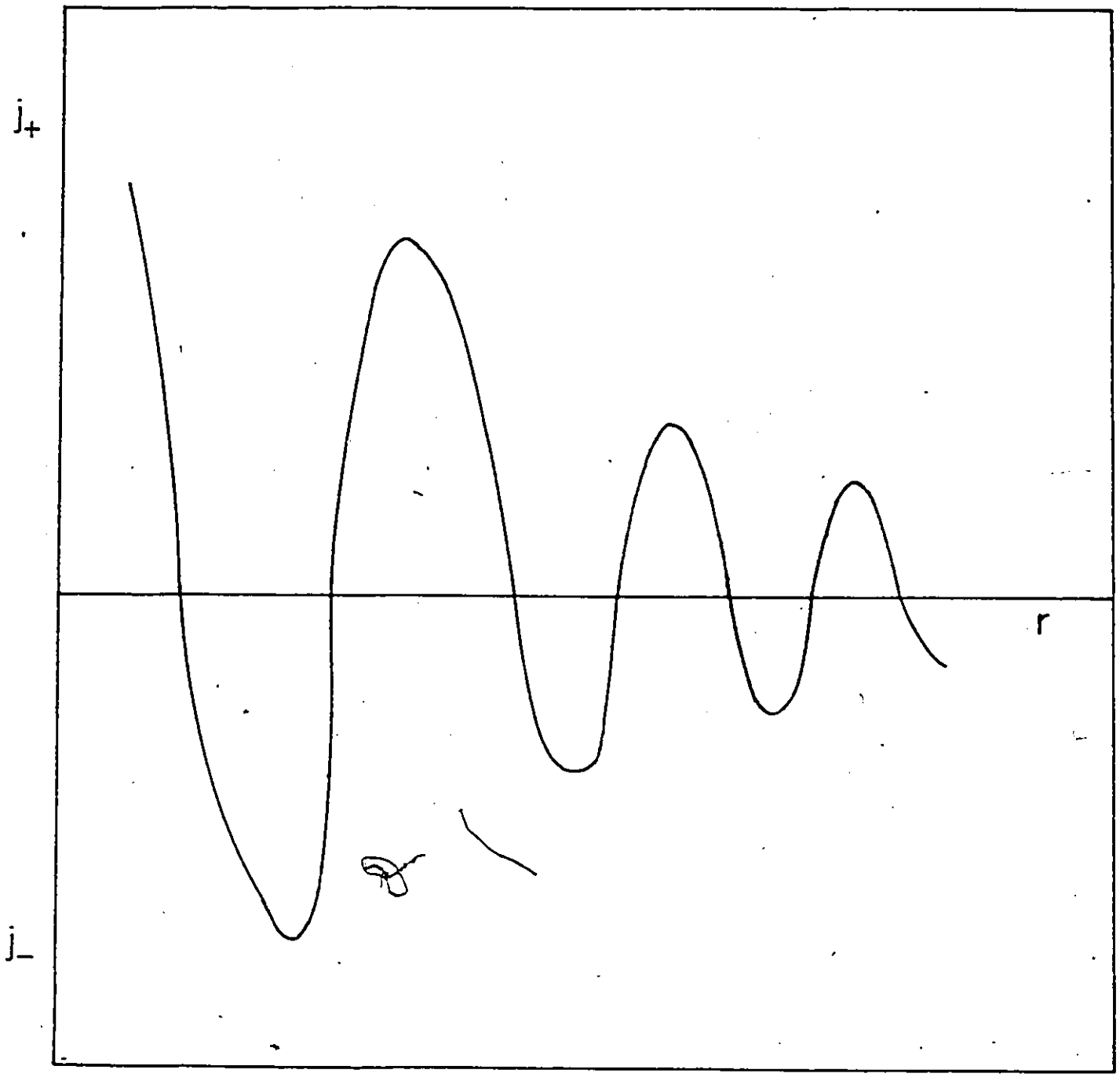

FIGURE 3.1 R.K.K.Y. Interaction

energy gaps (such as $Cd_{1-z}Mn_zTe$, $Zn_{1-z}Mn_zTe$, etc.) and the system under investigation $Cd_xZn_yMn_zSe$ have low charge carrier concentration and hence the effect of RKKY exchange interaction is negligible. In addition to this, the exchange coupling is believed to be solely antiferromagnetic, so there is no competing ferromagnetism to cause frustration.

However even when all exchanges have negative sign frustration can still occur from geometric consideration which is second source of frustration as shown by Deseze [11] and discussed by Villain [12]. In a face centered cubic lattice, consider three neighbouring face centers BCD to a given ion A, forming a tetrahedron as shown in the figure (3.2). All of these are nearest neighbours and so with antiferromagnetic exchange, should be anti-parallel. If A is ↑ then B will be ↓ now C is frustrated since interaction with A requires downward (↓) direction while interaction with B requires upward (↑) direction, similarly with D. In an antiferromagnetic case, where all sites A,B,C, and D are occupied by magnetic ions, the problem is solved by a system of regular sublattices giving type 1, type 2 etc. [1] ordering of antiferromagnet. However for the spin glass case, the occupation of the sites is not complete and the magnetic ions are arranged at random. As a result, when concentration is < 0.6, the equilibrium conditions corresponds to random arrangement of spin vectors on the various sites. This effect was predicted for the $Cd_xZn_yMn_zSe$ alloys by Kremer and Furdyna [13].

The magnetic susceptibility of a spin-glass shows, to some extent, similar behaviour to that of an antiferromagnet with a singularity occurring at the freezing temperature T_g [14-19].

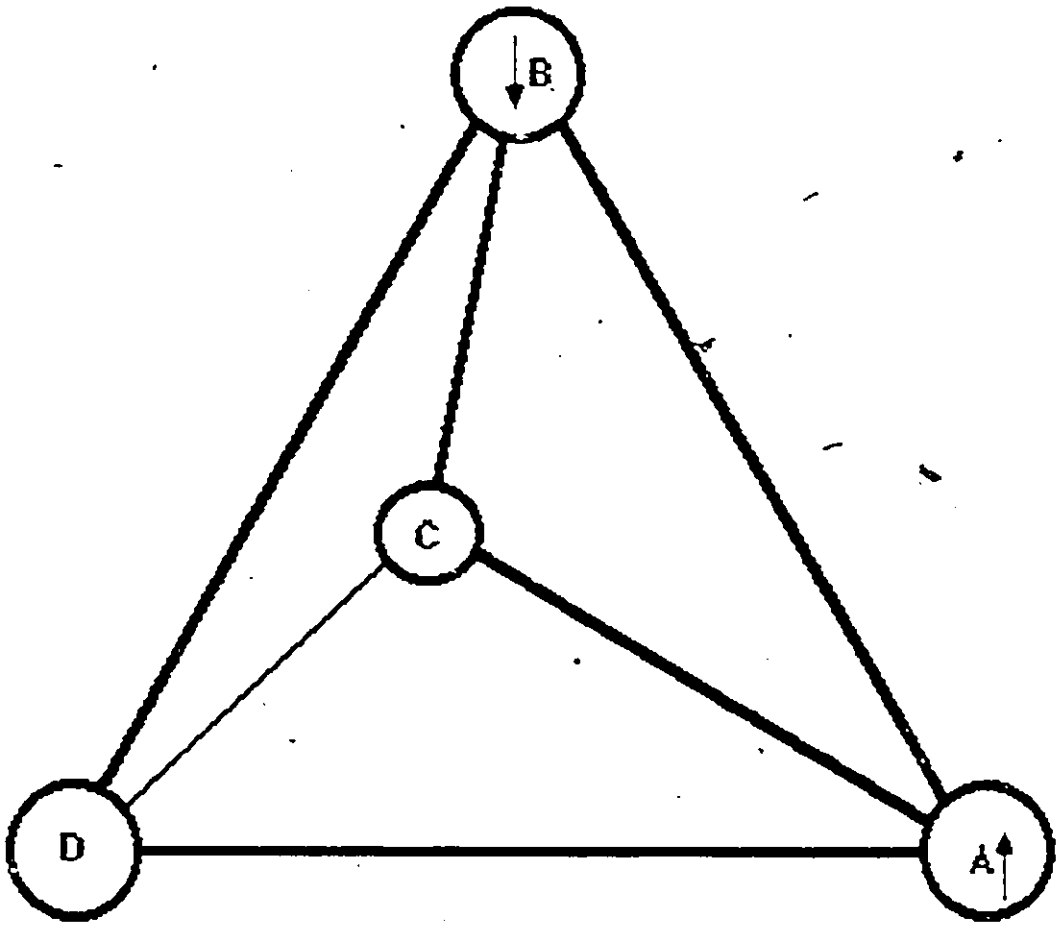

FIGURE 3.2 Tetrahedral bond arrangement

Experiments such as neutron diffraction [20-22] and Mössbauer effect [23-25] have shown the random freezing of spins. These results show that a magnetic phase transition occurs at this freezing temperature T_g, but no discontinuity at T_g has been observed in the specific heat behaviour [28,29]. In order to have a phase transition, a discontinuity must be seen in specific heat measurements over a narrow range of temperature rather than a unique temperatures [4,5,26,27]. This leaves some doubts about the type of transition which occurs in a spin-glass. This question is still not resolved although it is clear the transition is not a simple type. With regard to the question about the nature of the antiferromagnetic coupling between a pair of Mn ions, various suggestions have been put forward. The indirect exchange interaction between two localize moments, arising from the virtual transition between the filled valence band and the empty conduction band (Bloembergen-Rowland) [30] is relatively unimportant in these wide-gap materials, but becomes more important as E_g becomes small. Another mechanism, proposed by Geertsma et al [31], gives long range exchange interaction through virtual transitions between the valence band and a delocalized band of $3d^5$ states. We will discuss this in detail later in this chapter. The object of the present investigation of magnetic susceptibility is to try to determine which exchange mechanism is dominant in these alloys.

3.2 Measurement of susceptibility

The magnetic susceptibility of a magnetic material may be found by measuring the magnetization under the influence of an applied field. This was done by using a SQUID magnetometer. The word SQUID is an acronym for superconducting quantum interference device. This

instrument can be used to measure very small magnetic fields with an extremely high degree of accuracy. Due to the high sensitivity of the SQUID, a small amount of sample could be used for the measurements. Magnetization of samples as small as 20 mg were measured with the SQUID. Another advantage that SQUID magnetometer has over other types of magnetometer such as mutual inductance, torsion balance is that only a small applied magnetic field is needed to give sufficient magnetization of the sample to be detected. The superconducting ring-resonant circuit arrangement is called an rf-SQUID. When the sample is inserted into one of the pick up coils, the change in magnetic flux is transmitted to the SQUID producing a change in the magnetometer output proportional to the sample magnetization.

Figure (3.3) shows the experimental set up used to measure the susceptibility. This system was designed and developed by Dr. Gilles Lamarche, Physics Department, University of Ottawa. The cryostat is a typical double dewar system with liquid helium in the inner dewar and liquid nitrogen in the outer. A lead shield inside the helium bath surrounded the inner part of the system and so reduced any penetration from external stray fields. A solenoid and niobium cylinder were placed inside this shield in the helium bath. The solenoid provided a magnetic field which was trapped by the superconducting niobium when liquid helium was transferred into a dewar A field ranging between 25 to 30 gauss was applied through the solenoid. The niobium cylinder also provided additional magnetic shielding.

A S.H.E. Model 330 SQUID was used. The pair of oppositely wound superconducting pick-up coils were used to detect the

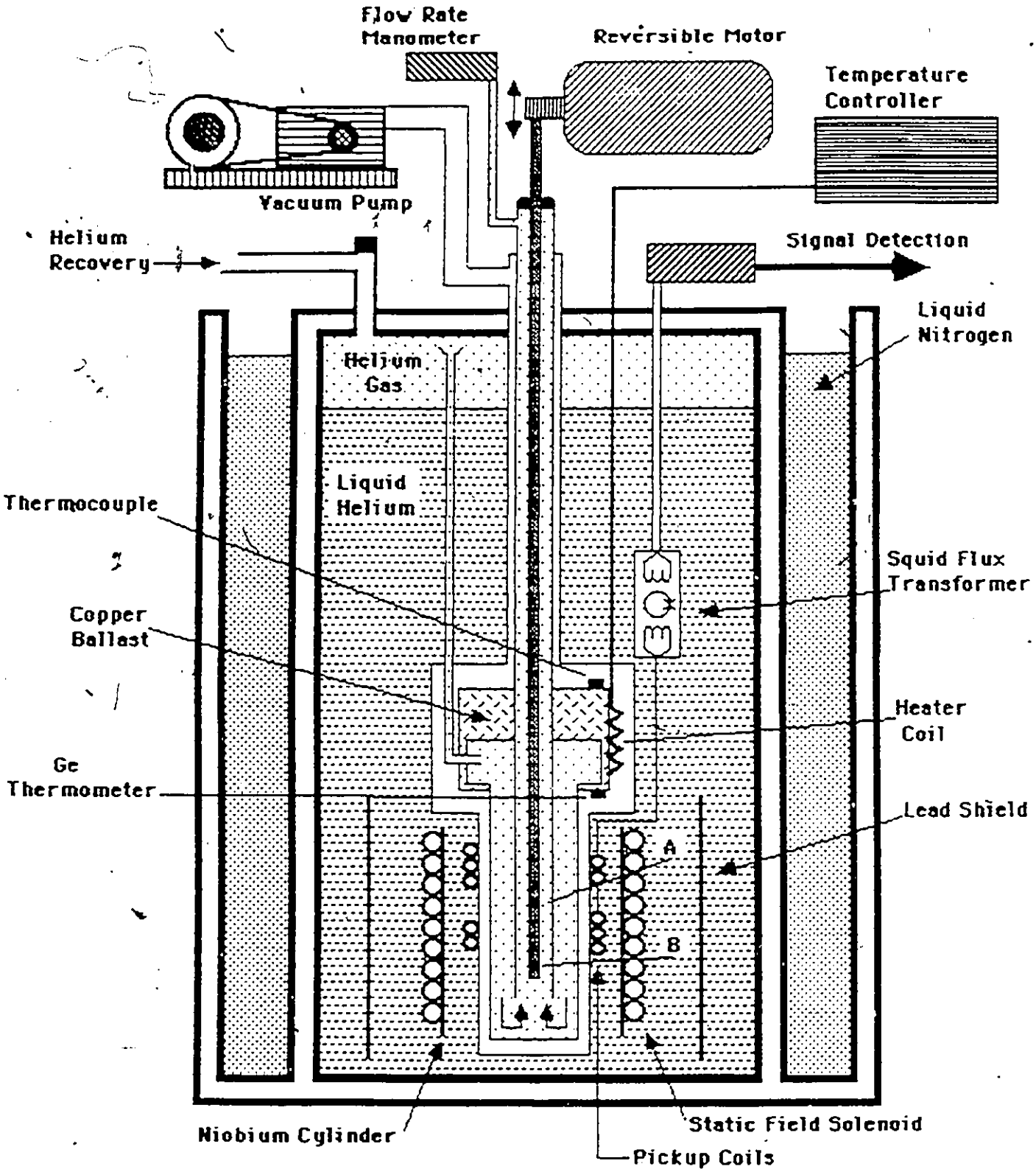

FIGURE 3.3 Magnetic susceptibility apparatus. A sample is placed in position B. A second sample or a paramagnetic salt is placed in position A.

magnetization. The superconductiong pick-up coils are located inside the niobium cylinder and are tightly bound to the outside wall of a vacuum can inside which an exchange helium gas is placed. The change in flux of these coils was measured by the SQUID in a flux transformer. The pick-up coils gave two measurements of magnetization of opposite polarity because the coils are oppositely wound. This gas chamber contains the sample holder which consists of a very pure copper container attached to a long plastic rod which extends outside the cryostat and is attached to a reversible motor. This enabled different samples to be inserted and extracted without opening the whole system as well as provided a means for driving the sample through the pick-up coils by a reversible motor.

The temperature of the system was controlled by circulating the gas around the sample. The gas from over the helium bath was allowed to enter the gas chamber through a tube which was wrapped several times around a copper ballast. A heating coil was also attached to a copper block. The copper ballast was heated so in turn it heated up the He gas as the latter was going around. With this set-up, we obtained temperatures in the range 4.2 K and 270 K. Three different thermometers placed at different locations were used to monitor the temperature. A chromel-gold 0.07% iron thermocouple was placed at the top of the copper block. A calibrated Ge resistance thermometer was placed near the bottom of the block. Finally a magnetic thermometer (a paramagnetic salt) was placed on the sample holder about 10 cm above the sample. After numerous measurements using three thermometers and after comparing the data only less than a degree difference was measured between the three thermometers. So

measurements were made without the magnetic thermometer and in its place another sample was used.

With this system we could measure the SQUID voltage from which the absolute magnetic susceptibility could be determined through the use of calibration relation which was determined by Dr. Gilles Lamarche as

$$\chi = \frac{(1.25\times10^{-5})V}{(i/2+0.23)M} \text{ emu/gm} \qquad 3.7$$

where V is the SQUID voltage, M is the mass of sample in grams and i the current through the solenoid in mA. The units of this equation (3.7) are electromagnetic units per gram of sample. By using these units for susceptibility, equation (3.5) becomes

$$\chi = \frac{ZN_A g^2 \mu_B^2 J(J+1)}{3k_B W(T+\theta)} \text{ emu/gm} \qquad 3.8$$

where N_A is Avogadro's number and z is the Mn concentration, W is the molecular mass of each sample.

3.3 Results

The magnetic susceptibility measurements were carried out for all the single-phase samples in the range of 4.2 K to 270 K. These measurements were made as a function of temperature to determine the values for spin-glass transition temperature T_g, the Curie-Weiss paramagnetic temperature θ, and the Curie constant C for the alloys. Fig. (3.4,3.5,3.6) shows the low temperature susceptibility measurement for different constant values of f where f = y/x+y. The results shown in Fig. (3.4,3.5,3.6) were obtained for zero-field cooled samples i.e. the samples were cooled before the magnetic field was applied. The results showed a sharp cusp in the values of susceptibility for zero

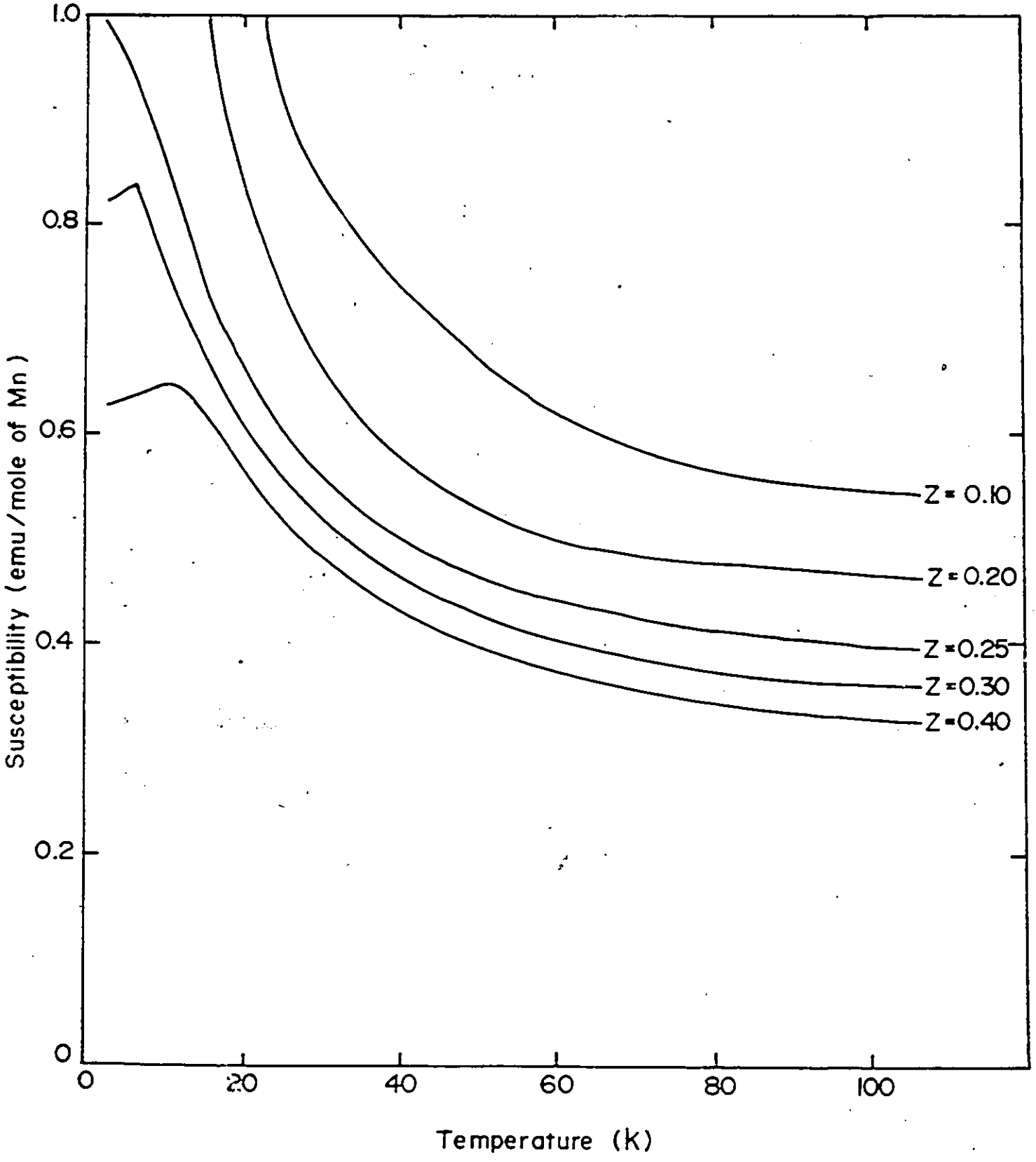

FIGURE 3.4 Results of measurements of magnetic susceptibility for some samples with f = 0 where f = y/x+y.

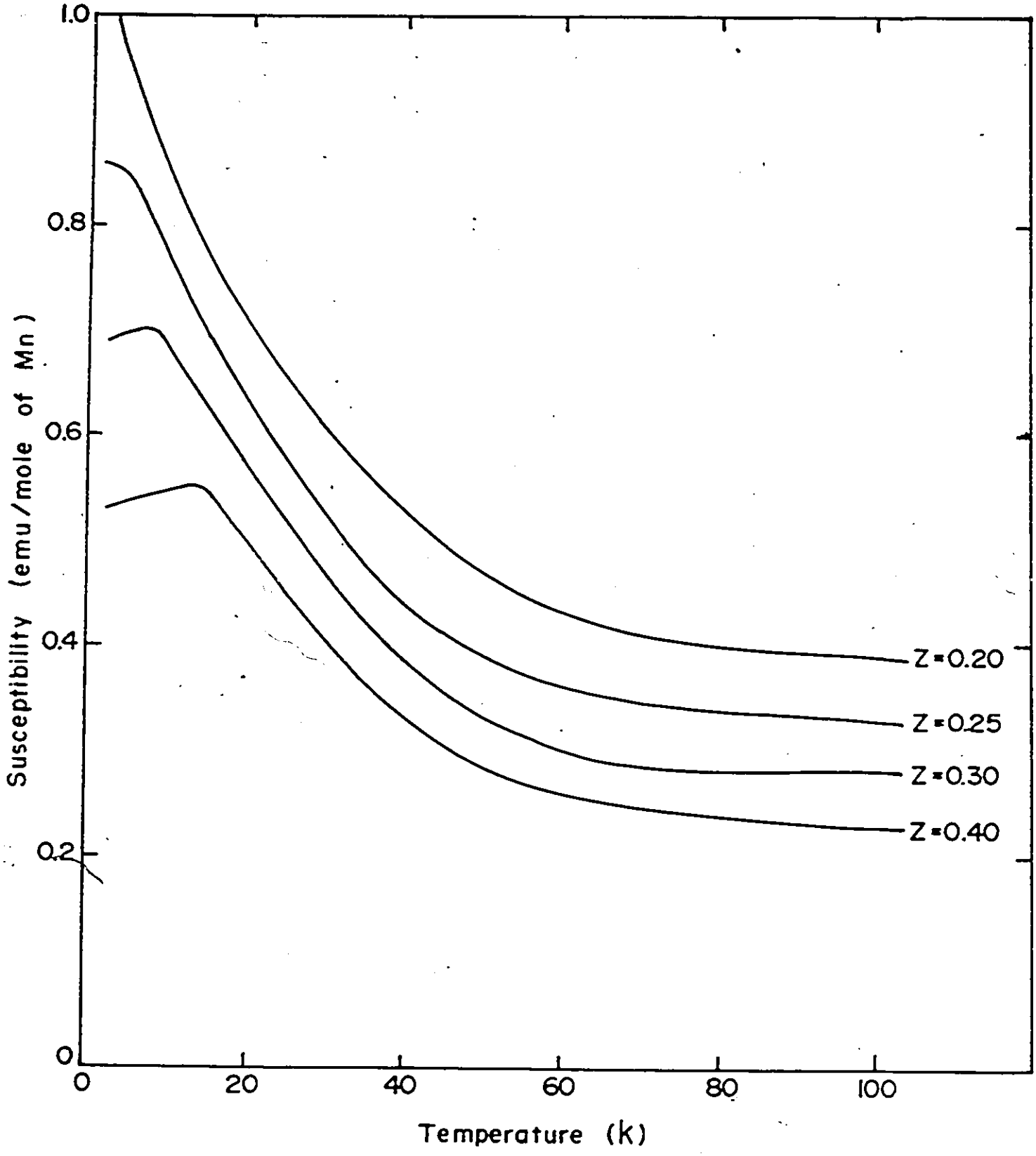

FIGURE 3.5 Results of measurements of magnetic susceptibility for some samples with f = 0.4 where f = y/x+y.

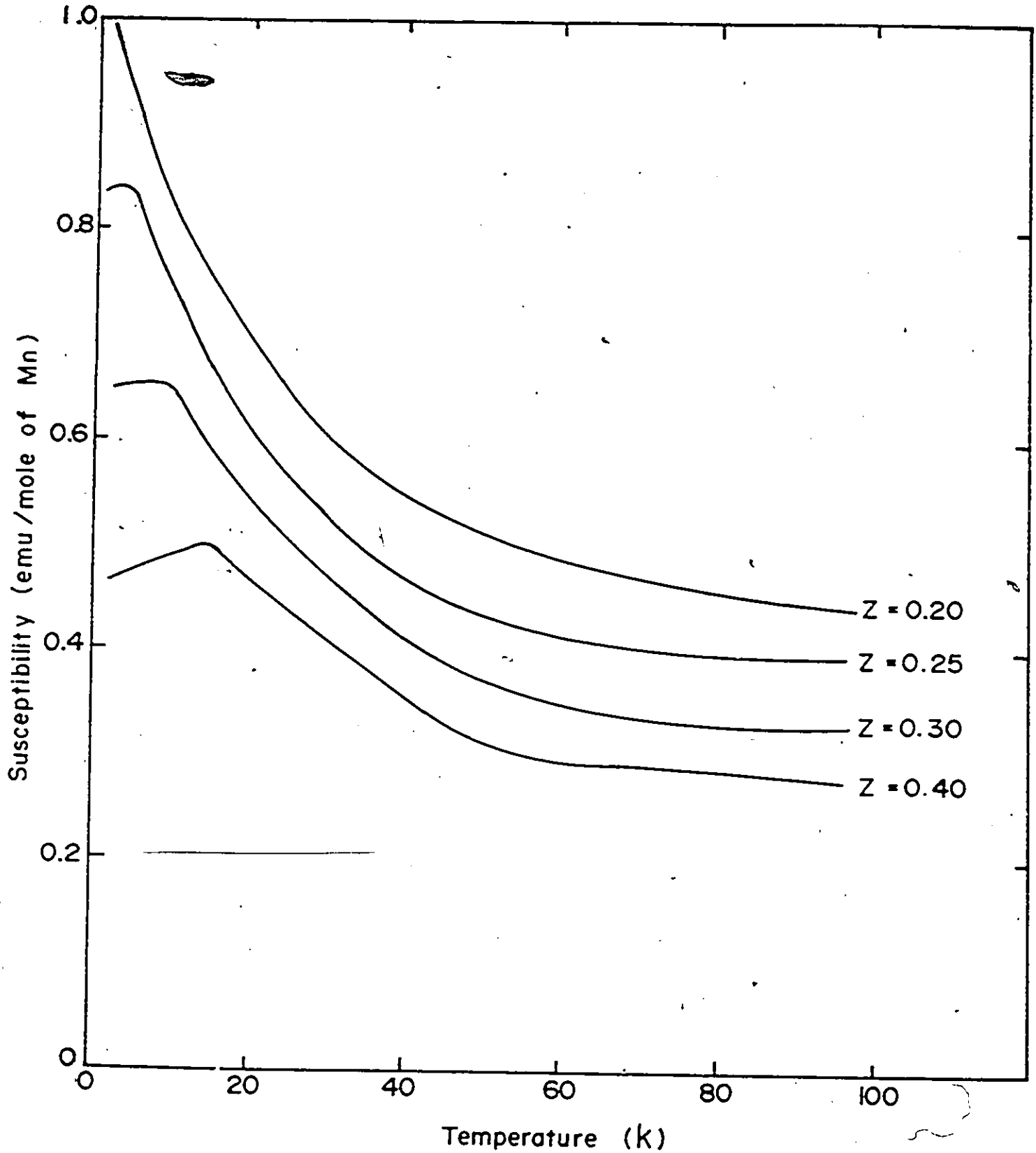

FIGURE 3.6 Results of measurements of magnetic susceptibility for some samples with f = 0.8 where f = y/x+y.

field cooled samples but the cusp was not as sharp when the samples were cooled in the presence of a magnetic field. Fig. (3.7) shows the behaviour of the susceptibility measurement for zero field cooled and field cooled samples. This indicates that an alignment of the spins by a magnetic field at higher temperature is to some extent retained by the spin system below the freezing point.

For zero field cooled samples, a well defined cusp could be observed in the curves of magnetic susceptibility χ as a function of temperature T when $z > 0.25$ and this peak of the cusp defines the spin-glass transition temperature T_g. For $z < 0.25$ the cusp would occur at or below 4.2 K, which is below the low temperature limit of the equipment used, and so was not observed. The values obtained for T_g are plotted in Fig. (3.8) as a function of f for values of constant z and in Fig. (3.9) values of T_g vs z at constant f. Also shown in Fig. (3.9) are values of T_g obtained by Novak et al [32] at temperatures < 4.2 K for $Cd_{1-z}Mn_zSe$ alloys. In the high temperature range, the temperature dependence of the reciprocal magnetic susceptibility $1/\chi$ should show the linear Curie-Weiss from $\chi = \frac{C}{T-\theta}$. The experimental curves of $1/\chi$ vs T (see Fig. 3.10) have been extrapolated to give the Curie-Weiss "Paramagnetic" temperature θ. Values of θ so obtained are shown in Fig. (3.11) as a function of f for various constant values of z, and in Fig. (3.12) as a function of z for various constant f values. The slope of the linear part i.e. the high temperature part of $1/\chi$ vs T graph gives the values of the Curie constant C. These values of C (per mole of sample) are plotted as a function of the alloy composition parameters in Fig. (3.13) and Fig. (3.14). At the temperature nearer to T_g, the values of $1/\chi$ fall below

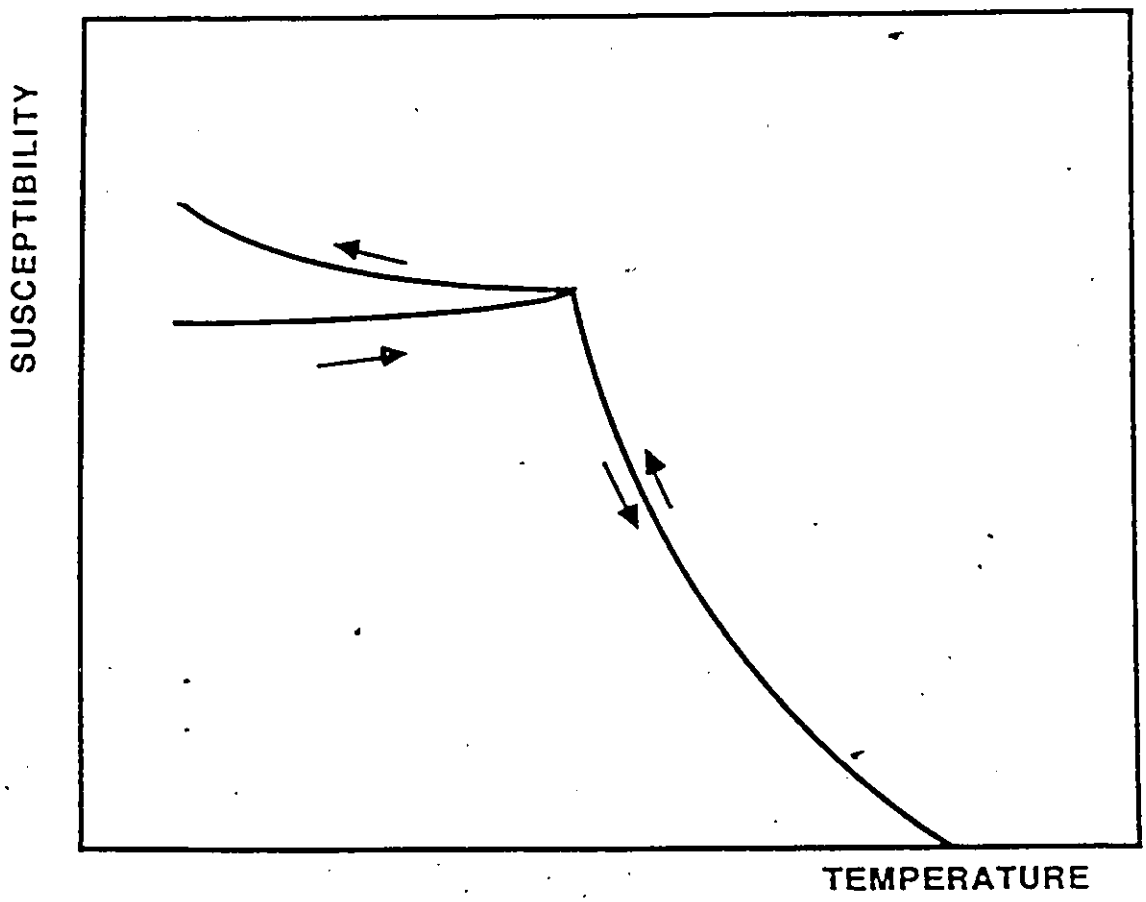

FIGURE 3.7 Irreversible effects in spin glasses. The arrows indicate the sequence of measurements which produced this result after the sample is initially cooled in zero field.

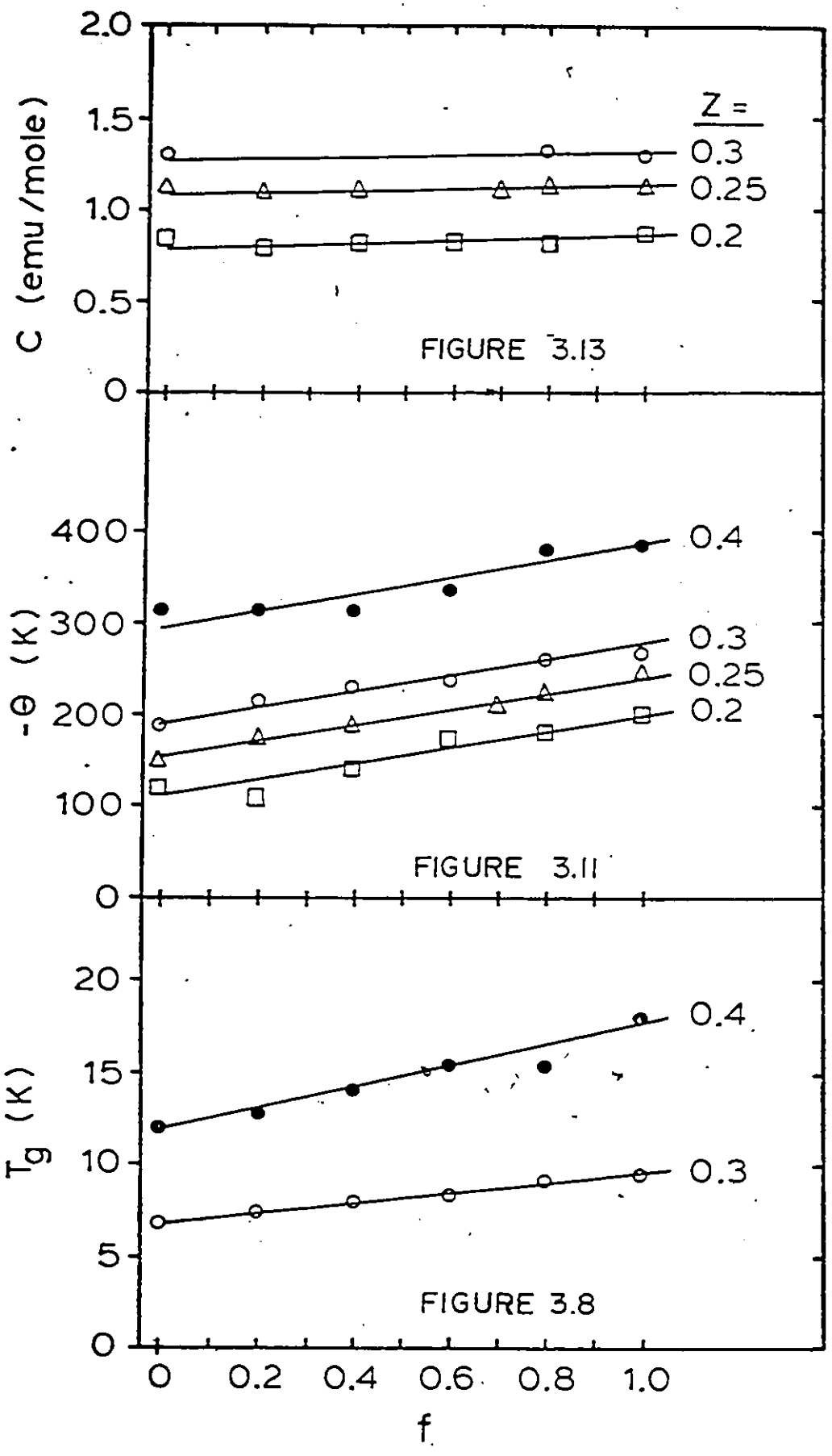

FIGURE 3.8, 3.11, 3.13 Plot of the parameter T_g, θ and c, obtained from susceptibility measurements versus f (where f = y/x+y).

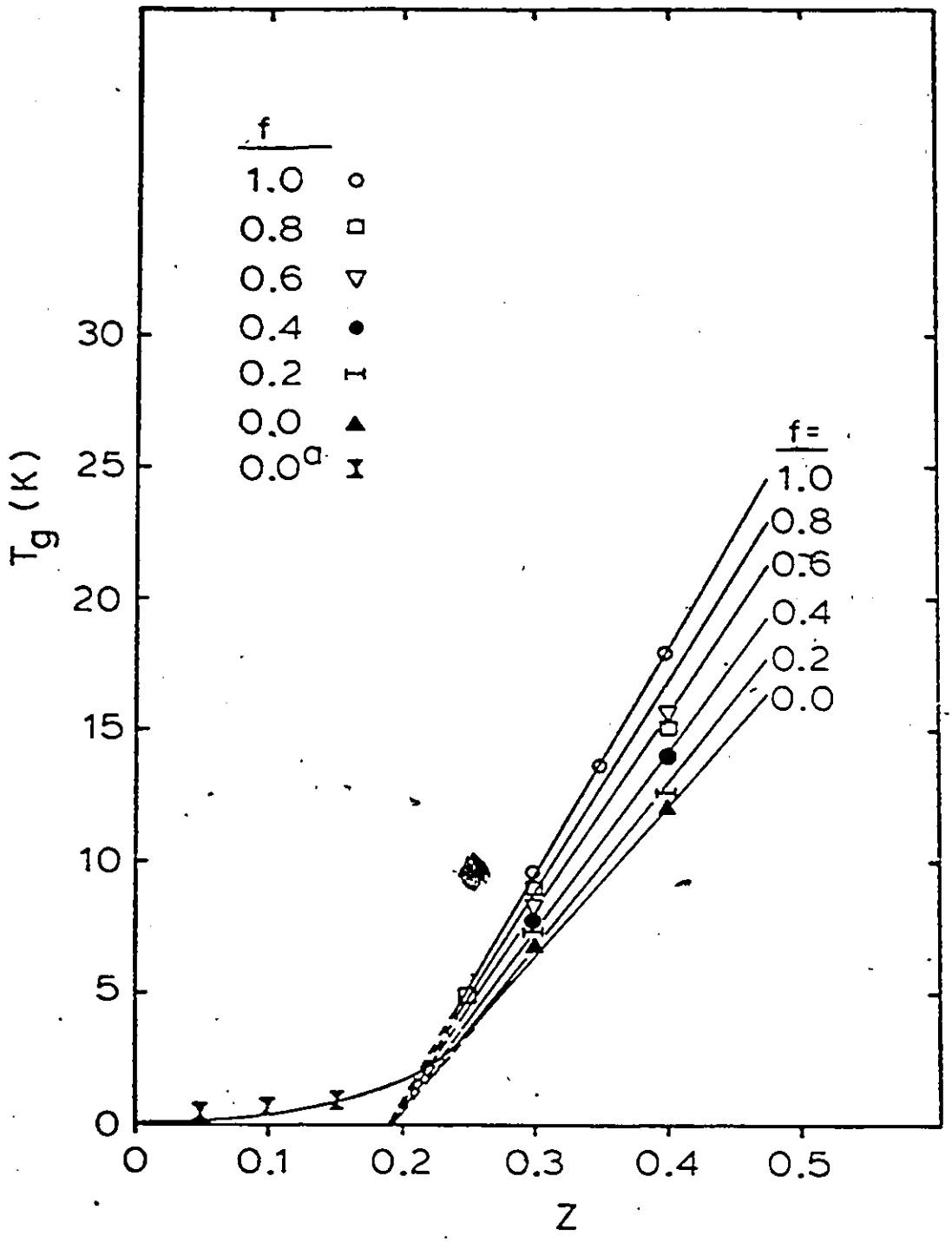

FIGURE 3.9 Plot showing the spin-glass transition temperature T_g, measured by magnetic susceptibility, versus the Mn concentration z.

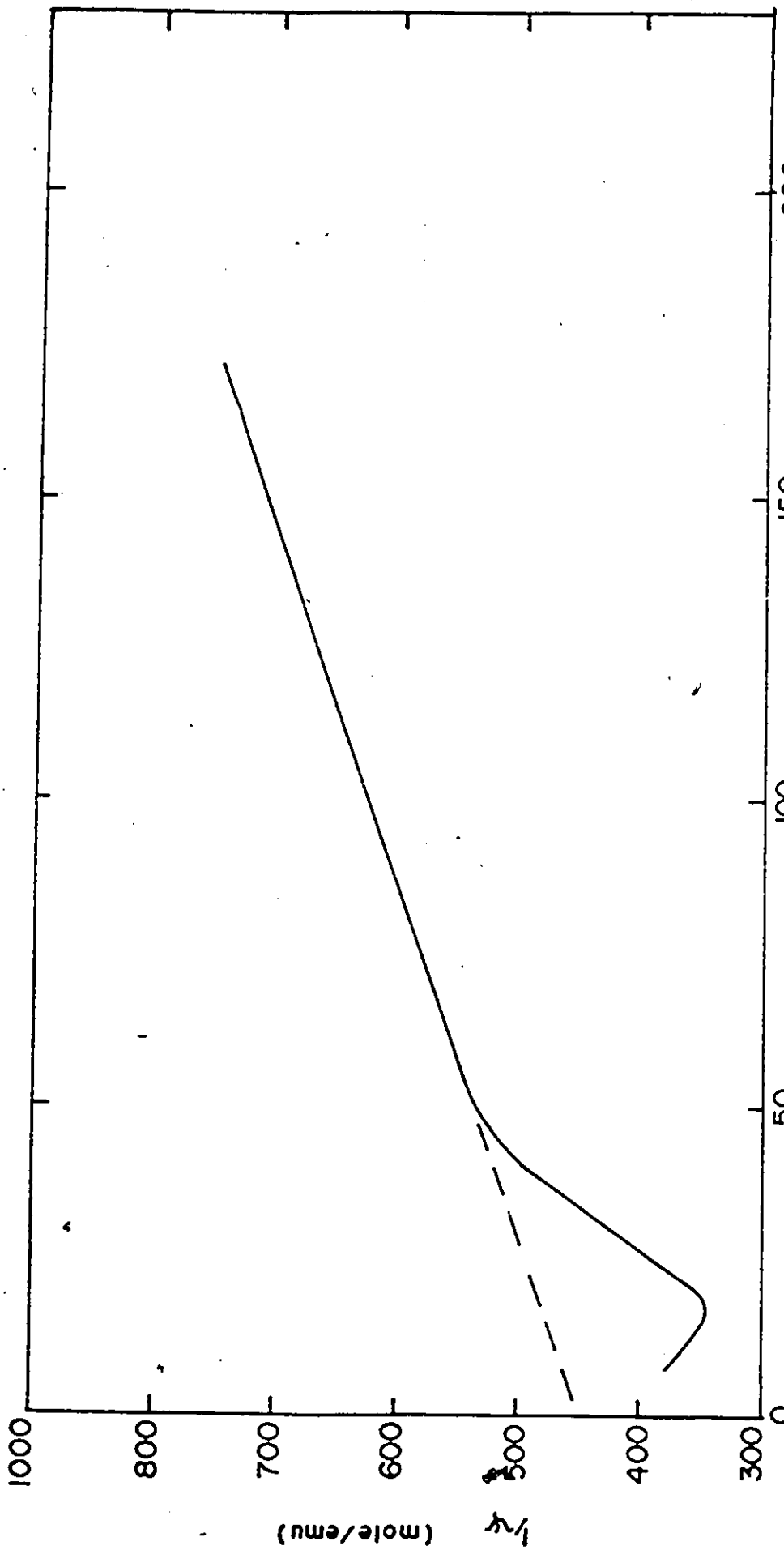

FIGURE 3.10 A typical curve showing the variation of the reciprocal magnetic susceptibility $1/\chi$ versus temperature (χ is measured in emu per mole of sample). The curve shown is for the sample with z = 0.4 of the alloys $Cd_xZn_yMn_zSe$ (48,12,40).

the Curie-Weiss line as shown in Fig. (3.10) and this effect is attributed to superparamagnetic effects in random Mn clusters.

3.4 Analysis

The plot of the inverse susceptibility graph versus temperature shows which type of interaction is taking place. At high temperature, Mn^{2+} spins interact weakly in a normal paramagnet fashion, giving the Curie-Weiss behaviour for the magnetic susceptibility, shown by the linear variation of $1/\chi$ vs T curve. If we extrapolate this linear portion of the curve it will intersect the negative T axis, implying that an antiferromagnetic interaction is taking place between the spins, so in this high temperature region the susceptibility is given by

$$\chi(T)_{\text{per mole}} = \frac{z\, N_A\, \mu_B^2\, g^2 S(S+1)}{3k(T-\theta)} \qquad 3.9$$

where z is the Mn concentration, N_A is Avogadro number and $\theta < 0$. As the temperature is lowered the spins begin to show more correlation i.e. tend to stay antiferromagnetically aligned in small clusters for a longer time. As the temperature continues to fall the range of the exchange interaction extends and Mn clusters show greater correlation. These growing interaction between the spins, and formation of finite clusters cause a superparamagnetic effect to come into play so that χ is increased and hence $1/\chi$ changes slope and falls below the Curie-Weiss line Fig. (3.10).

As we lower the temperature further, the correlation range extends to further independent spins; as a result the size of magnetic clusters increases until they begin making contact with each other i.e. they become strongly interacting. Finally at the temperature T_g a

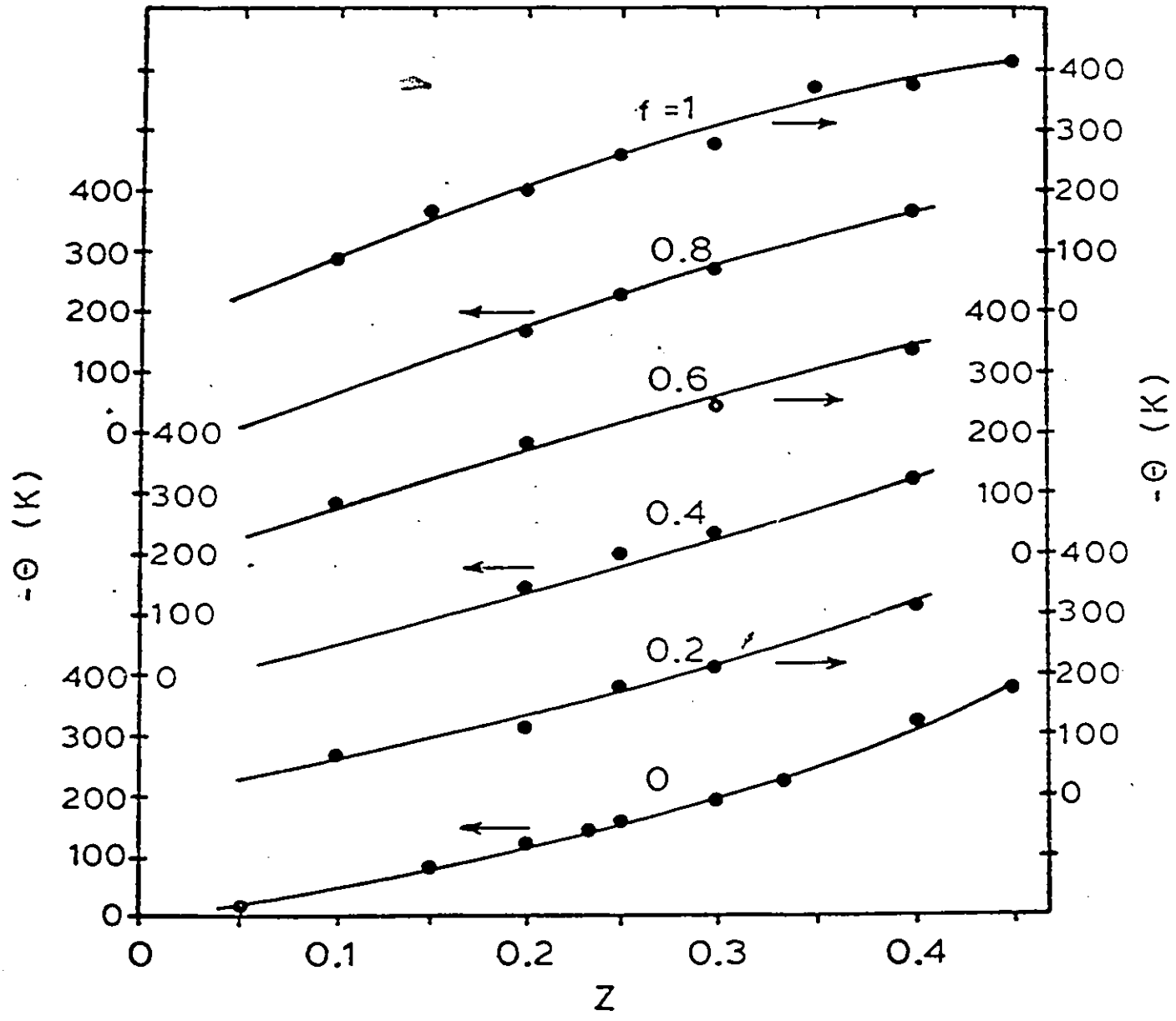

FIGURE 3.12 Plot of the Curie-Weiss "Paramagnetic" temperature θ versus the Mn concentration z for lines of constant f (where f = y/x+y). Note that each curve refers to a separate scale as indicated by the arrows.

percolation takes place which makes an infinite cluster of frozen spins. The spins inside the cluster are strongly correlated, and their directions are controlled by a field which is assumed to be randomly distributed over all directions. Thus the spins no longer react to the external field, this causes the magnetic susceptibility χ to show a cusp maximum at T_g.

Considering now the variations of the parameters obtained from magnetic susceptibility measurement. From Fig. (3.8), T_g varies and increases slightly with f, the reason for this could well be explained by the fact that the value of lattice parameter decreases with f, and consequently the distance between Mn ions become smaller towards the Zn side of pseudo-ternary diagram. In general, exchange interactions tend to increase with a decrease in separation between the magnetic ions. This would mean that spins would freeze at higher temperature.

Linear extrapolation of the T_g vs z graphs to zero gives $z = 0.19$ which is very close to the value of 0.195 calculated for the percolation limit for nearest neighbour interaction for an fcc lattice as calculated by various authors [33,34]. A similar value should apply for the wurtzite structure since wurtzite and zinc blende have the same nearest neighbours configurations. The behaviour of T_g has been previously explained by postulating that spin glass behaviour cannot occur for concentration less than this percolation limit. However results by Novak et al [32,35] have shown that values of T_g can be obtained at concentrations down to $z = 0.05$ indicating that interactions larger than nearest neighbour must occur. However for $z \sim 0.25$ the nearest neighbour interactions dominate and this is why the extrapolation from this range gives the nearest neighbour percolation limit.

It is convenient to discuss this point further by considering the analysis suggested by Escorne et al [36,37]. It is assumed that the exchange parameter J between two manganese ions can be written as

$$J = J_o \exp(-\alpha r) \qquad 3.11$$

where r is the distance between the ions. For a concentration z of Mn ions arranged at random on a cation sublattice of nearest neighbour spacing d, the mean Mn spacing can be written as $dz^{-1/3}$, and hence the mean exchange interaction between Mn ions is given by

$$J_m = J_o \exp(-\alpha d z^{-1/3}) \qquad 3.12$$

If it is also assumed that $kT_g = -AJ_m$ where A is a constant independent of z, this gives

$$\ln T_g = \ln(-A J_o/k) - \alpha d z^{-1/3} \qquad 3.13$$

The distance d is related to the lattice parameter, and for the zinc blende structure $d = a_c/\sqrt{2}$ while for hexagonal wurtzite structure $d = a_h$. Thus provided the initial assumption of eq. (3.11) is satisfied and α is a constant, the graph of $\ln T_g$ vs $dz^{-1/3}$ should be a straight line. In the work done here in our research group this has been shown to be the case for the alloys systems $Cd_xZn_yMn_zTe$, (38) $(Cd_{1-z}Mn_z)(Te_{1-y}Se_y)$ (39) and also for the system under investigation here, $Cd_xZn_yMn_zSe$. It is seen that these data fall on one of two lines, one corresponding to the cubic zinc blende structure and one to the hexagonal wurtzite structure. Both lines are straight up to a value of $dz^{-1/3}$ corresponding to z = 0.6. Above this value, the zinc blende points form a different line, and this is the range in which antiferromagnetic rather than spin glass behaviour occurs as shown by neutron diffraction [22,22], work and as discussed by Tom Donofrio in his work on the alloy system $Cd_xZn_yMn_zTe$ [38].

A linear extrapolation of the present data gives good agreement with the data of Novak et al [32,35] for $Cd_{1-z}Mn_zTe$ and $Cd_{1-z}Mn_zSe$ for values of z in the range $0.01 < z < 0.5$, indicating that eq. (3.11) is still valid at these low concentrations of manganese. These results indicate that, within the experimental error and for a given structure, the exponent α is constant and independent of composition, namely of the Mn concentration z.

As mentioned above, the result of ℓnT_g vs $dz^{-1/3}$ in Fig. (3.15) showed a linear variation implying that the exponent α is a constant, independent of z and r. Consequently α is independent of energy gap E_g (shown by other workers of the group T. Donofrio for $Cd_xZn_yMn_zTe$ and S. Chehab for $Cd_{1-z}Mn_z\ Te_{1-y}Se_y$ alloys [38,39]).

Equation (3.11) indicates that there is a fairly long range indirect antiferromagnetic exchange interactions between the Mn^{2+} ions which has an exponential variation with distance and for which the exponent α is independent of composition and hence of various other parameters which are composition dependent.

Turning to the exchange mechanisms which have been proposed to explain spin glass behaviour, clearly in this case direct exchange and R.K.K.Y. are eliminated as is superexchange through localized anion p orbitals. In the material under investigation the selenium p electrons are part of sp^3 hybridized valence conduction band system and the exchange via various indirect transitions needs to be considered. One mechanism proposed by Bloembergen and Rowland [30] and discussed by various authors [36,40] involves virtual transitions between valence and conduction bands. However although this exchange has an exponential variation with distance $\{J(r) \alpha \exp(\frac{-2mE_g}{\hbar^2})^{\frac{1}{2}} r\}$ the exponent is

a function of band gap E_g. Thus although this mechanism is important in low band gap materials e.g. $Hg_{1-z}Mn_zTe$ [40], it cannot be the dominant mechanism in the present case.

Two other exchange mechanisms giving exponential distance variation have been proposed. One, involving coupling through phonons [41], contains also a cosine term involving distance and so is not applicable here. The second mechanism was proposed by Geertsma et al [31] based on the work of Gonçalves da Silva and Falicov [42]. This gives long range exchange interaction through virtual transitions between the valence band and a delocalized band of 3d states. The exponential term in this case has an exponent which is a function of the energy difference between the two states and of the effective mass of the valence band. Since for these zinc blende and wurtzite semi-conductors, the valence band is insensitive to changes in composition, it appears reasonable that this exponent should have a constant value as described above. Thus this exchange mechanism would appear to have the form required to explain the present results.

In the analysis of Geertsma et al [31] it has been shown that to a good approximation the exchange can be taken to have the form

$$J(r) = I_o r^{-2} \exp(-\alpha r) \qquad 3.14$$

i.e. there is an additional r^{-2} factor compared with Escorne equation (3.11). When this term is included in the present analysis, equation (3.13) must be written as

$$\ln d^2 T_g \cdot z^{-2/3} = \ln \left(\frac{-AI_o}{k}\right) - \alpha d z^{-1/3} \qquad 3.15$$

In Fig [3.16] the data for the system under investigation, $Cd_xZn_yMn_zSe$, in this thesis, and for other systems investigated by the workers in the research group i.e. $Cd_xZn_yMn_zTe$, $Cd_{1-z}Mn_zSe_{1-y}Te_y$ are plotted as

$\ln d^2 T_g z^{-2/3}$ vs. $dz^{-1/3}$. It is seen in this case also that, within the limits of experimental error, the results lie on two straight lines, one for the cubic zinc blende and one for hexagonal wurtzite structure. Both the Escorne and Geertsma plots appears to be straight lines because the variation of d is relatively small and so has relatively little effect on the shape of the graph. Again it is found that the line shown in Fig. (3.16) $\ln d^2 T_g z^{-2/3}$ vs $dz^{-1/3}$ extrapolate to the points representing the data of Novak et al [32,35] at low z values.

From the slope and intercept of each of the lines in Fig. (3.16) values of α and AI_o/k can be determined for each structure: these are

zinc blende $\alpha = 6.1 \pm 0.4$ nm^{-1} $\quad AI_o/k = -(2.03 \pm 0.5) \times 10^2$ Knm^2

wurtzite $\alpha = 8.0 \pm 0.4$ nm^{-1} $\quad AI_o/k = -(4.35 \pm 0.9) \times 10^2$ Knm^2

As indicated by Anderson [43], the parameter A can be equated to S(S+1). The values of Curie-Weiss C in these materials show that in all cases S = 5/2, so that the values of I_o/k can be obtained from the above data and these are for zinc blende $I_o/k = -(23 \pm 6)$ Knm^2 and for wurtzite $I_o/k = -(50 \pm 11)$ Knm^2.

These results for I_o/k allow values to be determined for the exchange between nearest neighbour and next nearest neighbour sites (J_1 and J_2 respectively) which can be compared with particular values given in the literature. For the case of $Cd_{0.95}Mn_{0.05}Se$ Aggarwal et al [44] from measurements of A-exciton splitting gives the value of J_1/k as -8.7 ± 0.3 K, while for the same alloy Shapira et al [45] from high field magnetization measurements give $J_1/k = 8.3 \pm 0.7$ K. In the present work, the value of d for this composition is 0.4292 nm and hence from equation (3.14) the value of J_1/k is -8.7 ± 0.7 K. Shapira

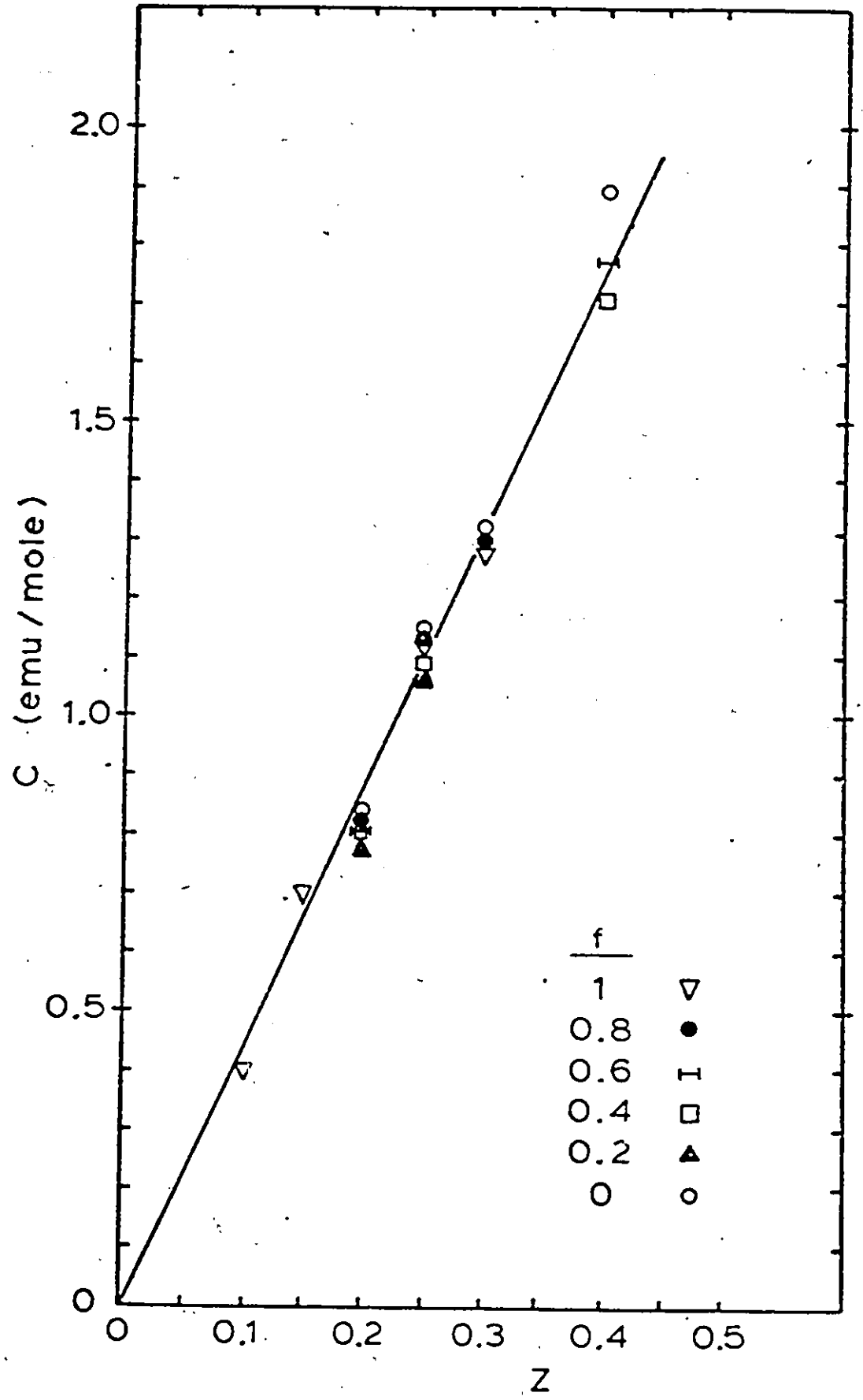

FIGURE 3.14 Plot of the Curie constant c versus Mn concentration z at various values of f (where f = y/(x+y)). (c is measured in e.m.u./mole of sample).

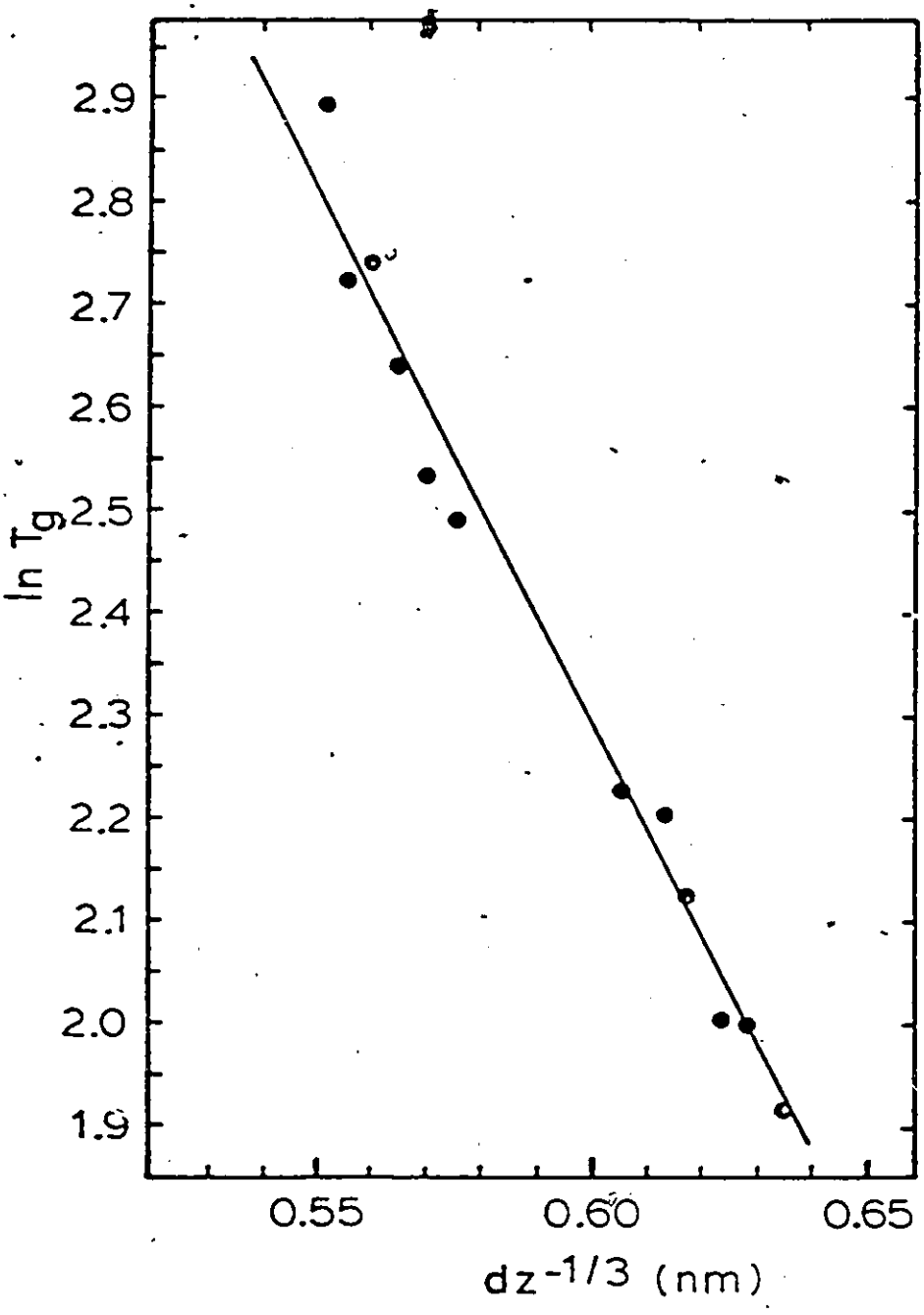

FIGURE 3.15 Plot of ℓnT_c versus $dz^{-1/3}$ for the alloy system $Cd_xZr_yMn_zSe$.

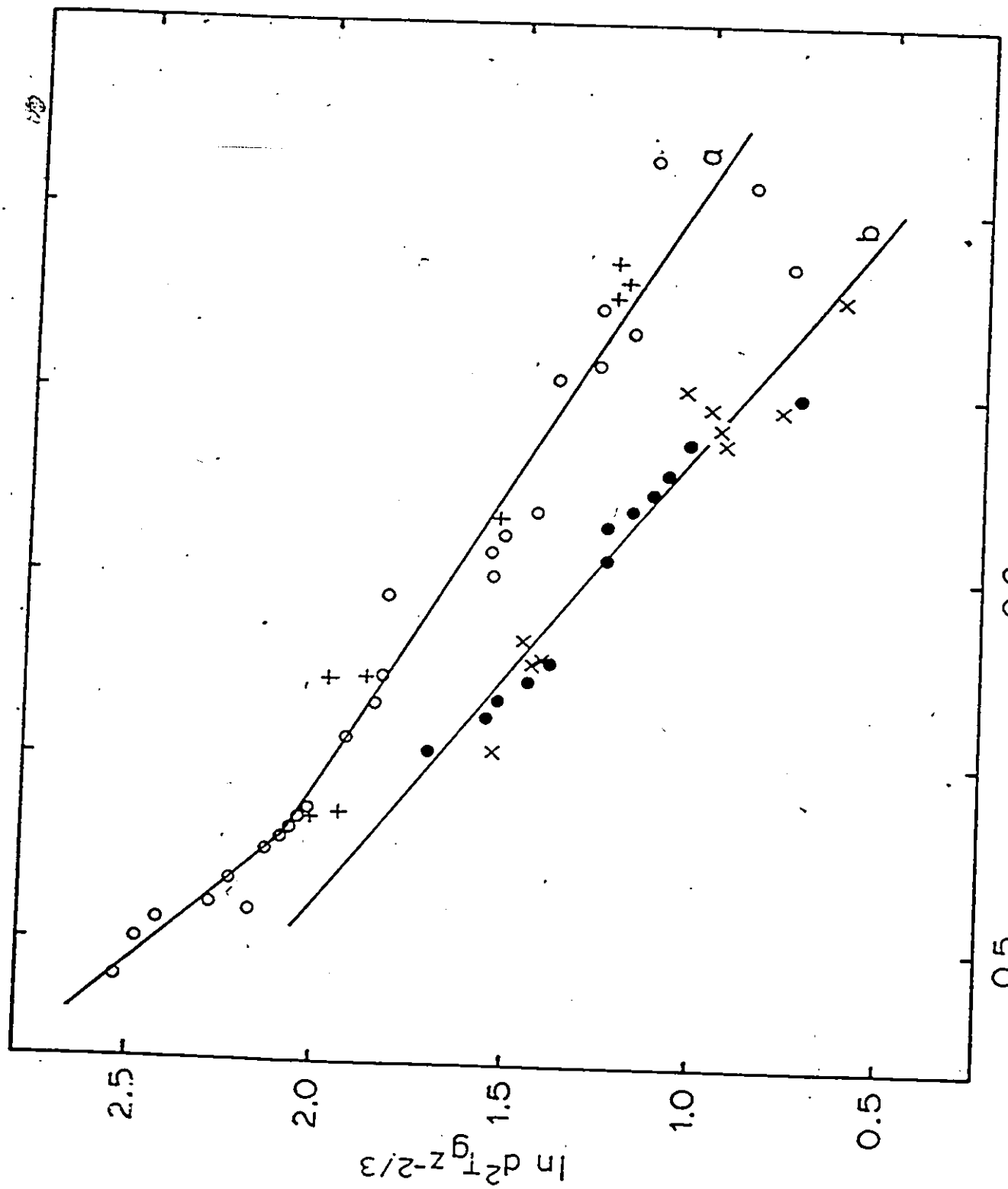

FIGURE 3.16 Variation of ln $d^2T_g z^{-2/3}$; a) zinc blende structure, o $Cd_xZn_yMn_zTe + Cd_{1-z}Mn_zTe_{1-y}Se_y$; b) wurtzite structure $Cd_xZn_yMn_zSe$ X $Cd_{1-z}Mn_zTe_{1-y}Se_y$.

et al [45] also indicated that for $Zn_{0.97}Mn_{0.03}Se$ they obtained J_1/k = -13 K, and from the present data for $Zn_{0.97}Mn_{0.03}Se$ which has zinc blende structure and so d = a/√2 where a, the cubic lattice parameter is 0.5654 nm, the value obtained for $J_1/k = -12.7 \pm 0.9$ K.

The analysis of Geertsma et al [31] indicates that the exponent α has the value $2(2\varepsilon m^*/h^2)^{\frac{1}{2}}$ where ε is the energy difference in the virtual transition and m* is the effective mass for the valence band. A reasonable estimate of m* is given by the heavy hole mass for CdTe, which is close to the free electron mass m_o [46]. Thus with m* taken as m_o the above values of α give values of ε of 0.34 ± 0.05 eV for the zinc blende structure and 0.61 ± 0.06 eV for the wurtzite case.

Turning now to Curie-Weiss temperature θ, it is noted that magnitude of the "paramagnetic" Curie temperature θ, is observed to increase with both f and z. The variation with z in Fig. (3.12) is non-linear, with the lines for f 0.5 bend upwards while those for f 0.5 bending downwards. This effect can be related to the variation of the lattice parameter in the alloys (see chapter two). As in chapter (2) Fig. (2.6) it is observed that the lattice parameter decreases with increasing z for f 0.5, and increases for f 0.5, the extremes of these conditions occur at f = 0, and 1 respectively. The reduction of the lattice parameter with higher z (f 0.5) increases the interaction between Mn ions and results in an increase in θ above the linear variation, while the opposite effect is observed for the f 0.5 case.

After this qualitative description of the dependence of θ on composition, let us try now and make some quantative predictions of the values of θ for our alloys and then compare with experimental results.

The standard mean field theory [47] gives

$$\theta = 2/3 \frac{S(S+1)}{K} \sum_i n_i J_i \qquad 3.16$$

where $\sum_i$ represents the summation over consecutive sets of neighbours i.e. 1^{st} nearest neighbours, 2^{nd} next nearest neighbours etc., and where n_i is the number of neighbours in each case and J_i is the appropriate value of the exchange parameter. If J_i is assumed to satisfy eq. (3.14), and with concentration z of paramagnetic ions, n_i is replaced by zn_i then

$$\theta = 2/3\ S(S+1)\ J_o/k\ z \sum_i \frac{n_i \exp(-\alpha r_i)}{r_i^2} \qquad 3.17$$

For both structures, values of n_i and r_i were calculated by Dr. Woolley out to seventh nearest neighbours (Table 1). Then with S, I_o/k and lattice parameter values known, values of θ were determined from equation (3.17) and compared with the experimentally determined values. In Fig. (3.12) the points are the experimental values and the curves values, calculated from equation (3.17). It is seen that very good agreement is obtained.

Finally the remaining physical constant that can be determined from the magnetic susceptibility measurement is the Curie constant C. The variation of the Curie constant C(per mole of sample) is linear with z and extrapolates to the origin of coordinates (Fig. 3.14) within experimental error. This result is independent of the alloy composition f. Fig. (3.13) shows that the variation of C with f for constant z is very small. These results are to be expected since in the Curie-Weiss range C should depend only upon the concentration of Mn ions.

Table 1. Values of r_i, distances between cations, and n_i, the number of neighbours at distance r_i, in terms of d the nearest neighbour cation spacing. Values for the zinc blende structure ($d = a/\sqrt{2}$) and wurtzite structure ($d = a$).

Zinc blende

r_i	d	$\sqrt{2}d$	$\sqrt{3}d$	$2d$	$\sqrt{5}d$	$\sqrt{6}d$	$\sqrt{7}d$
n_i	12	6	24	12	24	8	48

Wurtzite

r_i	d	$\sqrt{2}d$	$\frac{8}{3}d$	$\sqrt{3}d$	$\frac{11}{3}d$	$2d$	$\sqrt{5}d$	$\frac{17}{3}d$
n_i	12	6	2	18	12	6	12	12

3.5 Conclusion

The results from the magnetic susceptibility measurements proved to be very useful in giving valuable information on the magnetic behaviour of the $Cd_xZn_yMn_zSe$ alloys and all other materials belonging to same class. The values of the spin-glass freezing temperature T_g were determined, and when plotted against z, the Mn concentration extrapolation to $T_g = 0$ gives $z \sim 0.2$, in very good agreement with the theoretically calculated percolation limit for nearest neighbour interaction [48,49,50]. However values of T_g were obtained by Novak et al [35] for concentration down to $z = 0.05$ which could be explained on the basis of next and next next nearest neighbour interaction by using the analysis suggested by Escorne et al [36] according to which $\ln T_g$ should decrease in a linear fashion when the mean spacing between the Mn ions increases with decreasing z, which is true in our case and even for $z < 0.2$. This exchange causes an antiferromagnetic interaction between Mn^{2+} ions, which decreases exponentially with distance and the exponent is independent of composition. An exchange mechanism proposed by Geertsma et al [31] seems to satisfy these requirements. It involves virtual transitions between valence band and delocalized 3d state. From the analysis, very good agreement can be obtained with values of J_1/k and J_2/k determined from very different measurements.

Also the results can be used to give a very good prediction of the value of θ for the alloys, without any adjustable parameter. The values of the energy separation ε determined above are useful to indicate whether the exchange is due to interaction of the valence band with a 3d band or the conduction band. The valence band 3d transition would probably involve the transition of an electron from the top of

valence band to the $3d^5$ state, converting it to $3d^6$ with a resultant energy increase of ε. As indicated above, ε should be independent of composition for a given structure with values determined here of 0.35 eV for zinc blende and 0.61 eV for wurtzite samples. For all the samples $E_g > 1.56$ eV and hence in all cases, the valence-conduction band spacing is too large for any appreciable interaction. However in case of $Hg_{1-z}Mn_zTe$, the results of Mycielski et al [51] shows that when E_g is comparable with ε, virtual valence-conduction band transitions play a significant role.

The exchange interaction in our alloys system was found to be antiferromagnetic interaction as indicated by the fact that values of Curie-Weiss paramagnetic temperature θ were found to be negative; thus confirming the antiferromagnetic interactions between the Mn^{2+} spins and an increase in the magnitude of the θ values with increasing z which indicates an increase in antiferromagnetic interaction.

With the values of Curie constant C we were able to calculate the spin of the Mn^{2+} ion, and this was found to be 5/2.

With the help of magnetic susceptibility measurement we are able to get a good agreement between the experimental and calculated values of J_1/k, J_2/k and θ, and the exchange mechanism between the Mn spins in the alloys.

REFERENCES

1. Allan H. Morrish, "The Physical Principal of Magnetism", Robert E. Krieger, Publishing Company Inc. 1980, Ch. 2, 6, 7 and 8.

2. C. Kittel, Introduction to Solid State Physics, Fifth Ed. chapter 14, 15 and 17, p. 435, Wiley Totonto 1976.

3. CRC Handbook of Chemistry and Physics, CRC Press, Boca Raton, Florida.

4. Peter J. Ford, Contemp. Phys. vol. 23, no. 2, 141 (1982).

5. J.A. Mydosh, J. Mag. Mag. Mat. 7 237-248 (1978); "Magnetism in Solids" Some Current topics, edited by A.P. Cracknell and R.A. Vanghan, Published by the Scottish Universities Summer School in Physics, chap. 4.

6. K.H. Fischer, Physica B86-88, 813 (1977).

7. A.P. Marani, J. Mag. Mag. Mat. 5, 95 (1977).

8. G. Toulouse, Comm. Phys. 2, 115 (1977).

9. G. Toulouse, "Modern trend in the theory of condensed matter", Lecture note in Physics, 115 edited by A. Pekalski and J. Przystawa, P. 195 (1980).

10. J. Ziman, "Principle of Theory of Solids", Cambridge University Press, ch. 10, (10.6).

11. L. Deseze, J. Phys. C10, L 353 (1977).

12. J. Villain, Z. Phys. B33, 31 (1979).

13. R.E. Kremer, J.K. Furdyna, Phys. Rev. B31, 1 (1985).

14. V. Cannella, and J.A. Mydosh, Phys. Rev. B6, 4220 (1972).

15. V. Cannella, and J.A. Mydosh A.I.P. Conf. Proc. 10, 785 (1973).

16. C.N. Guy, J. Physics F5, L242 (1975).

17. C.N. Guy, J. Physics F7, 1505 (1977a).

18. C.N. Guy, J. Physica B 86-88, 877 (1977b).

19. C.N. Guy, J. Phys. F8, 1304 (1978).

20. H. Sato, S.A. Werner and R. Kikuchi, J. Physics (Paris) 35, C4#25 (1976).

21. A.P. Murani, Phys. Rev. Lett. 37, 450 (1976).

2. A.P. Murani, and J.L. Tholena, Solid State Commun. 22, 25 (1977).

23. C.E. Violet, and R.J. Borg, Phys. Rev. 149, 540 (1966).

24. C.E. Violet, and R.J. Borg, Phys. Rev. 162, 608 (1967).

25. A.P. Murani, J. Physique C6, 1647 (1978a).

26. K.H. Fisher, Physica B86-88, 813 (1977).

27. A.P. Murani, J. Mag. Mag. Mat. 5, 95 (1977).

28. L.E. Wenger, and P.H. Keesom, Phys. Rev. B11, 3497 (1975).

29. L.E. Wenger, and P.H. keesom, Phys. Rev. B13, 4053 (1976).

30. N. Bloembergen and T.J. Rowland, Phys. Rev. 97, no. 6, p. 1679 (1955).

31. W. Geertsma, C. Hass, G.A. Sawatzky, and Vertogen, Physica 86-88B, 1039 (1977).

32. M.A. Novak, O.G. Symko, D.J. Zheng, and S. Oseroff, Physica B126, 469 (1984).

33. G.S. Grest and E.G. Grabl, Phys. Rev. Lett. 43, 1182 (1979).

34. C. Domb and N.W. Dalton Proc. Phys. Soc. 89, 859 (1966).

35. M.A. Novak, S.B. Oseroff, and O.G. Symko, Physica B107, 313 (1981).

36. M. Escorne, A. Mauger, R. Triboulet and J.L. Thalence, Physica B107, 309 (1981).

37. M. Escorne and A. Mauger Phys. Rev. B25, 4674 (1982).

38. T. Donofrio Ph.D. Thesis, University of Ottawa (1986).

39. S. Chehab Ph.D. Thesis, University of Ottawa (1986).

40. C. Lewiner, J. Gaj and G. Bastard, J. Phys. 41 (1980).

41. Z.S. Gulacsi, M. Gulacsi, and M. Crisav, J. Mag. Mag. Mat. 40, 247 (1984).

42. C.E.T. Gonçalves da Silva and L.M. Falicov, J. Phys. C5, 63 (1973).

43. P.W. Anderson, Solid State Physics 14, p. 142 (1963).

44. R.L. Aggarwal, S.N. Jasperson, Y. Shapira, S. Foner, T. Sakakibara, T. Goto, N. Miura, K. Dwight and A. Wold, Proc. 17th Intern. Conf. Phys. semicond. San Francisco (1984) p. 1419.

45. Y. Shapira, S. Foner, D.H. Ridgley, K. Dwight, and A. Wold, Phys. Rev. 30, 4021 (1984).

46. K. Zmio, Semiconductors and Semimetals 13, 91 (1978).

47. J.S. Smart, Magnetism, vol III, eds. G.T. RAdo and H. Suhl (Academic Press, New York, 1963) p. 63.

48. C. Domb and N.W. Dalton, Proc. Phys. Soc. London 89, 889 (1966).

49. G.S. Grest and E.G. Gable, Phys. Rev. Lett. 43, 1182 (1979).

50. H.L. Frisch, E. Sonnemblick, V.A. Vyssotsky and J.M. Hammersley, Phys. Rev. 124, 1021 (1961).

51. A. Mycielski, G. Rigaux, M. Menant, T. Dietland, M. Otto, Solid State Commun. 50, 257 (1984).

Chapter IV

ELECTRON SPIN RESONANCE MEASUREMENTS

4.1 Brief History

Paramagnetic resonance was discovered in Kazan by Ye. K. Zavoyskiy (1944). His first experiments dealt with resonance absorption in salts of the iron group ions. Electron paramagnetic resonance (EPR) has become one of the most powerful tools of physical research. Its application is extremely broad. In ionic crystals it makes it possible to determine the structure of the energy levels in magnetic centers, explain the fine structure of the crystalline lattice, and define the parameters that characterize the kinetics of magnetization. We can study crystal lattice defects by means of electron paramagnetic resonance (EPR). In liquid salt solutions electron paramagnetic resonance provides the possibility of investigating solvate shell structure. With EPR we can study the properties of conduction electrons in metals and semi-conductors. In nuclear physics, paramagnetic resonance has proved valuable as a method for determining nuclear moments, and it is one of most effective means of polarizing nuclei.

Also the method of paramagnetic resonance has been very useful in chemistry. It has enabled the first detection of free radicals in 10^{-10} to 10^{-13} mole quantities. Also it has been useful to biological materials and most recently paramagnetic resonance has found important applications in radio engineering in the construction of a new kind of low-noise amplifier.

4.2 Introduction

A free magnetic ion which has a resultant angular momentum quantum number J would give 2J + 1 different degenerate levels. The application of the static magnetic field H will produce Zeeman splitting of the 2J + 1 states into the levels with energies of $E = g\mu_B M_J H$, where M_J is the magnetic quantum number, g is the Lande splitting factor, and μ_B is the Bohr magneton. For the alloy system being investigated, ions form a part of a crystalline solid and are not free, therefore the angular momentum may be described by a spin quantum number S i.e. J = S. In a field H, the energies of the split 2S + 1 levels can again be written as $M_S g\mu_B H$ and g is expected to be very close to 2.0. Without any other considerations, the form of the splitting would be given by Fig. (4.1).

In electron spin resonance (ESR), transitions between the levels can be induced by the application of an oscillating magnetic field (i.e. alternating electromagnetic field) and the resulting absorption is measured. According to quantum mechanics, a selection rule operates so that for magnetic dipole radiation, only the transitions between adjacent levels for which $\Delta M_S = \pm 1$ is allowed, and frequency of oscillating magnetic field is given

$$\hbar\omega = g\mu_B H \qquad (4.0)$$

It can be seen that the resonance may be observed by either fixing the frequency ω and varying H or vice versa. In normal ESR the former method is used, with the frequency fixed at some point in the microwave range.

It should be mentioned that the condition represented by eq. (4.0) may be modified by fine and hyperfine splitting. In the former

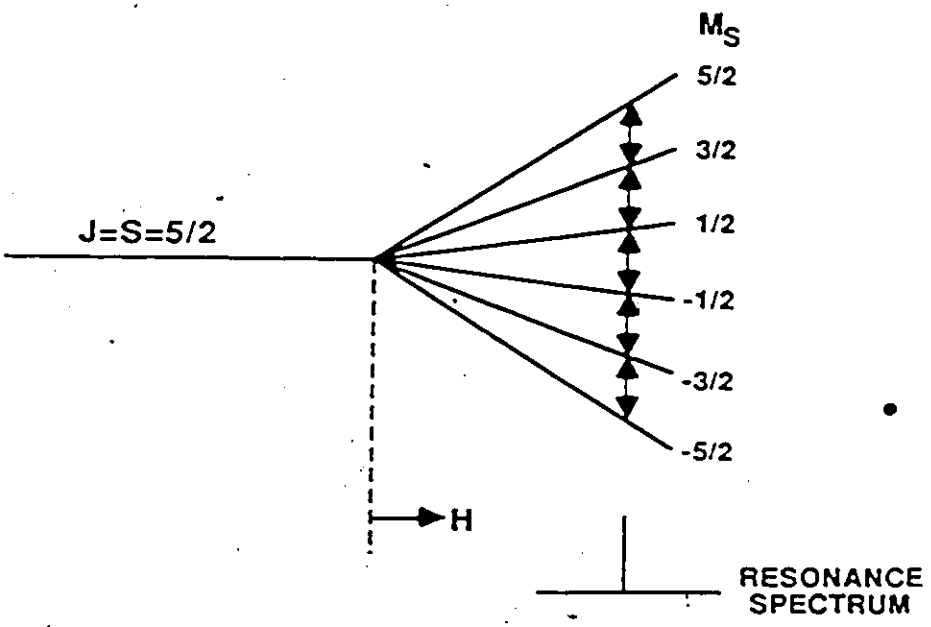

FIGURE 4.1 Zeeman splitting of a $3d^5$ level. In this example there is only one resonance line.

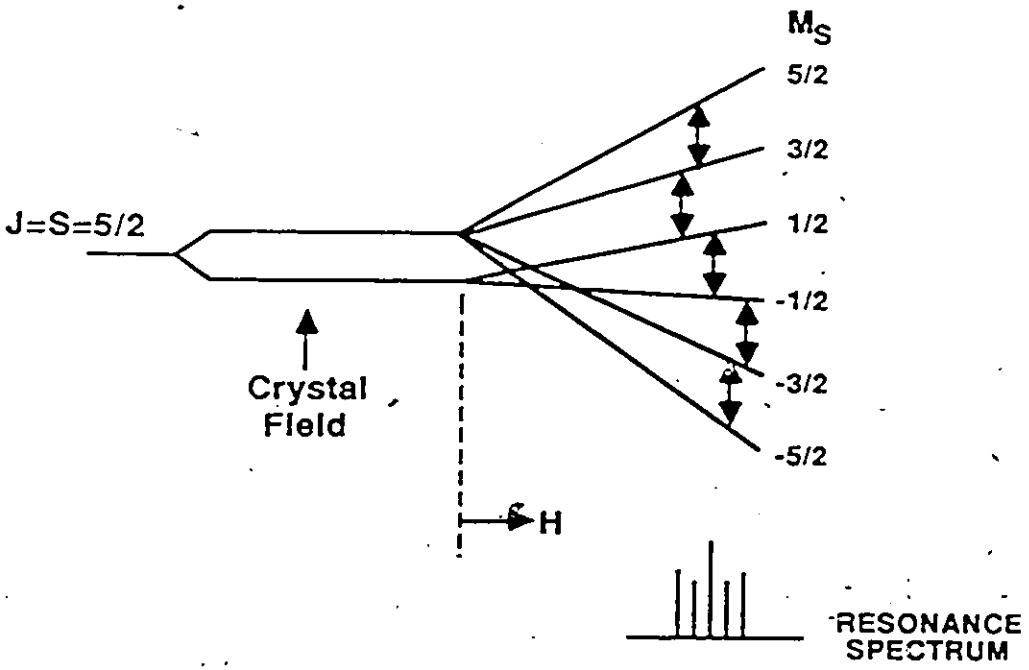

FIGURE 4.2 Zeeman splitting of a $3d^5$ level with fine splitting. The single resonance line is split into five by the presence of a crystal field.

case, some of the degenerate levels are split initially by the crystalline field as shown in Fig. (4.2) when a magnetic field is applied, multiple resonance points would occur, resulting in the observation of more than one line. With hyperfine splitting, the nuclear magnetic moments are coupled to the electron moments to produce an extra splitting of each level. In the materials $Cd_{1-z}Mn_zSe$, $Cd_{1-z}Mn_zTe$ the ESR spectra due to the above effect have been observed in diluted samples ($z < 0.05$) by Oseroff et al [1].

As with all resonance effects, some broadening of the line occurs due to various factors. The line width may be related to several different effects, including various types of relaxation phenomena, such as spin-spin and exchange interaction [2]. Another factor which may affect this linewidth, referred to as ΔH, is inhomogeneous broadening and is caused by an overlapping of any fine or hyperfine structure, as well as by the presence of inhomogeneous fields in the crystal [2]. The main aim in performing the present ESR measurements was to determine ΔH as a function of temperature and composition and to investigate the cause of broadening.

4.3 E.S.R. Measurement Apparatus

The ESR measurements were made in Dr. Armen Manoogian laboratory under his supervision and with the assistance of technician specialist B.W. Chan.

The apparatus consists of a klystron producing microwave power at x-band microwave frequency (~9.2 GHz). The produced microwave power can propagate in a microwave bridge, known as "magic" T, which consists of four-armed wave guide structure (as shown in the figure)

allowing the microwave power to feed into the sample cavity through one arm, and the power that is reflected back from the cavity to leave by a separate arm to the detection system. The slide-screw tuner contains a pin which can be inserted into the path of the microwaves, and can also be moved along the length of the waveguide comprising the slide screw tuner. The attenuator consists of a mica card covered with carbon that can absorb nearly all the microwave power that is not reflected back by the pin and hence that reaches the attenuator. As a result the pin depth of the slide-screw tuner changes the amplitude of the microwave, while the position of the pin along the tuner changes the microwave phase. The crystal detector consists of a silicon rectifier mounted in the wave guide. The rectifier detects the high frequency microwave power and changes it to a direct current (d.c.) voltage. Lower frequencies however, even up to several tens of megacycles, are able to pass through without being changed to d.c. The microwave resonant sample cavity is a piece of a waveguide with copper plates soldered on each end, one end of which has a hole of $\frac{1}{4}$ inch in the center to allow the microwaves to enter the cavity. The length of the cavity is one wavelength.

A frequency stabilizer keeps the microwave frequency stabilized against the resonance frequency of the sample cavity. A phase sensitive detector (PSD) is employed when recording signals on a chart recorder. While it is being swept, the magnetic field is modulated at 100 KHz by means of a pair of Helmotz coils mounted on the two opposite walls of the cavity which face the two poles of the magnet. The derivative of the ESR absorption lines is then produced on the chart recorder; and the peak to peak linewidth ΔH is measured with

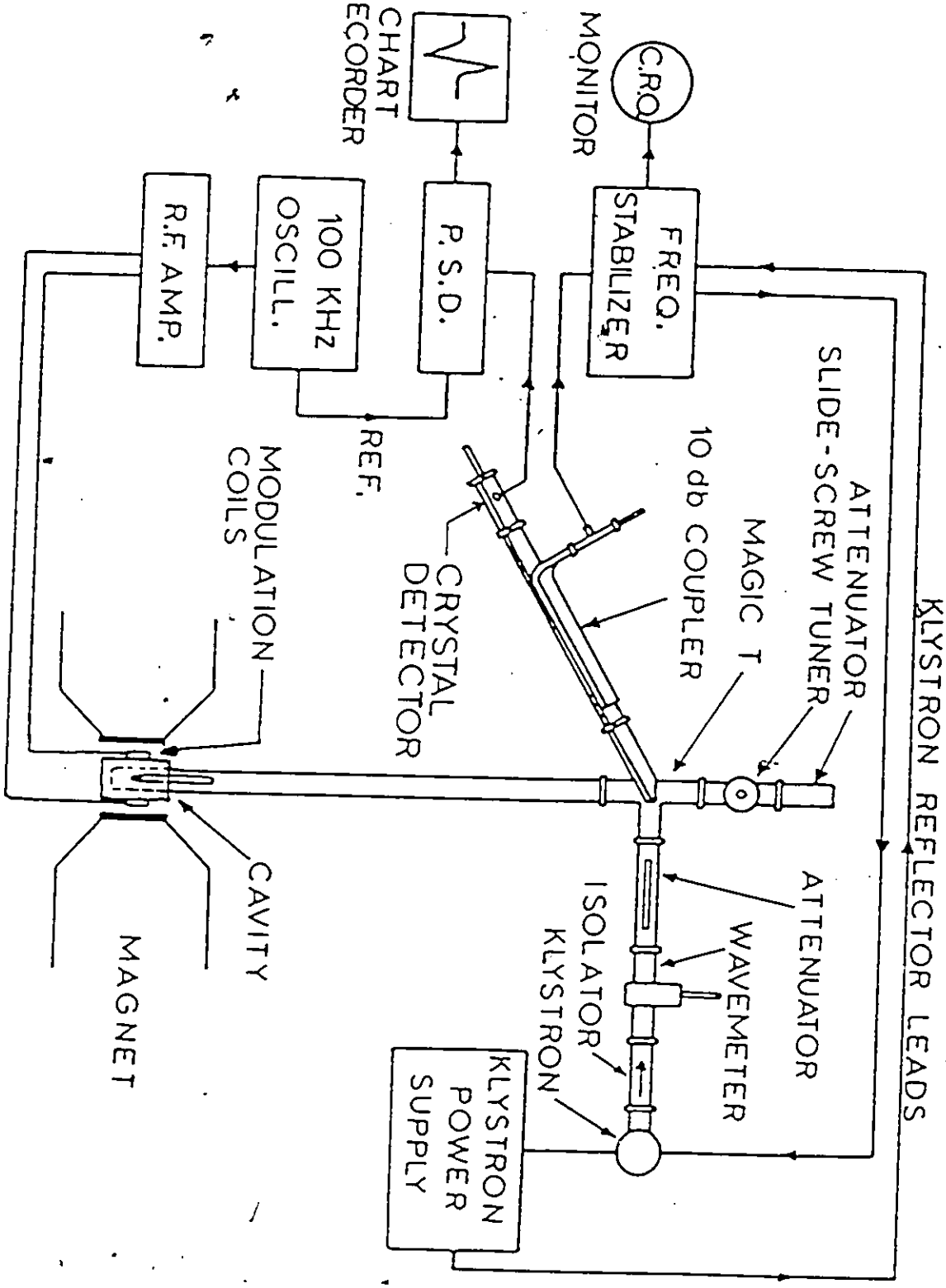

FIGURE 4.3 Electron spin resonance spectrometer system

an NMR gaussmeter; also the resonance field H_R is defined from the zero of the derivative curve.

The temperature of the sample can be controlled in the range between 10 K to 500 K. Circulating nitrogen gas around the sample cavity is used for the temperature control between 500 K and 90 K whereas helium gas is used between 90 K and 10 K. The temperature of the sample is measured by means of a thermocouple which can be in direct contact with the sample. A gold-chromel thermocouple is used for temperature below 300 K, and a copper-constantan thermocouple for temperature above 300 K. The ESR measurements can be carried out at various temperatures.

4.4 Results

The ESR measurements were carried out on all the samples in the single phase region. The resonance absorption for different compositions was observed over a wide temperature range, (10 K to 500 K). At higher temperatures (i.e. room temperature and above) all of the single phase samples produced a single symmetric line with a g-value very close to 2.0. Plots of ΔH versds temperature for a wide range of concentrations are presented in Figs. (4.4,4.5). In all cases it was observed that the symmetric Mn resonance linewidth increased with decreasing temperature remaining symmetrical in the higher temperature range. However at low temperature where ΔH began to increase appreciably, the lineshape was observed to broaden asymmetrically. When this occurred, the low field peak of the derivative line remained essentially the same while the high field peak became greatly broadened and flattened out. An example of this is in

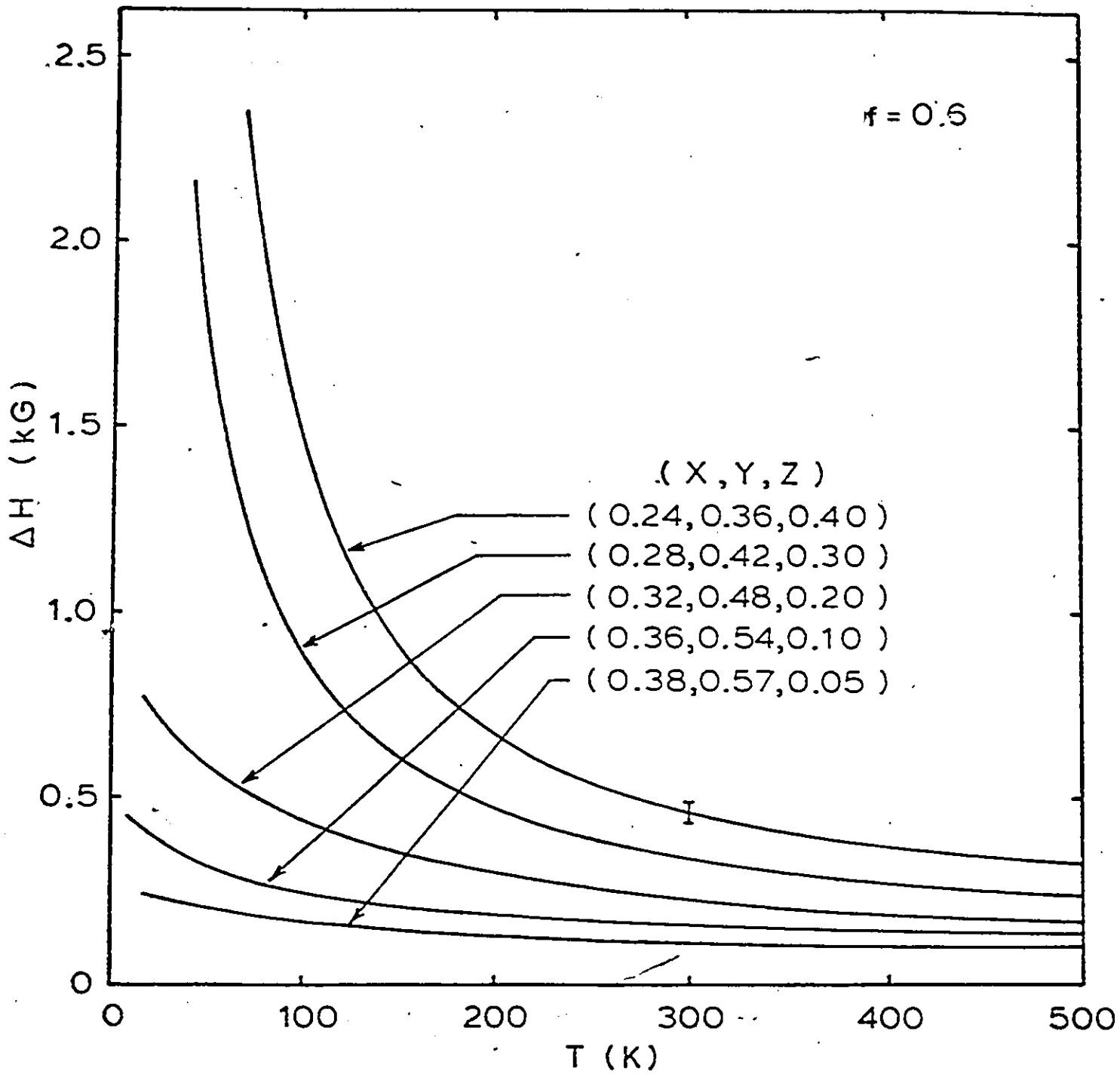

FIGURE 4.4 Mn ESR linewidth ΔH versus temperature for alloys $Cd_xZn_yMn_zSe$ with f = 0.6 (where f = y/x+y). A typical error bar for the experimental results is shown on one of the curves.

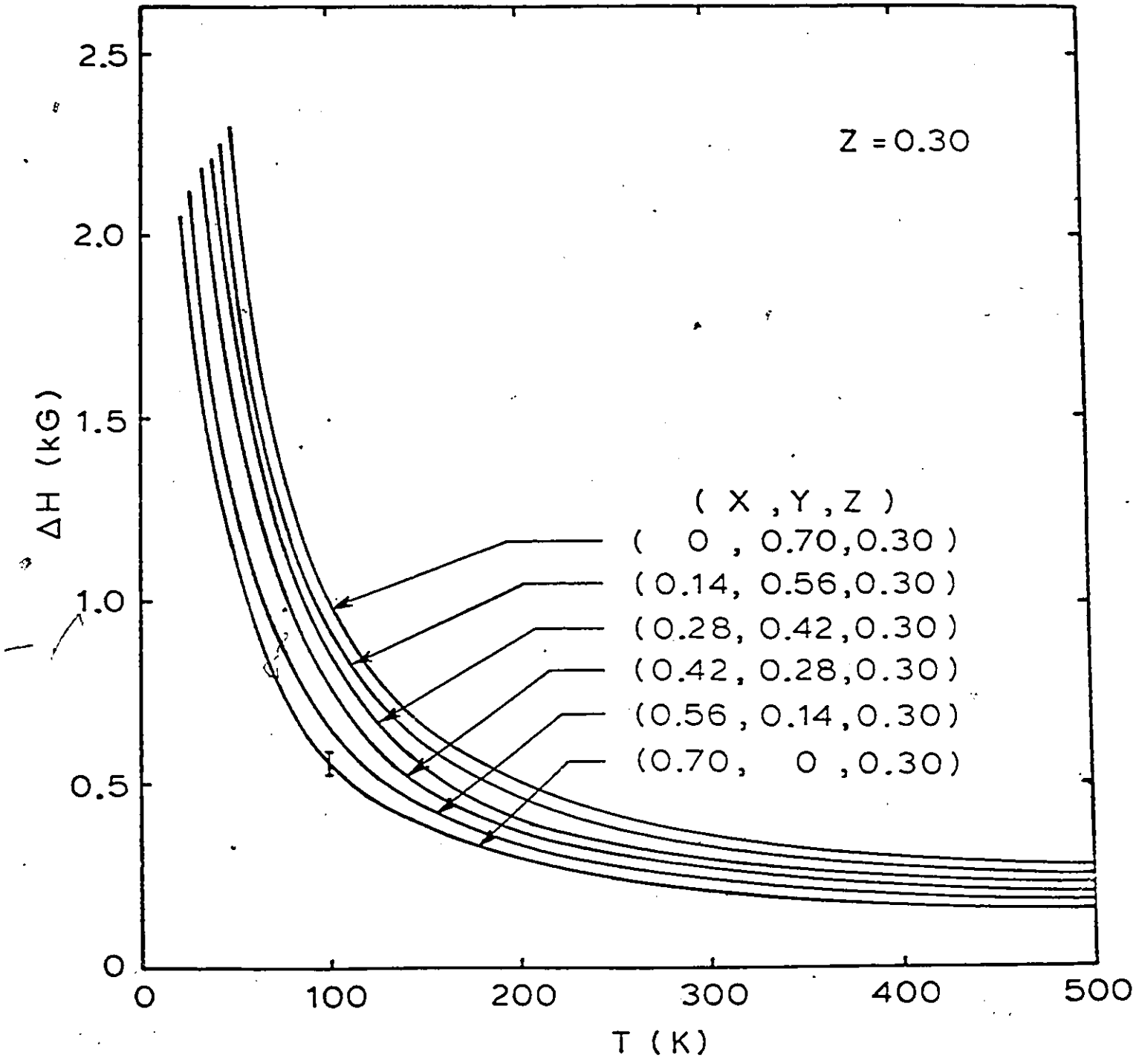

FIGURE 4.5 Mn ESR linewidth ΔH versus temperature for alloys $Cd_xZn_yMn_zSe$ with Mn concentration z = 0.30. A typical error bar for the experimental results is shown on one of the curves.

Fig. (4.6). At this point the line intensities decreased and quickly fell to almost zero with further cooling of the sample. This effect was most readily observed for samples with $z > 0.25$, since in those cases this low temperature behaviour occurred above the 10 K lower temperature limit of the equipment used. This effect has also been noted in other materials being investigated by the research group, e.g. $Cd_{1-z}Mn_zTe_{1-y}Se_y$ [3] and $Cd_xZn_yMn_zTe$ [4]. As indicated by Sayad and Bhagat, in their ESR work on $Cd_{1-z}Mn_zTe$ [5], the ESR lineshape for each of these alloys remains symmetrical down to certain temperature below which the line becomes assymmetric.

4.5 Analysis of ESR Linewidth and Discussion

In the ESR measurements of all the alloy samples it was observed that the symmetric Mn resonance linewidth increased with decreasing temperature, eventually becoming asymmetric at low temperature. As an example given in Fig. (4.6) in which it is seen that the low field half of the line is broadened and flattened out. The same kind of ESR line shapes were calculated by Searl et al [6-8] for a random polycrystalline assembly of uni-axial crystals having uni-axial g-value anisotropy. For more detail see reference Searl et al [6-8].

To analyse the variation of linewidth with temperature, initially the method of Oseroff et al [1] for $Cd_{1-z}Mn_zSe$ and $Cd_{1-z}Mn_zTe$ was used with the expression

$$\Delta H = A \left\{ \frac{T_c}{T - T_c} \right\}^{\alpha} + B \qquad (4.1)$$

developed by Huber [9] where B is the higher temperature linewidth, T_c is the "transition temperature", α is a critical exponent, and A is

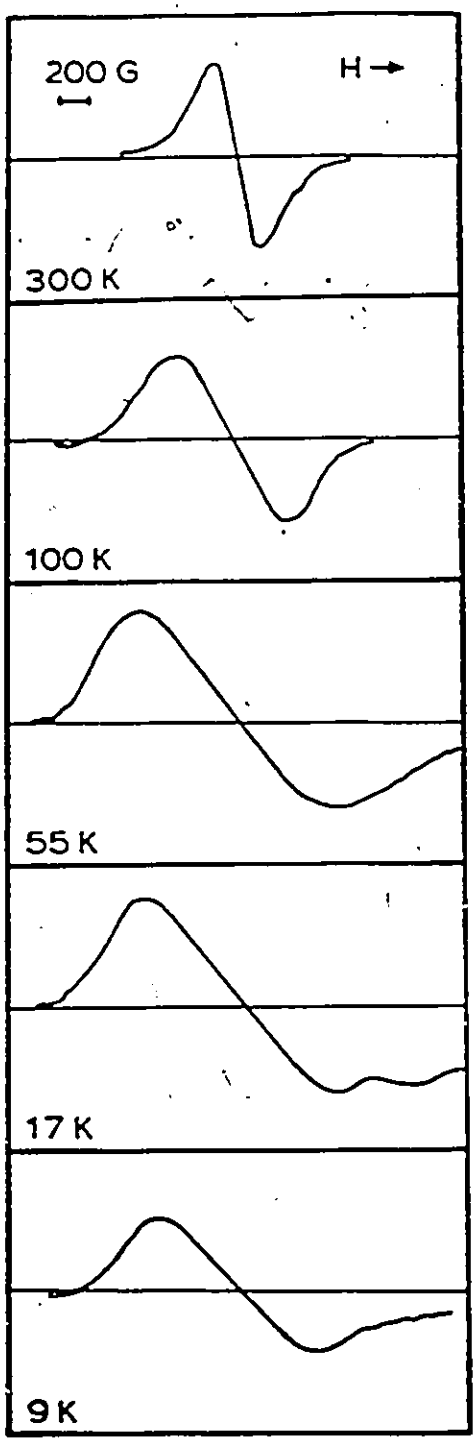

FIGURE 4.6 An example of asymmetric broadening of the ESR linewidth. At the lowest temperature, the resonance line splits into two.

a parameter dependent of T. This is the standard form used to analyse critical phenomenon results. The results obtained by Oseroff gave values for all four parameters T_c, A, B and α from a least square fit condition. However the values of A and α were inconsistent with composition variation, especially the value of α "the critical exponent" which varied by as much as an order of magnitude. Thus in the initial work on the present alloy, which is $Cd_xZn_yMn_zSe$, we analysed the data by employing a log-log plot such as

$$\log (\Delta H - B) = \alpha \log [T_c/(T-T_c)] + \log A \qquad (4.2)$$

The values of T_c used in this analysis were chosen as the temperature at which the linewidth became very large. These values are considerably higher than the T_g values obtained from the magnetic susceptibility. It was found that a linear variation of the type indicated in the equation (4.2) could be obtained only for the case B = 0. The values of α were then found to fall within the range of $\alpha = 0.33 \pm 0.08$.

But, a zero value of B is not physically meaningful, because it is not possible to have a zero linewidth at very high temperature ($T \to \infty$) in the paramagnetic region, which was implied by this analysis. Also it is not possible that the existence of the linewidth and its broadening at all temperatures is a result only of critical effects represented by the term $A\left(\frac{T_c}{T - T_c}\right)^{\alpha}$. Consequently equation (4.1) had to be discarded as a good expression representing ΔH vs T in our case.

In subsequent work [10-12] Oseroff used a modified Huber expression to fit the data of ΔH vs T for $Cd_{1-z}Mn_zTe$ and $Cd_{1-z}Mn_zSe$.

$$\Delta H = A(T_c/T-T_c)^{\alpha} + B(1-\theta/T) \qquad (4.3)$$

The equation is little more complicated than equation (4.1), because the parameter B is replaced by the term $B(1 - \theta/T)$, giving a 1/T variation for the high temperature linewidth, θ is the "paramagnetic Curie Weiss temperature" which is negative in these materials. This new term was introduced for antiferromagnets by Dormann and Jaccarino [13], to account for the non-critical high temperature dependence of the ESR linewidth. The results obtained using the equation (4.3) by Oseroff varied for α between 0.2 to 2.0, so this equation was discarded, because theoretically the value of critical exponent should be constant for the same critical phenomenon.

It has been suggested by Webb and co-workers [14] that the variation of ΔH with temperature is due to the resonance line being broadened because of the inhomogeneity which must be present with the random distribution of Mn^{2+} ions, and which results in an effective clustering of the ions. Webb et al [14] suggest that the variation of ΔH due to this effect can be written as an empirical expression of the form

$$\Delta H = \Gamma \exp\left(\frac{-T}{T_o}\right) + \Gamma_o \qquad (4.4)$$

where Γ_o is high temperature linewidth and Γ and T_o are empirical parameters associated with the interaction of the spins. This expression seemed to work quite well over a wide range of T, more specifically in the lower temperature region. However it was not clear how the high temperature linewidth Γ_o values were chosen by Webb et al [14] in every case. Apparently in most cases Γ_o was chosen as the value of ΔH at T = 300 K, the highest temperature at which ESR measurements were taken. In the present work the measurements were extended up to T = 500 K, and ΔH showed a noticeable variation between

300 K and 500 K. Knowing that for a given composition the values of these parameters (T_o and Γ) should be constant independent of the high temperature linewidth, convinced us further that our high temperature linewidth term $B(1-\theta/T)$ is the one to be used. Therefore the expression becomes

$$\Delta H = \Gamma \exp(-T/T_o) + B(1-\theta/T) \qquad (4.5)$$

From the value of ΔH in the range where the inhomogeneity broadening is negligible, i.e. at high T, values of θ and B could thus be obtained by plotting $T\,\Delta H$ vs T. Equation 4.5 can be written as

$$T\,\Delta H = F(T) + B(T-\theta) \qquad (4.6)$$

where $F(T) = T\Gamma \exp(-T/T_o)$. It can be seen that the second term in the equation (4.5) is linear in T and so plots of $T\,\Delta H$ vs T should give straight lines for the high temperature range, where the paramagnetic term is valid. In Figs. (4.7-4.10), which shows examples of such plots for the lines $f = 0$, $f = 0.2$, $f = 0.8$, and $f = 1$, it is observed that for each plot a linear behaviour is obtained down to a certain temperature below which there is a deviation from linearity. The slope of the line will give the value of parameter B and intercept will give the value of θ. The values obtained for θ in this way for all the samples were in good agreement with those obtained from the magnetic susceptibility measurement (see chapter 3), also the values for B varied systematically with composition. These result justified the use of the term $B(1-\theta/T)$ in describing the ESR linewidth dependence on temperature in purely paramagnetic high temperature regions. However it was found that at lower temperatures the $B(1-\theta/T)$ term appeared to overestimate the paramagnetic contribution, so that in some cases the rapid increase in ΔH appeared to be dominated by the

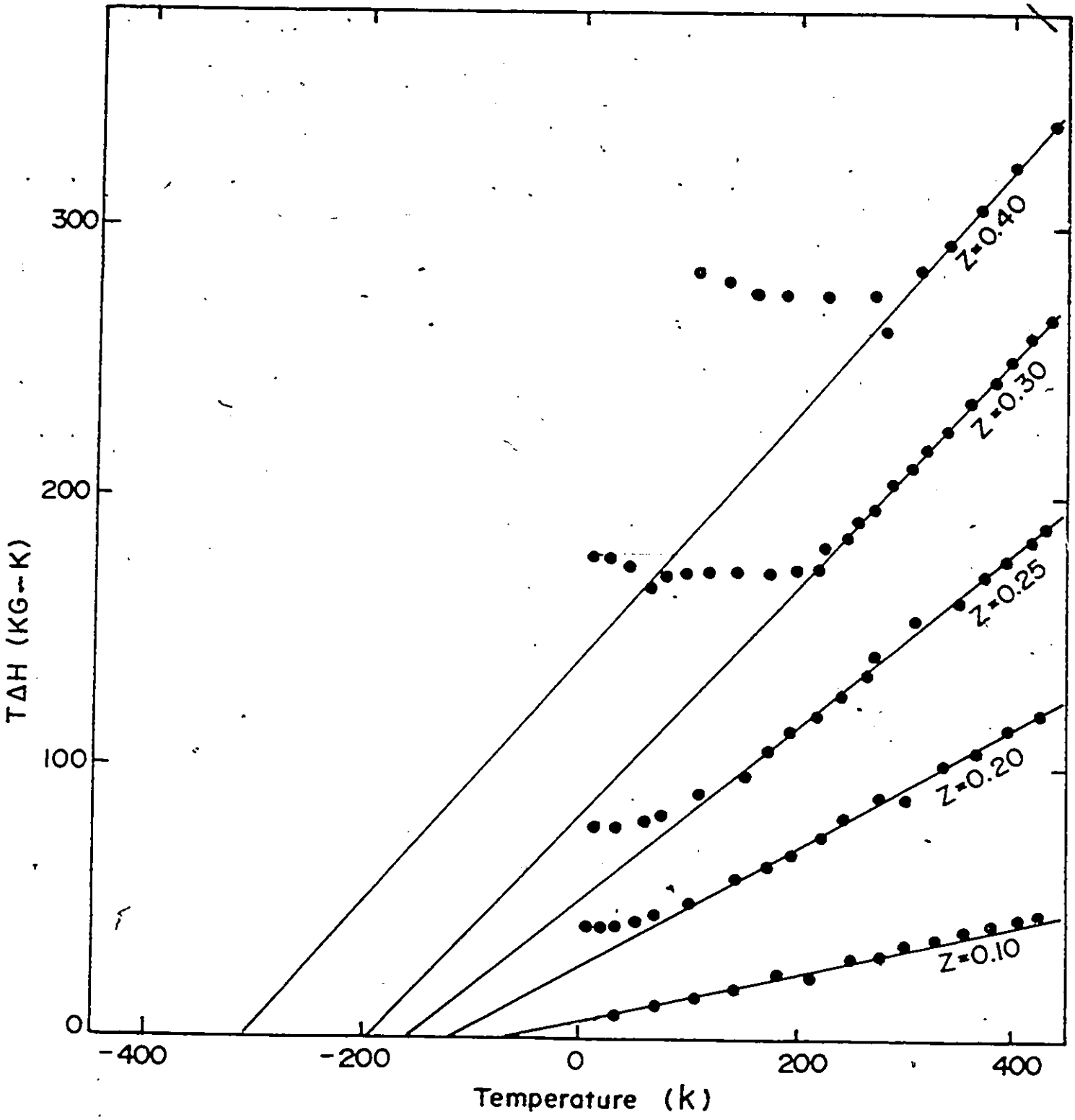

FIGURE 4.7 Variation of the values of TΔH with temperature for the alloys with f = 0 (where f = y/x+y).

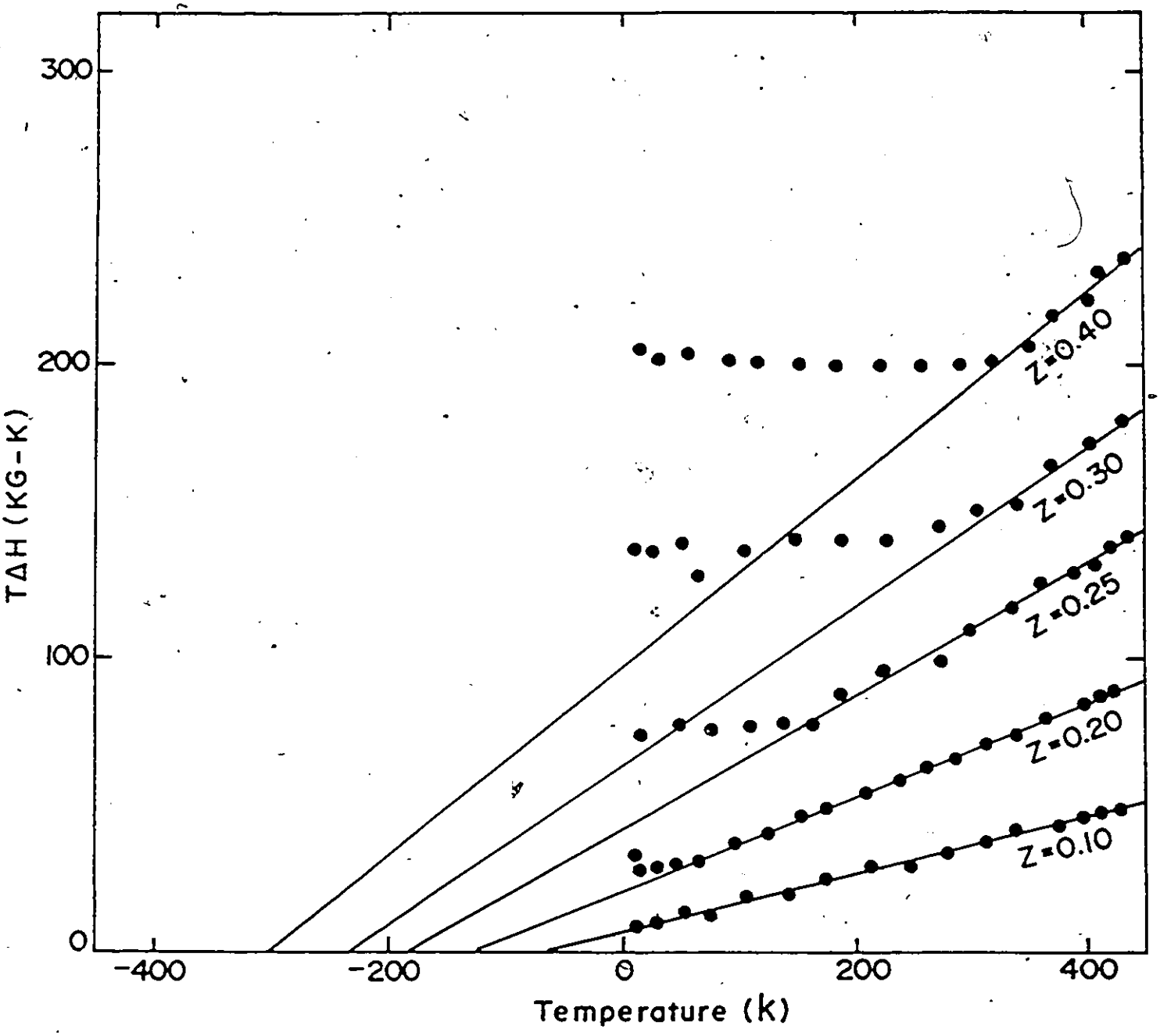

FIGURE 4.8 Variation of the values of TΔH with temperature for the alloys with f = 0.2 (where f = y/x+y).

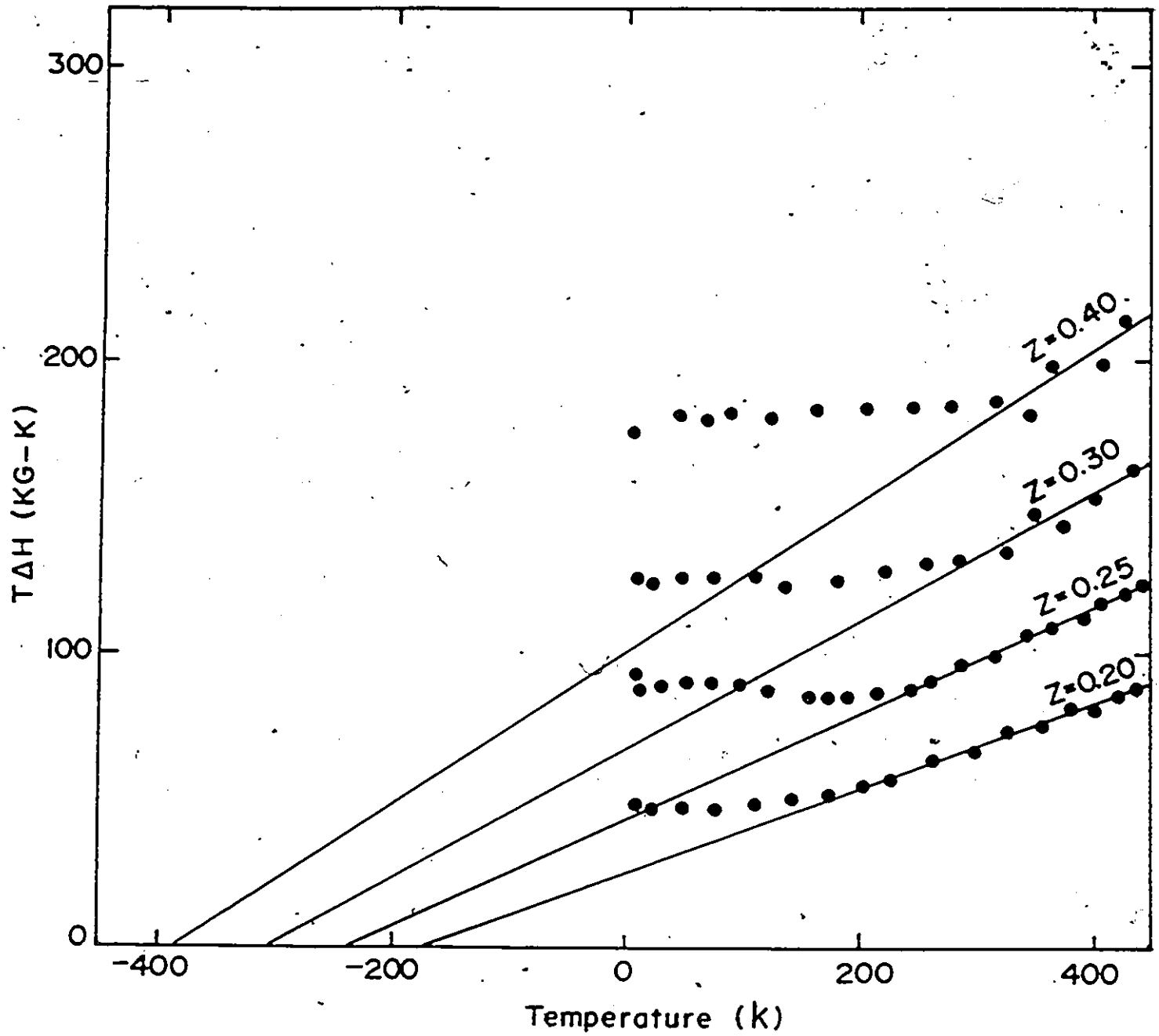

FIGURE 4.9 Variation of the values of TΔH with temperature for the alloys with f = 0.8 (where f = y/x+y).

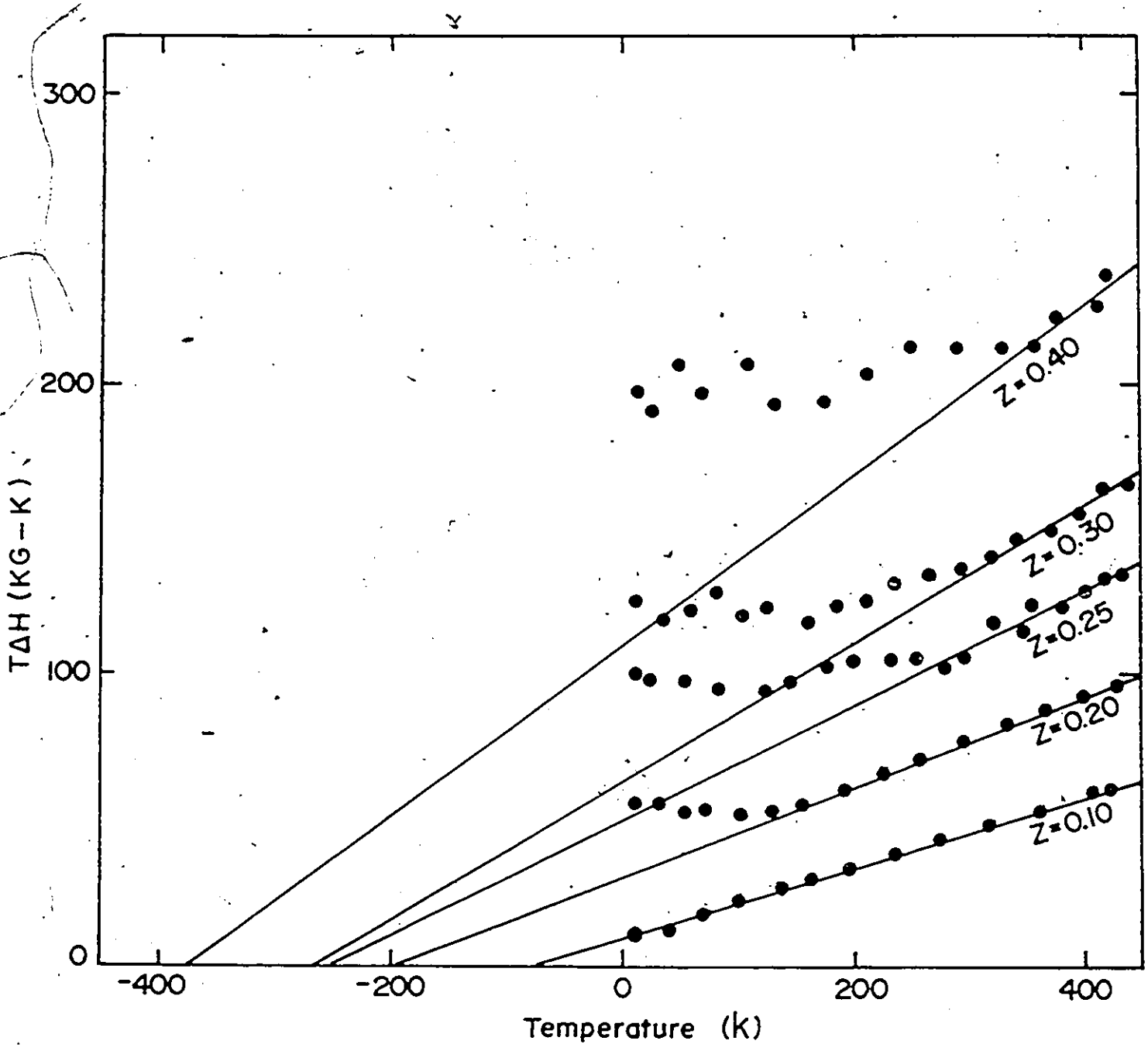

FIGURE 4.10 Variation of the values of TΔH with temperature for the alloys with f = 1 (where f = y/x+y).

paramagnetic term rather than that due to the inhomogeneity effect. This can be attributed to the fact that the paramagnetic contribution is due to the free Mn^{2+} spins all of which can be assumed to contribute at high temperatures. However at lower temperatures where exchange effects become important, the increased correlation between the spins mean that the effective number of free spins is reduced. To allow for this, the B coefficient in the paramagnetic relation needs to be modified and so has been written as $B\{1-\exp(-T/T_o)\}$. Hence this term is made to decrease at a rate compatible with the increase in the exchange effect. The experimental values of ΔH versus T were then fitted to the equation

$$\Delta H = \Gamma \exp(-T/T_o) + B\{1 - \exp(-T/T_o)\}\ (1-\theta/T) \qquad (4.6)$$

Values of θ were taken from the susceptibility measurements and Γ, T_o and B were determined by a least square fit to the experimental values of ΔH from the maximum temperature of 500 K down to that at which the line showed appreciable assymmetry. Indeed when the line shows asymmetry, the value of ΔH cannot be clearly determined. The least squares calculations were carried out using an Apple II microcomputer programme written by Tom Donofrio, a member of the research group.

In all cases, the fit to experimental points was very good with standard deviation in the order of 0.01 k gauss. Also the values of B obtained with this method, were in good agreement with those obtained graphically.

The variation of the parameters B, Γ and T_o with the composition variables f and z for a typical section of the alloy phase diagram, are shown in Fig. (4.11-4.14). The variation with alloy composition of the parameters B, Γ, and T_o obtained from the analysis

of the ESR results provides additional insight into the behaviour of the materials. In each case the parameter values are observed to vary linearly with f, (see Fig. 4.11), with the magnitude of the parameter being greater with increased manganese concentration z. The variation with f serves to show the trend of the parameter variation as cadmium is replaced by zinc.

The paramagnetic parameter B shows the paramagnetic behaviour of the material, as is seen from equation (4.6), B giving the linewidth ΔH at high temperature ($T >> \theta$). From Fig. (4.12) it is seen that within the limits of experimental error B shows a linear variation with z at constant f, so that B can be expressed as $B_o + \gamma z$. It is of interest to consider how the parameters B_o and γ vary for the system under investigation. Firstly it is seen from Fig. (4.12) that the intercept B_o has the same value ~60 gauss for all of the $Cd_xZn_yMn_zSe$ alloys. Secondly with regard to the slope γ, within a given crystal structure γ is found to vary smoothly with cation composition, increasing as Cd is replaced by Zn, as is seen in our case. This is illustrated by the limiting values for $Cd_xZn_yMn_zSe$ system

Wurtzite $Cd_{1-z}Mn_zSe$ γ = 250 Gauss $Zn_{1-z}Mn_zSe$ γ = 440 Gauss

The variation in ΔH indicated by γ can be attributed to line broadening due to spin-spin interaction, for which the dominant effect can be expected to be the indirect exchange which is responsible for the spin-glass behaviour at lower temperatures. Abragam and Bleaney [15] have discussed this line broadening effect and obtain an expression for the second moment of the form

$$h^2 \langle \Delta\nu^2 \rangle = 1/3\ S(S+1) \sum_j \sum_i (3\ J'_{zz}/2)^2_{ij} \qquad (4.7)$$

where J'_{zz} is a component of the total spin-spin interaction tensor. To

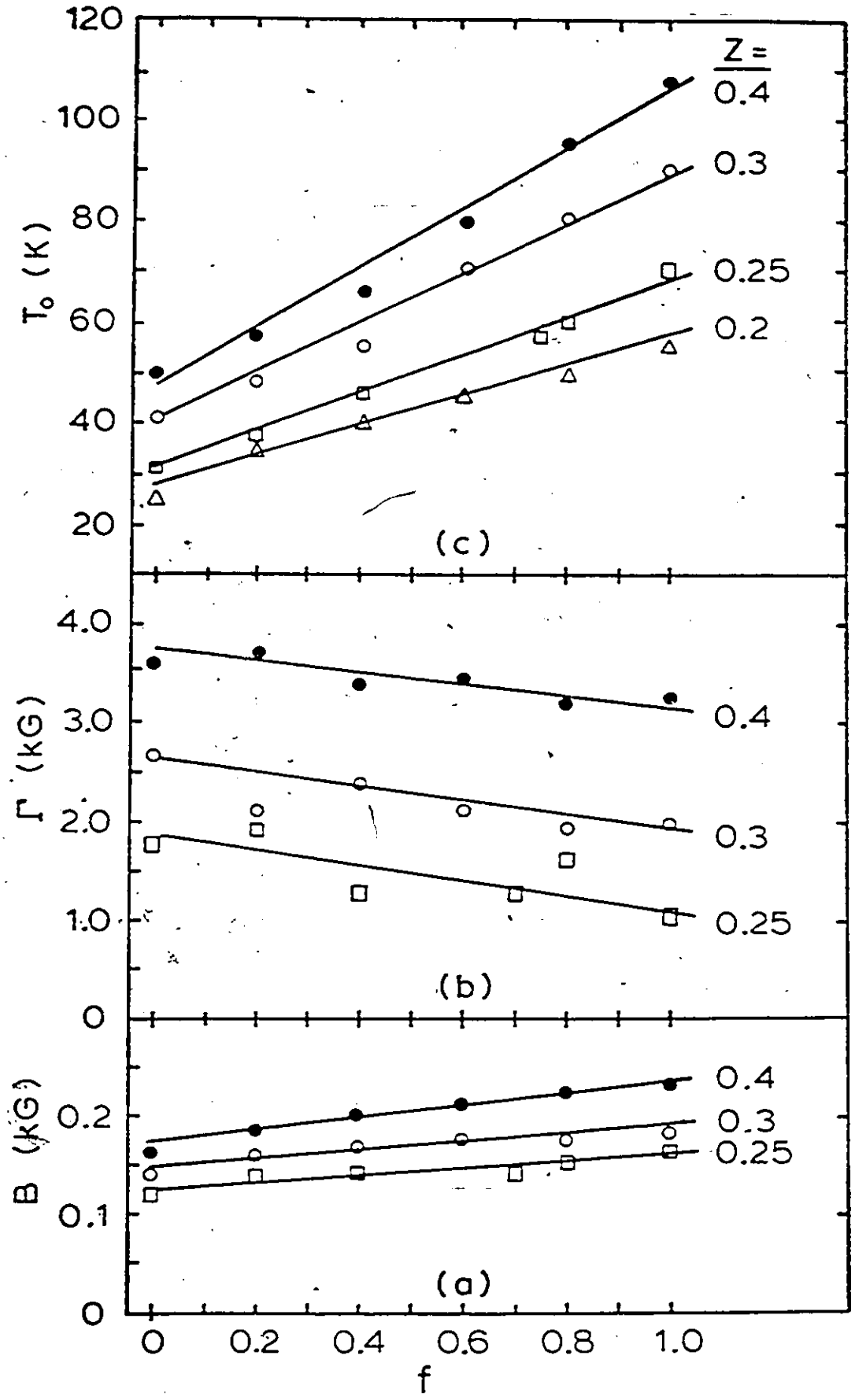

FIGURE 4.11 Plots of parameter B, Γ, and T_o versus f (where f = y/x+y), determined by fitting equation 4.6 to the ΔH vs T curves for various Mn concentrations z.

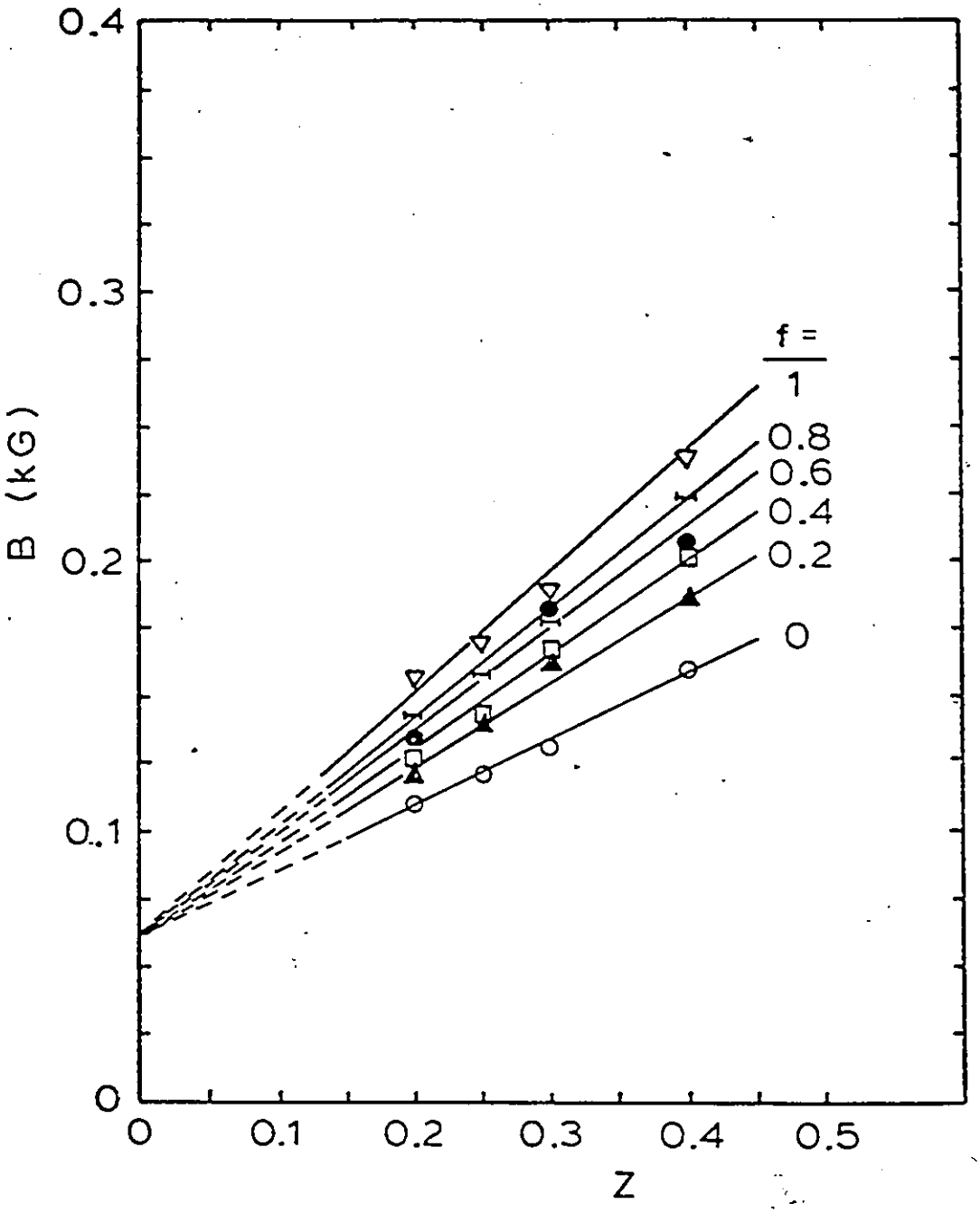

FIGURE 4.12 Variation of the parameter B in equation 4.6' versus the Mn concentration z determined by fitting equation 4.6' to the ΔH vs T curves for the indicated f values.

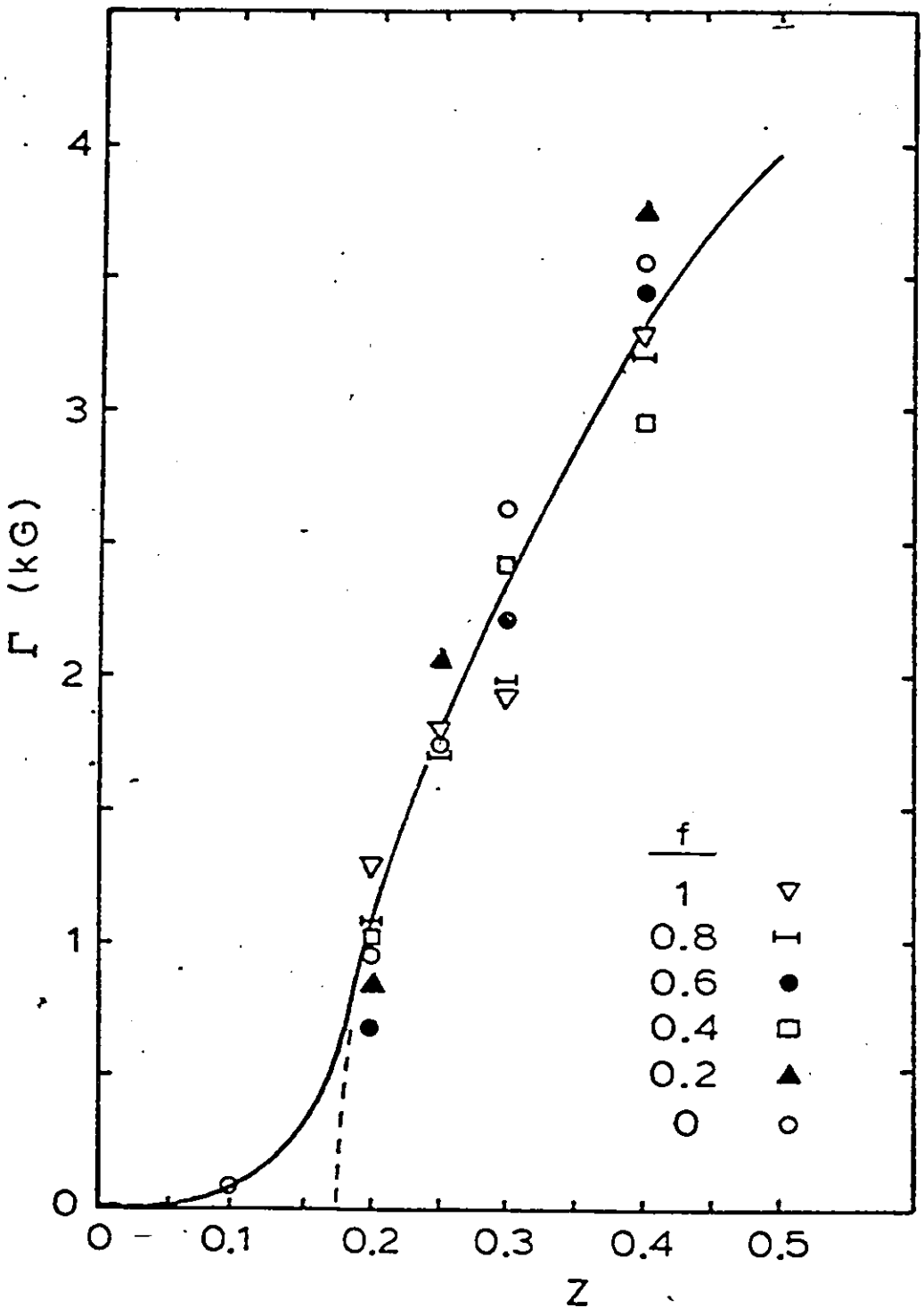

FIGURE 4.13 Plot of the parameter Γ in equation 4.6/ as a function of Mn concentration z for various alloy composition f determined by fitting equation 4.6/ to the ΔH vs T curves.

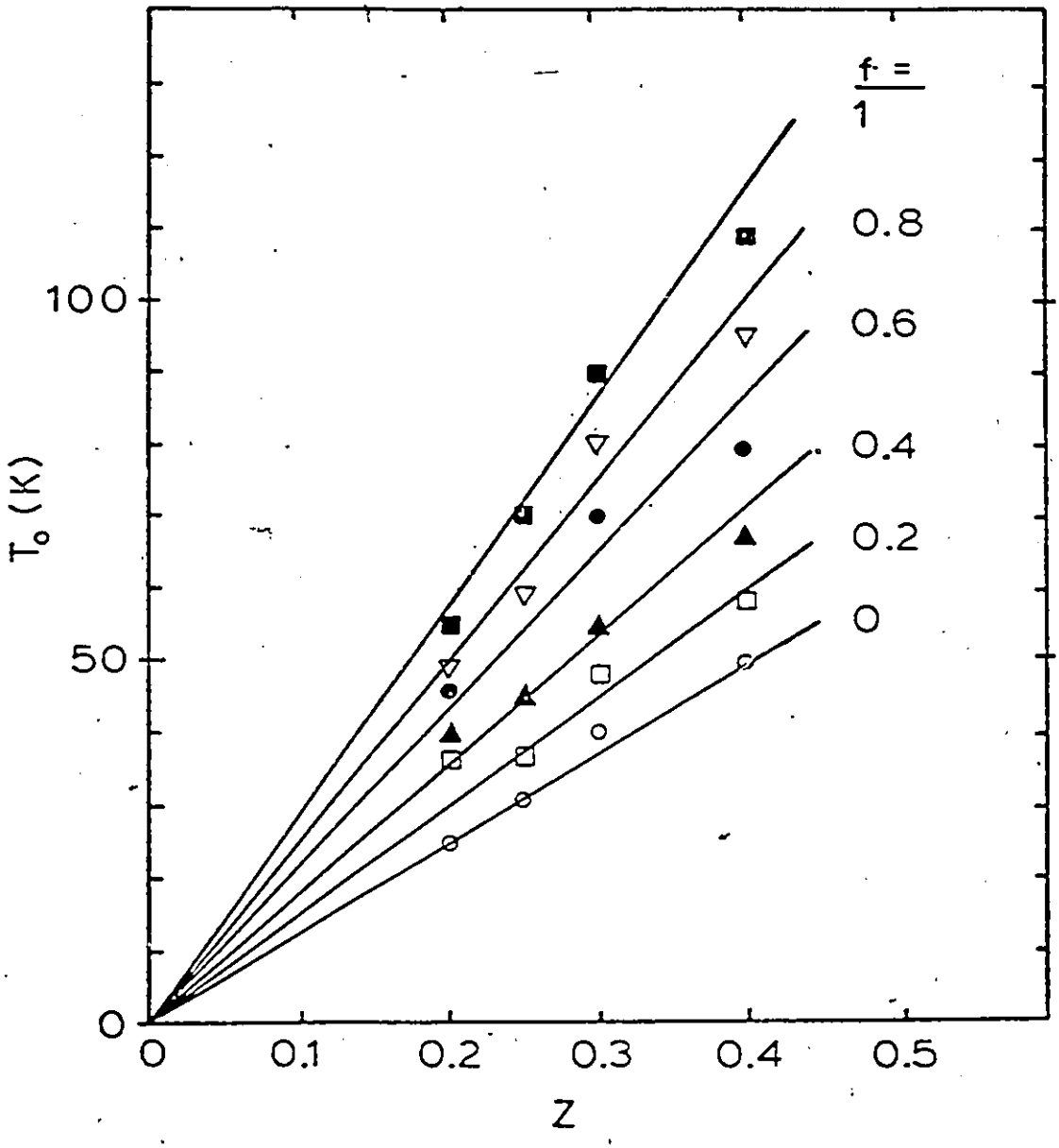

FIGURE 4.14 Plots of the parameter T_o in equation 4.6/ as a function of Mn concentration z for various alloy composition f determined by fitting equation 4.6/ to the ΔH vs T curves.

a reasonable approximation, the second moment may be taken as proportional to the square of the linewidth [16].

Given the exponential form of the exchange interaction previously postulated [17], which gives a good fit to the parameters of the spin-glass behaviour, all components of J may be expected to vary in a similar way as the cation is changed from zinc to cadium. Thus the ratios of the nearest neighbour exchange parameter J_1 determined previously [17], may be used to give an indication of the ratios of the second moment to be expected and hence the ratios of γ as cadmium is replaced by zinc. As shown previously in chapter 3, J_1 for $Cd_{1-z}Mn_zSe$ is 8.5 K and that of $Zn_{1-z}Mn_zSe$ is 13 K giving a zinc to cadmium ratio 1.5. From the above results the corresponding ratio for γ is 1.7.

In the plot of the variation of Γ with z, Fig. (4.13), the graph is represented by single line because of the scatter of the points within the interval of f values at each z. The plot shows that the line for $z < 0.2$ extrapolates to zero Γ at $z = 0.17$. However as in case of the T_g values, for $z < 0.2$ non-zero values of Γ are obtained and curve appears to change slope at about $z = 0.2$ and pass through the origin. Γ is determined by the width of the distribution of the local field seen by Mn ion in the lattice. In any random arrangement as is obtained in these alloys, the relative width of such a distribution is proportional to $z(1-z)$. At the same time, the total number in the distribution is proportional to z, the number of Mn atoms in the system. Thus the actual width of the distribution might be expected to be proportional to $z^2(1-z)$. i.e. Γ should vary as $\Gamma = Dz^2(1-z)$. In Fig. (4.15) the experimental values of Γ are plotted against $z^2(1-z)$ for the alloy $Cd_xZn_yMn_zSe$ under investigation and a reasonable straight line variation is obtained with the parameter D being 36 k gauss.

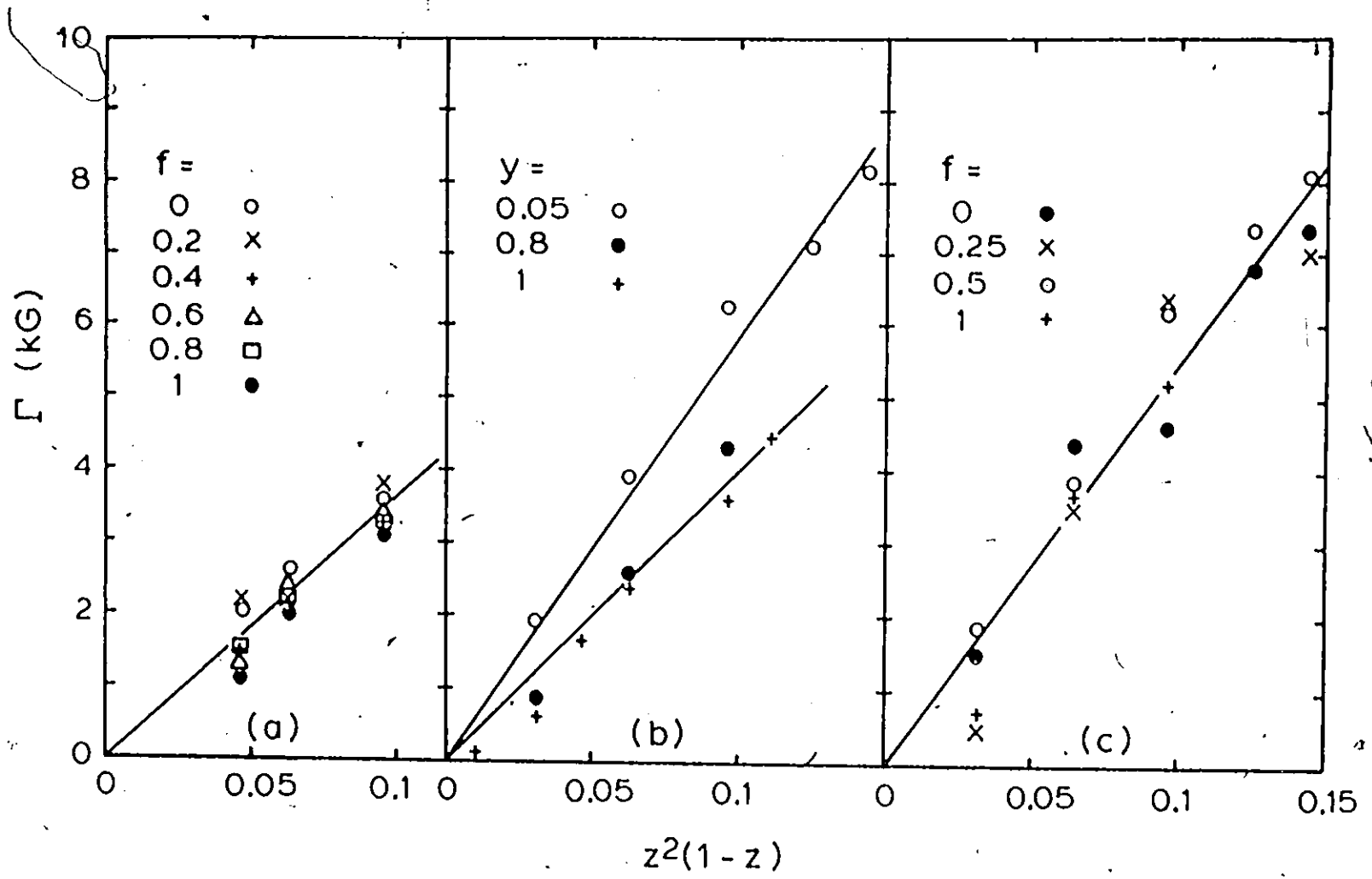

FIGURE 4.15 Plot of parameter Γ vs $z^2(1-z)$ for the alloys (a) $Cd_xZn_yMn_zSe$ (b) $Cd_{1-z}Mn_zTe_{1-y}Se_y$ and (c) $Cd_xZn_yMn_zTe$.

With regard to the physical significance of the parameter T_o, Sayad and Bhagat [5] have suggested that T_o is a measure of the potential barrier separating two neighbouring ground states of a disordered spin system. It is seen from Figs. (4.11,4.12) that within the limits of experimental error, T_o varies linearly with appropriate composition variable within a given phase field.

For the variation of T_o as a function of z Fig. (4.12) a series of straight lines can be drawn through the points of constant f, with all the lines extrapolating to the origin.

The values of dT_o/dz at constant f (where $f = y/x+y$) and of dT_o/df at constant z can be determined and these are shown in Fig. (4.16). It is seen that dT_o/dz varies linearly with f and that dT_o/df varies linearly with z and is zero at $z = 0$. Thus in general for these alloys, the relation between T_o and composition can be written as

$$T_o = (\alpha + \beta f)z \qquad (4.8)$$

If a least square fit is made to the experimental data for the $Cd_xZn_yMn_zSe$ alloys, the relation $T_o = (117 + 156\ f)z$ K with a standard deviation $\sigma = 2.8$ K is obtained.

Similarly the alloys $Cd_xZn_yMn_zTe$ [4] gives the relation for zinc blende

$$T_o = (146 + 86\ f)z \text{ K with } \sigma = 4.4 \text{ K}$$

One factor which may have some effect on these values of T_o is the variation of the lattice parameter a, since for a given z if a increases then the effective number of Mn atoms per unit volume decreases. This can be allowed for by using a corrected value z' in equation (4.8). Thus for any given value of f, z' has been taken as $z(a_o/a)^3$ where a_o is the lattice parameter at $z = 0$. In the present

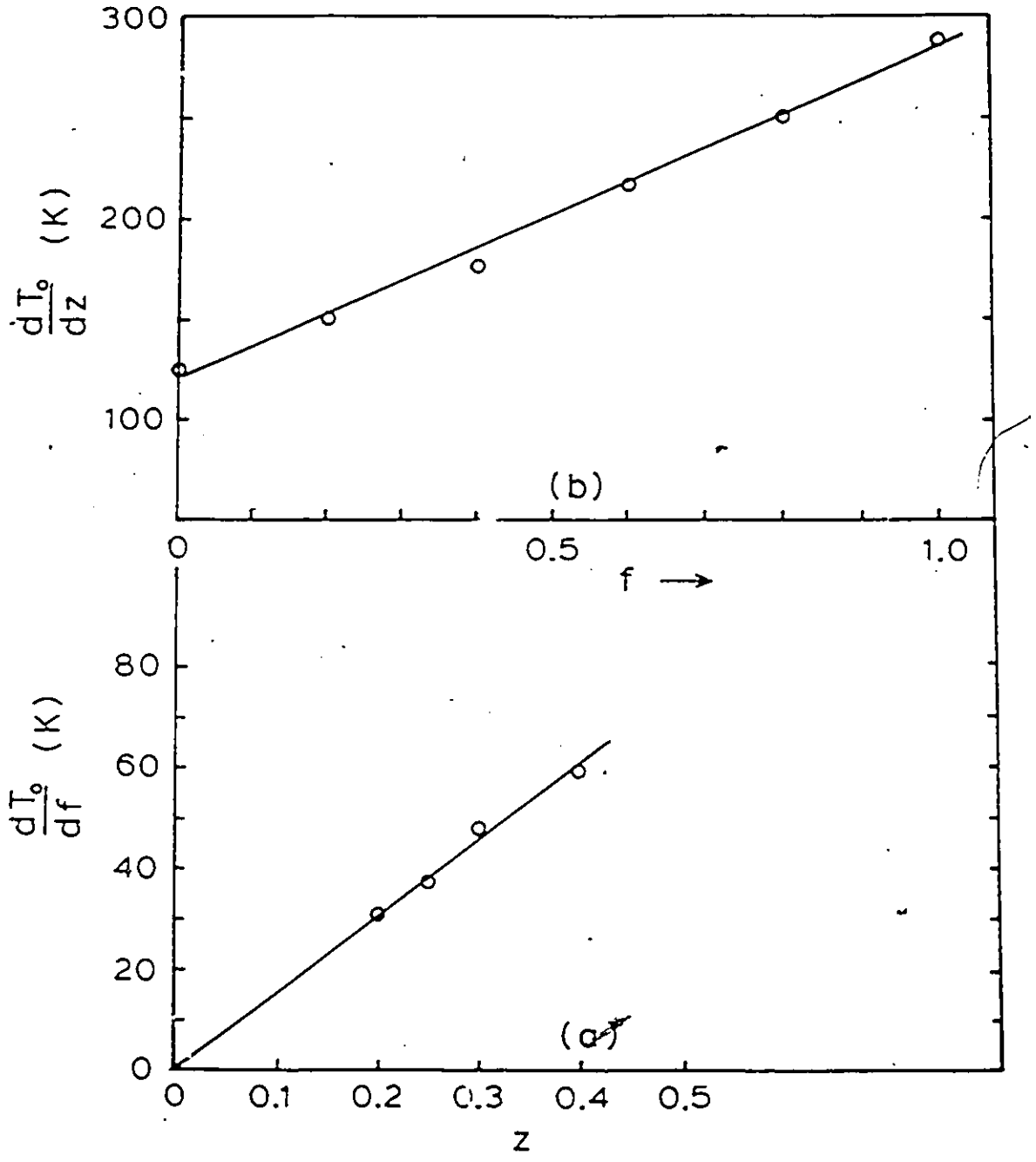

FIGURE 4.16 Plot of (a) dT_o/df vs z and (b) dT_o/dz vs f for the $Cd_xZn_yMn_zSe$ alloys.

case the structure is wurtzite and c/a is practically constant at 1.63, so that this correction is valid. Using z' instead of z in the fit to equation (4.8), it is found that only small changes in α and β are observed. Thus for $Cd_xZn_yMn_zSe$ alloys β becomes 173 K as opposed to the previous value of 156 K. Thus, at this stage, the effects of lattice parameter on T_o can be neglected.

These results for the T_o analysis can be seen to be consistent with the qualitative comments of Kremer and Furdyna [18] on the variation of the ESR linewidth ΔH with composition at constant z and constant temperature T, since at constant T, an increase in T_o will give an increase in ΔH. Kremer and Furdyna indicated that for constant T and z, the linewidth ΔH increases as the atomic number of the non-magnetic cation decreases (i.e. Cd → Zn in this case) and the above values of β are consistent with this. The question of what physical parameter is producing this effect is not clear at this time. One possible effect is the change in the amount of Mn-anion p hybridization recently discussed by Hass et al [19]. The values given in that work for the J_{sp-d} exchange constants indicate that J_{sp-d} decreases as the non-magnetic cation is changed from Cd to Zn.

4.6 Conclusions

The variation of the values of ESR linewidth ΔH with temperature can be well fitted in terms of the spatial inhomogeneity effect, represented by the form $\Gamma \exp(-T/T_o)$, as proposed by Webb et al [14] plus a paramagnetic term. The parameters Γ, B and T_o appear to be characteristic of the material investigated. T_o, which according to Sayad and Bhagat [5] is a measure of the potential barrier separating

neighbouring ground states of the disordered spin system, is found to be well fitted by the relation $(\alpha + \beta f)z$. It is found that when Zn is substituted for Cd on the cation sublattice the coefficient β is positive while in case of $Cd_{1-z}Mn_zTe_{1-y}Se_y$ when Se is substituted for Te [3], the coefficient β has negative value. This is consistent with the qualitative comment of Kremer and Furdyna [18] on the variation of ΔH with composition at constant T and constant z. It is suggested that the values of β may be determined by the changes in the exchange constant J_{sp-d} [19] with composition.

The parameter Γ can be taken as a measure of the width of the distribution of the local fields as seen by the Mn ions and it is argued that Γ should be proportional to $z^2(1-z)$. Graphs of Γ vs $z^2(1-z)$ give reasonable straight lines in all cases and the slopes of these lines appears to be characteristic of the crystal structure, being ~37 k gauss for wurtzite and ~56 k gauss for zinc blende.

The parameter B, which characterizes the paramagnetic behaviour and gives the linewidth ΔH at high temperatures, is found to vary linearly with z i.e. $B = B_o + \gamma z$ for all cases of constant, non-magnetic cation ratio. The values of B_o are found to be independent of cation composition and to depend upon anion type (and/or crystal structure). The parameter γ can be attributed to the effects of spin-spin line broadening and for a given crystal structure shows good correlation with the values of exchange interaction determined from analysis of the spin-glass behaviour at low temperatures.

REFERENCES

1. S. Oseroff, R. Calvo, W. Giriat, J. Appl. Phys. 50, 7738 (1979).

2. A.H. Morrish, The Physical Principles of Magnetism, p. 78, Krieger, New York (1980).

3. S. Chehab, Ph.D. Thesis, University of Ottawa.

4. T. Donofrio, Ph.D. Thesis, University of Ottawa.

5. H.A. Sayad and S.M. Bhagat Phys. Rev. 31B, 591 (1985).

6. J.W. Searl, R.C. Smith, S.J. Wyard, Proc. Phys. Soc. 78, 1174 (1961).

7. J.W. Searl, R.C. Smith, S.J. Wyard, Bulletin Ampere, Fasc. special, 9th year, p. 236 (1960).

8. J.W. Searl, R.C. Smith, S.J. Wyard, Proc. Phys. Soc. 74, 491 (1959).

9. D.L. Huber, Phys. Rev. B6, 3180 (1972).

10. S.B. Oseroff, Phys. Rev. 25B, 6584 (1982).

11. S. Oseroff, R. Calvo, W. Giriat and Z. Fisk, Solid State Commun. vol. 35, p. 539 (1980).

12. S.B. Oseroff, R. Calvo, Z. Fisk and F. Acker, Phys. Lett. vol. 80A, p. 311 (1980).

13. V. Jaccarino and E. Dormann, Phys. Lett. 48A, 81 (1974).

14. D.J. Webb and S.M. Bhagat, J.K. Furdyna, J. Appl. Phys. 55, 2310. (1984).

15. Abragam and Bleany, "Electron Paramagnetic Resonance of Transition Ions", Clarendon Press-oxford, p. 142-148, 438-442, 467-470 (1970).

16. C.P. Poole Jr., Electron Spin Resonance (Interscience, New York, 1967) p. 779.

17. J.C. Woolley, S.F. Chehab, T. Donofrio, S. Manhas, G. Lamarche and A. Manoogian, J. Magn. Magn. Mat. 61 (1986) 13.

18. R.E. Kermer and J.K. Furdyna, Phys. Rev. 1331 (1985) 1.

19. K.C. Hass, B.E. Larson, H. Ehrenreich and A.E. Carlsoon, J. Magn. Magn. Mat. 54-57 (1986) 1283.

Chapter V

Conclusion

In this thesis an investigation of some of the properties of the pseudo-ternary alloy $Cd_xZn_yMn_zSe$ has been presented. The alloys of this system which are known as semi-magnetic semi-conductors have interesting properties such as disordered magnetic behaviour, spin glass transition, antiferromagnetically correlated spins in clusters and other magnetic effects. Three different types of measurements were performed on these materials; the determination of lattice parameter, magnetic susceptibility, and ESR linewidth.

Once the limits of solid solution were defined with the help of lattice parameter values, the magnetic properties of the alloys were studied. This was done by carrying out magnetic susceptibility and electron spin resonance measurements.

The magnetic susceptibility measurements made on the wurtzite and zinc blende single-phase samples, as described in chapter 3. We were thus able to determine the spin-glass freezing temperature T_g, the Curie-Weiss paramagnetic temperature θ, and the Curie constant C. It was found that the variation of these parameters depend mainly on the Mn concentration z. Also when the concentration of the Zn component in a sample was increased while keeping the manganese concentration constant, the results showed a change in magnetic effect as well as lattice value. It was found that for both T_g and θ, this increase was directly attributable to an increase in the exchange energy which resulted from a decrease in the lattice parameter. Another interesting aspect of the T_g results was that ℓnT_g was found to decrease in a

linear fashion when the mean spacing between the Mn ions increases with decreasing z. This indicated that the exchange interaction decreases exponentially with distance between the magnetic spins. An exchange mechanism proposed by Geertsma et al., involving virtual transitions from the valence band to Mn 3d levels was assumed as the one occurring in these wide gap semi-conductors. Using the expression for this exchange, $J(r) = I_o r^{-2} \exp(-\alpha r)$ (see Chapter 3 for details), in conjunction with the mean field theory we were able to predict values for J_1 and J_2, the nearest and next nearest neighbour exchange parameters, as well as the values for the Curie-Weiss paramagnetic temperature θ. All these calculated values agreed very well with the experimental values, which was strong evidence in support of our assumption that the Geertsma exchange mechanism is the one having maximum effect.

The results of electron spin resonance experiment revealed some other magnetic properties of the alloy. The ESR line was found to broaden in a symmetric fashion down to a certain temperature depending upon composition of the sample below which the line starts broadening assymmetrically. The linewidth dependence on temperature was fitted to an empirical equation (Chapter 4). The parameter (B, T_o, and Γ) values obtained from the fit showed consistent dependence on composition. With regard to the physical significance of these ESR parameters, as discussed in Chapter 4, B represents the linewidth at highest possible temperature, T_o is a measure of the potential barrier separating two neighbouring ground states of the disordered spin system, while Γ is determined by the variation in the magnetic environment of a Mn ion in the lattice.

Finally the investigation of the $Cd_x Zn_y Mn_z Se$ alloys system presented in this thesis, has yielded valuable information which was very useful in giving better understanding of some aspects of the physical behaviour of this new class of materials called semi-magnetic semi-conductors.